EPIGENETIC REGULATION OF OLIGODENDROCYTE DEVELOPMENT AND REGENERATION IN THE CENTRAL NERVOUS SYSTEM

APPROVED BY SUPERVISORY COMMITTEE

Q. Richard Lu, Ph.D. (Mentor)

W. Lee Kraus, Ph.D. (Chair)

Jane E. Johnson, Ph.D.

Eric N. Olson, Ph.D.

DEDICATION

To my supportive friends and family,

my significant other and so on and so forth.

EPIGENETIC REGULATION OF OLIGODENDROCYTE DEVELOPMENT AND REGENERATION IN THE CENTRAL NERVOUS SYSTEM

by

DANYANG HE

DISSERTATION

Presented to the Faculty of the Graduate School of Biomedical Sciences

The University of Texas Southwestern Medical Center

In Partial Fulfillment of the Requirements

For the Degree of

DOCTOR OF PHILOSOPHY

The University of Texas Southwestern Medical Center

Dallas, Texas

December, 2016

EPIGENETIC REGULATION OF OLIGODENDROCYTE DEVELOPMENT AND REGENERATION IN THE CENTRAL NERVOUS SYSTEM

Danyang He, Ph.D.

The University of Texas Southwestern Medical Center, 2016

Supervising Professor: Q. Richard Lu, Ph.D.

Oligodendrocytes (OLs) produce myelin sheaths that electrically insulate axons and promote rapid propagation of action potentials in the CNS. The onset and timing of CNS myelination and remyelination requires precise coordination between epigenetic programming and transcriptional regulation. In this thesis, I present my findings on two epigenetic regulatory complexes Chd7/Sox10 and lncOL1/Suz12 in CNS myelination and remyelination.

First, we show that chromatin remodeler Chd7 is required for proper onset of CNS myelination and remyelination. Genome-occupancy analyses, coupled with transcriptome profiling, reveal that Chd7 interacts with Sox10 and targets the enhancers of key myelinogenic genes, and identify novel Chd7 targets including bone formation regulators *Osterix/Sp7* and *Creb3l2*, which are also critical for oligodendrocyte maturation. Thus, Chd7

coordinates with Sox10 to regulate the initiation of myelinogenesis and acts as a molecular nexus of regulatory networks that account for the development of a seemingly diverse array of lineages including oligodendrocytes and osteoblasts, pointing to the hitherto previously uncharacterized Chd7 functions in white matter pathogenesis in CHARGE syndrome.

To understand the role of lncRNAs in CNS myelination, we establish dynamic expression profiles of lncRNAs at different stages of oligodendrocyte development and uncover a cohort of stage-specific oligodendrocyte-restricted lncRNAs including a conserved chromatin-associated lncOL1. Genetic inactivation of lncOL1 causes defects in CNS myelination and remyelination following injury. Functional analyses illustrate that lncOL1 interacts with Suz12, a component of PRC2, to promote oligodendrocyte maturation in part through Suz12-mediated repression of a differentiation inhibitory network that maintains the precursor state.

Collectively, these studies show that epigenetic circuitry between lncRNAs and transcription factors with chromatin-modifying complexes play roles in balancing inhibitory and activating gene program, allowing the timely CNS myelination and myelin repair.

TABLE OF CONTENTS

PRIOR PUBLICATIONS

1. **He D**, Marie C, Zhao C, Kim B, Wang J, Deng Y, Clavairoly A, Frah M, Wang H, He X, Hmidan H, Jones BV, Witte D, Zalc B, Zhou X, Choo DI, Martin DM, Parras C, Lu QR. (2016). Chd7 cooperates with Sox10 and regulates the onset of CNS myelination and remyelination. NAT NEUROSCI; 19(5):678-89
2. **He D**, Wang J, Lu Y, Deng Y, Zhao C, Xu L, Chen Y, Hu Y, Zhou W, Lu QR. lncRNA functional networks in oligodendrocytes reveal stage-specific myelination control by a lncOL1/Suz12 complex in the CNS. Neuron. Manuscript Revised.
3. Lopez Juarez A*, **He D***, Richard Lu Q. (2016). Oligodendrocyte progenitor programming and reprogramming: Toward myelin regeneration. Brain Res.; 1638(Pt B):209-20
4. Lu F, Chen Y, Zhao C, Wang H, **He D**, Xu L, Wang J, He X, Deng Y, Lu EE, Liu X, Verma R, Bu H, Drissi R, Fouladi M, Stemmer-Rachamimov AO, Burns D, Xin M, Rubin JB, Bahassi el M, Canoll P, Holland EC, Lu QR. (2016). Olig2-Dependent Reciprocal Shift in PDGF and EGF Receptor Signaling Regulates Tumor Phenotype and Mitotic Growth in Malignant Glioma. Cancer Cell; 9;29(5):669-83.
5. Zhang L, He X, Liu L, Jiang M, Zhao C, Wang H, **He D**, Zheng T, Zhou X, Hassan A, Ma Z, Xin M, Sun Z, Lazar MA, Goldman SA, Olson EN, Lu QR. (2016). Hdac3 Interaction with p300 Histone Acetyltransferase Regulates the Oligodendrocyte and Astrocyte Lineage Fate Switch. Dev Cell.; 36(3):316-30

LIST OF FIGURES

LIST OF TABLES

LIST OF DEFINITIONS

CNS	Central Nervous System
OPC	Oligodendrocyte Precursor Cells
OL	Oligodendrocyte
iOL	immature Oligodendrocyte
mOL	mature Oligodendrocyte
RNA-Seq	RNA Sequencing
ChIP-Seq	Chromatin Immunoprecipitation Sequencing
RIP	RNA Immunoprecipitation
PDGFRα	Platelet-derived growth factor receptor alpha
NG2/Cspg4	Neural/glial antigen 2
Olig1	Oligodendrocyte transcription factor 1
Olig2	Oligodendrocyte transcription factor 2
Mbp	Myelin basic protein
Plp1	Proteolipid Protein 1
Cnp	2',3'-Cyclic Nucleotide 3' Phosphodiesterase
Mag	Myelin-associated glycoprotein
MOG	Myelin Oligodendrocyte Glycoprotein
APC/CC1	Adenomatous Polyposis Coli
Sox10	SRY (sex determining region Y)-box 10
Sox9	SRY (sex determining region Y)-box 9

Hes1	Hairy and enhancer of split 1
Hes5	Hairy and enhancer of split 5
Id2	Inhibitor of DNA Binding 2
Id4	Inhibitor of DNA Binding 4
Myrf/Gm98	Myelin regulatory factor
Sox5	SRY (sex determining region Y)-box 5
Sox6	SRY (sex determining region Y)-box 6
Zeb2/Sip1	Zinc Finger E-Box Binding Homeobox 2
HDAC	Histone deacetylase
HAT	Histone acetyltransferase
HMT	Histone methyltransferase
TET	Ten-eleven translocation methylcytosine dioxygenase
Ezh2	Enhancer Of Zeste 2
Eed	Embryonic Ectoderm Development
Suz12	Suppressor Of Zeste 12 Protein Homolog
CHD	Chromodomain-helicase-DNA-binding
Brg1/Smarca4	SWI/SNF Related, Matrix Associated, Actin Dependent Regulator Of Chromatin, Subfamily A, Member 4
Sirt2	Sirtuin (Silent Mating Type Information Regulation 2 Homolog) 2
H3k27ac	Acetylation at the 27^{th} lysine residue of the histone protein 3
H3K27me3	Trimethylation at the 27^{th} lysine residue of the histone protein 3

H3K4me3	Trimethylation at the 4 th lysine residue of the histone protein 3
Igf2	Insulin Like Growth Factor 2
H19	Imprinted Maternally Expressed Transcript
Cyp1b1	Cytochrome P450 Family 1 Subfamily B Member 1

CHAPTER ONE

INTRODCUTION

OLIGODENDROCYTE DEVELOPMENT AND REGENERATION

Oligodendrocyte and Myelin

Within the vertebrate nervous system, motor, sensory, and cognitive functions require rapid impulse propagation, which is facilitated by the insulation of axons by myelin sheaths. Myelin is a specialized structure that extends compacted multilayered membrane around the axons and reduces the transverse capacitance and increases the transverse resistance of the axonal plasma membrane. By limiting action potentials to short unmyelinated axonal segments, myelin sheaths provide the structural basis for saltatory propagation, which accelerates nerve conduction by 20-100 folds. In the central nervous system (CNS), myelin is generated by oligodendrocytes. Using silver carbonate impregnation method, Del Río Hortega first discovered and systematically described oligodendrocytes as glia cells with very few processes in 1928(P., 1928). Though Del Río Hortega predicted that oligodendrocytes were functionally similarly to Schwann cells in the CNS and responsible for myelination (P., 1922), yet cellular connection between oligodendrocytes and myelin sheaths was not demonstrated until 1960s when electron microscopy was introduced (Bunge, 1968). An oligodendrocyte extends many processes, each of which contacts and repeatedly envelopes a stretch of axon with subsequent condensation of this multispiral membrane-forming myelin (Bunge et al., 1962). Ultrastructurally, oligodendrocytes can be identified by

their generally round, dark nuclei (with condense chromatin), which are surrounded by dark cytoplasm containing short granular endoplasmic reticulum, polyribosomes, short mitochondria, and Golgi apparatus(Sandell and Peters, 2002).

Oligodendrocyte Specification and Differentiation

Developmentally, oligodendrocytes are generated by subventricular cells from the ventral neuroepithelium of the neural tube in early embryonic development and from dorsal spinal cord and hindbrain/telencephalon of the brain at later development (Vallstedt et al., 2005). Those progenitors, under the influence of extracellular ligands such as sonic hedgehog (Shh), give rise to committed oligodendrocyte progenitor cells (OPCs) that remain highly proliferative and motile, dividing as they migrate out throughout the CNS. Once in their final position, OPCs exit the cell cycle, undergo differentiation into premyelinating oligodendrocytes, which, given the appropriate environmental cues, will further mature and myelinate nearby receptive axons. These highly dynamic differentiation processes are characterized by the dramatic increase in morphologic complexity and the expression pattern of specific markers, and could be divided into four different steps: oligodendrocyte precursor cells (OPC), pre-oligodendrocytes (or late OPC), immature (or pre-myelinating) OL and mature (or myelinating) OL (Figure 1-1). OPC are identified with the specific expression of platelet-derived growth factor receptor α (PDGF-Rα), ganglioside A2B5 and proteoglycan NG2. OPC first give rise to preoligodendrocytes that extend multipolar short processes and start to express sulfatide recognized by the O4 antibody. Upon loss of A2B5 and NG2

markers, immature OL become post-mitotic cells with long ramified branches and are committed to the oligodendroglial lineage with the appearance of galactocerebroside C (GalC). In the final stages of OL development, mature OL extend membranes that form compact enwrapping sheaths around the axons and express myelin proteins such as myelin basic protein (MBP), proteolipid protein (PLP), myelin associated glycoprotein (MAG), and finally myelin oligodendrocyte glycoprotein (MOG) (Figure 1-1)

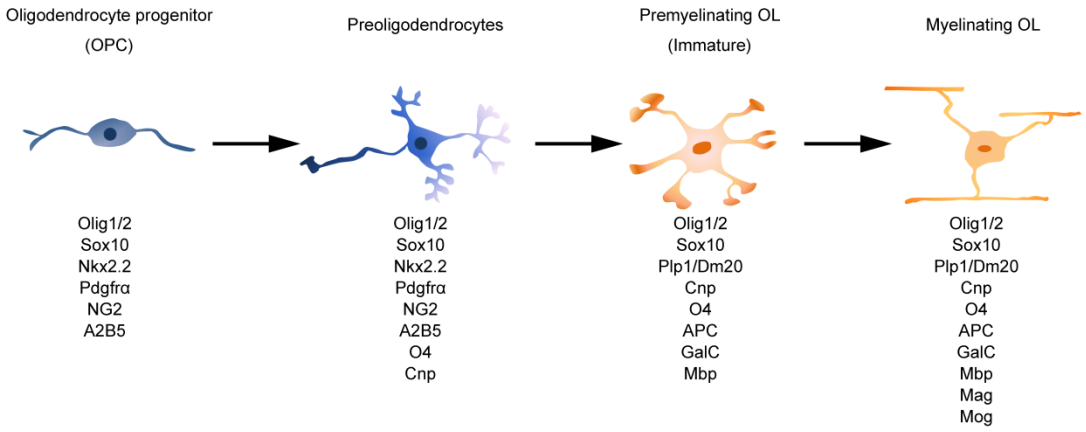

Figure 1-1 Stepwise differentiation and maturation of oligodendrocytes.

Oligodendrocyte Regeneration and Remyelination

Oligodendrocyte and myelin sheaths are critical to facilitate saltatory conduction, maintain axonal integrity and support survival of CNS neurons (Chamberlain et al., 2015). Disturbances to oligodendrocyte function or myelination in the developing or injured brain impairs axonal conduction (Waxman, 2006) and is associated with neuronal degeneration (Das Sarma et al., 2009). CNS is capable to spontaneously regenerate oligodendrocytes and

replace myelin (remyelination) following acute demyelination (Franklin and Ffrench-Constant, 2008). In response to injury, neighboring OPCs undergo a switch from an essentially quiescent state to a regenerative phenotype and rapidly migrate to the site of injury. Following recruitment, the OPCs differentiate into oligodendrocytes to remyelinate recently denuded axons. This differentiation phase encompasses three distinct steps: establishing contact with the axon that is to be remyelinated, activating myelin genes and generating a myelin membrane, and finally wrapping and compacting the membrane to form the sheath (Franklin and Ffrench-Constant, 2008). The remyelination is found to be incomplete or fail in inherited and acquired neurological diseases such as leukodystrophies and devastating multiple sclerosis (MS) (Mar and Noetzel, 2010; Trapp et al., 1998). Despite the presence of oligodendrocyte precursor cells (OPCs), myelination fails to proceed in demyelinating lesions in MS patients (Chang et al., 2002). At present, the factors that promote the initiation of OPC differentiation and overcome the block for successful remyelination in demyelinating diseases are poorly defined.

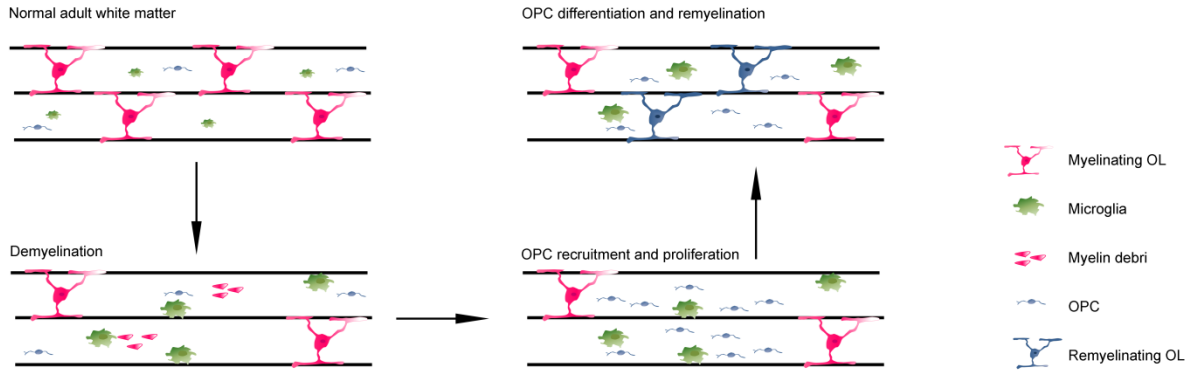

Figure 1-2 The phases of remyelination. Following acute demyelination, local OPCs are activated and recruited to lesion sites. Once recruited, OPCs then engage demyelinated

axons as they begin the differentiation phase. (Adapted from (Franklin and Ffrench-Constant, 2008))

Transcriptional Regulation of Oligodendrocyte Specification and Differentiation

These highly dynamic processes of OL lineage progression, which occur on an ongoing basis during both development and in adulthood, are coordinated and fine-tuned by equally dynamic changes in the expression and activity of transcription factors. Here I will summarize some of the major transcriptional programs and key molecules that mediate development of the OL lineage and myelination in the CNS (Figure 1-3).

bHLH Factors Olig1/2 Olig genes are identified as the earliest markers of oligodendrocyte progenitors (Lu et al., 2000; Zhou et al., 2000) and both Olig1 and Olig2 are required for oligodendrogenesis throughout the CNS (Zhou and Anderson, 2002). Olig2 is essential for the generation of early ventrally derived OPC and their differentiation (Lu et al., 2002). Genome-wide binding studies (ChIP-Seq) found that Olig2 targets specific enhancers that regulate oligodendrocyte-lineage progression in a stage-specific manner (Yu et al., 2013b). Although Olig1 is expressed from early in the lineage, it does not appear to be vital for OPC generation. Olig1-null mutants exhibit a defect in terminal differentiation and maturation of OPCs (Dai et al., 2015; Xin et al., 2005). Consistent with the observed delay or loss of mature markers in Olig1 null mice, Olig1 promotes transcription from the MBP promoter in luciferase assays (Li et al., 2007a; Xin et al., 2005), implicating MBP as a direct target gene.

SoxE Factors Sox9/10 Specification of OPCs requires the Sox9/Sox10 transcription factor, whereas terminal differentiation depends on the closely related Sox10. In the absence of Sox10, OL terminal differentiation is disrupted but OPCs developed normally (Stolt et al., 2002). However, deletion of both Sox10 and Sox9 within the OL lineage results in a marked reduction in the density of Olig2-positive OPCs, suggesting that Sox9/10 have partially redundant but critical roles in OPCs (Finzsch et al., 2008). Sox10 interacts with cell type-specific transcription factors at some loci to induce myelin gene expression, and it occupies active enhancers of genes critical for myelination (Lopez-Anido et al., 2015; Zhao et al., 2016).

SoxD Factors Sox5/6 Sox5 and Sox6 are expressed in neural progenitor cells and OPCs, and downregulated during differentiation (Stolt et al., 2006). Sox5 and Sox6 act to antagonize Sox10's prodifferentiation role and ablation of Sox5 and Sox6 genes in the OL lineage results in precocious expression of mature markers (Stolt et al., 2006), highlighting their role in limiting OL differentiation *in vivo*.

BMP Effectors Id2/4 Id2 and Id4 are downstream from the BMPs (Samanta and Kessler, 2004) and translocated from nucleus to cytoplasm as OPC differentiate (Wang et al., 2001). Overexpression of Id2 inhibits OPC differentiation, whereas absence of Id2 induces premature oligodendrocyte differentiation *in vitro* (Wang et al., 2001), suggesting that Id2 is a component of the intracellular mechanism that times oligodendrocyte differentiation. Id2/4 can complex with the bHLH proteins Olig1 and Olig2 and may prevent Olig1 and Olig2 from

entering the nucleus and inhibit the expression of target genes such as myelination-related genes (Samanta and Kessler, 2004).

Notch Effectors Hes1/Hes5 Hes1 and Hes5 function as the transcription effectors of Notch and negatively regulates OPC differentiation. Similar to Id2/4, Hes5 null mice display accelerated expression of myelin genes, and forced expression of Hes5 in cultured OPCs blocks their differentiation into OLs (Liu et al., 2006). Mechanistically, Hes5 interacts with and competes with the transcriptional activator Sox10, directly preventing and sequestrating its activity at myelin promoters (Liu et al., 2006).

Myelin Regulatory Factor Myrf/Gm98 Myrf is strongly induced during the early stages of OL differentiation and persists in myelinating oligodendrocytes. Myrf is necessary and sufficient to promote OL maturation and myelination. Mice lacking Myrf display a complete failure of OL terminal differentiation and subsequent myelination, and cannot survive due to severe neurological abnormalities (Emery et al., 2009). Myrf is also required for the maintenance of the myelin; conditional ablation of the gene in myelinating OLs in the adult CNS results in a degeneration of the myelin sheaths (Koenning et al., 2012). Genome-wide binding studies (ChIP-Seq) reveal that Myrf directly targets a wide range of genes underpinning the morphological development and myelination by OLs (Bujalka et al., 2013).

Sip1/Zeb2 Sip1 was initially identified as a direct transcriptional target of Olig2 and a downstream of Olig1 (Weng et al., 2012). Sip1 ablation in oligodendrocyte lineage cells resulted in a severe failure of myelin sheath formation without affecting OPC proliferation, indicating that Sip1 is required for the transition of OPCs to myelinating oligodendrocytes

(Weng et al., 2012). At least part of Sip1's function is likely to be through antagonism of BMP-Smad regulatory pathway as well as induction of the Smad7, a negative-feedback regulator of the BMP signaling complexes (Weng et al., 2012).

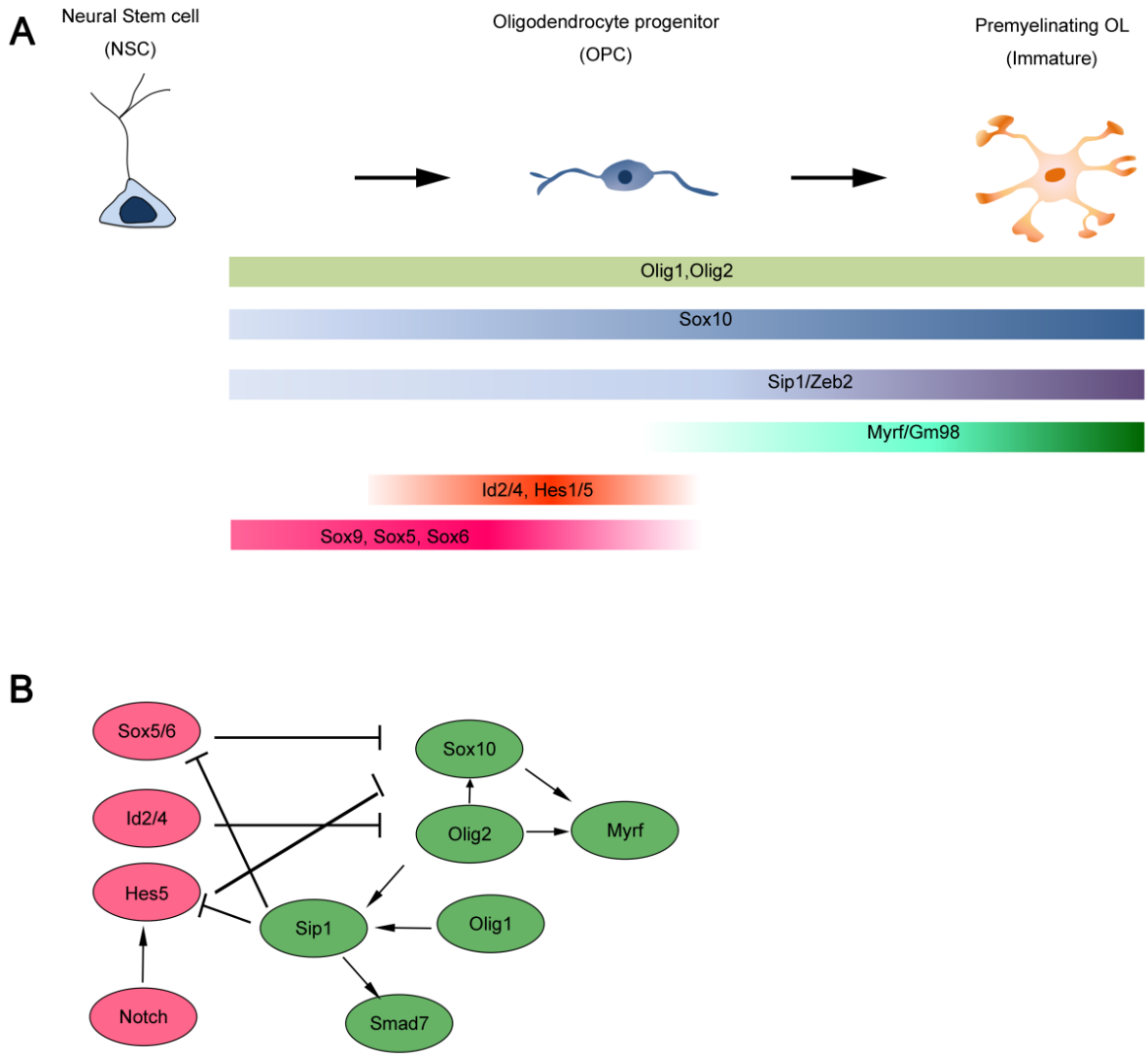

Figure 1-3 Transcriptional regulation of oligodendrocyte specification and differentiation (A) Expression levels of relevant transcription factors in NSCs, OPCs and

premyelinating OLs. (B) The balance between proliferation/maintenance and terminal differentiation is maintained by anti- and prodifferentiation factors. Red circles represent anti-differentiation factors and green circles represent pro-differentiation factors. (Adapted from (Emery and Lu, 2015))

Epigenetic Regulation of Oligodendrocyte Specification and Differentiation

The transcriptional program of OL differentiation and myelination is highly influenced and reliant on a parallel process of epigenetic regulation, which plays a fundamental role in governing the accessibility of transcriptional machinery to DNA sequences and comprises DNA methylation, histone modifications, ATP-dependent chromatin remodeling, a network of noncoding RNAs (e.g., microRNAs and lncRNAs) (Figure 1-4).

HDACs Histone deacetylases (HDACs) are a class of chromatin modifying enzymes that remove acetyl groups from lysine residues on a histone, allowing chromatin compaction and gene silencing. HDACs can be subdivided into four classes based upon sequence/structural homology to yeast counterparts: class I (HDAC1–3, and 8), class II (HDAC4–7 and 9–10), NAD-dependent class III (SIRT1–7), and class IV (HDAC11) (Falkenberg and Johnstone, 2014). Pharmacological inhibition and siRNA-mediated silencing of HDAC1/2 impair OL differentiation *in vitro* and *in vivo* (Marin-Husstege et al., 2002; Shen et al., 2005). Ablation of HDAC1 and HDAC2, but not individual HDACs, blocks OL differentiation and myelination, suggesting functional redundancy of HDAC1 and HDAC2 in myelination (Ye et al., 2009). HDAC1/2 are often found together with multiprotein co-repressor complexes to inhibit expression of OPC differentiation inhibitors

(He et al., 2007; Ye et al., 2009). HDAC1 recruits YY1 to the promoter of OPC differentiation inhibitors such as Id2/4 and Hes5 and repress their expression. In addition, HDAC1 and HDAC2 can disrupt the β-catenin/TCF transcription complex, and thereby prevent expression of Wnt signaling target genes (Ye et al., 2009). Different from HDAC1/2, HDAC3 functions as a molecular switch for oligodendrocyte and astrocyte lineage determination. HDAC3 ablation in oligodendrocyte lineage cells results in a severe failure of myelination in CNS, with a significant increase of astrocytes and a concomitant loss of oligodendrocytes (Zhang et al., 2016). Genome-wide occupancy analysis reveals that Hdac3 interacts with p300 to activate oligodendroglial lineage-specific genes, while suppressing astroglial differentiation genes (Zhang et al., 2016). At present, the role of other HDACs in OL development remains to be defines. A class III HDAC (NAD+)-dependent deacetylase sirtuin 2 (SIRT2) is enriched in OLs and has been implanted in OL cytoskeleton remodeling and process arborization (Li et al., 2007b). Class IV HDAC11 is reported to regulate OL-specific gene expression and cell development in an oligodendroglial cell line (Liu et al., 2009).

HMTs HMTs (Histone methyltransferases) are histone-modifying enzymes that catalyze the transfer methyl groups to lysine and arginine residues of histone proteins. Enhancer of zeste homolog 2 (Ezh2) is a Polycomb group protein which deposits triple methyl groups on lysine residue K27 of histone H3 (H3K27me3). Overexpression of Ezh2 in differentiating NSCs resulted in an increase in oligodendrocytes and a reduction in astrocytes, whereas silencing of Ezh2 led to completely opposite effects (Sher et al., 2008).

In oligodendrocytes, Ezh2 directly targets and represses genes associated with neuronal and astrocytic lineage and suppression of Ezh2 activity in oligodendrocytes resulted in derangement of the oligodendrocytic phenotype and re-expression of neuronal and astrocytic genes (Sher et al., 2012). Recently genome-wide profiling of the repressive histone marks uncovers that H3K9me3 marks are increased during OL differentiation, at genes related to neuronal lineage and regulation of membrane excitability(Liu et al., 2015). Silencing H3K9 HMT impaired oligodendrocyte differentiation and functionally altered the response of oligodendrocytes to electrical stimulation (Liu et al., 2015).Those observations suggest a working model that initial loss of neurogenic ability from neural stem cells to OPC is likely established through repression of neuronal genes by the deposition of H3K27me3 marks by EZH2, which is active at the OPC stage whereas later changes related to decreased excitability of OPCs and differentiation into myelinating OLs are dependent on the deposition of repressive H3K9me3 mark (Liu et al., 2015).

ATP-dependent Chromatin remodeling enzymes In addition to histone modifications, accessibility of transcription factors to specific binding sites in differentiating oligodendrocytes can be achieved via displacement of nucleosomes by ATP dependent chromatin remodeling complexes. So far, Smarca4/Brg1 is the only chromatin remodeling enzyme defined in oligodendrocyte lineage progression. BRG1-dependent chromatin remodeling is required for the transition from OPCs to OLs but dispensable during the later stage of oligodendrocyte maturation (Bischof et al., 2015; Yu et al., 2013b). BRG1 chromatin

remodeler is prepatterned with OLIG2 to facilitate expression of oligodendrocyte lineage-specific genes (Yu et al., 2013b).

MicroRNAs miRNAs function mainly to inhibit the expression of anti-differentiation factors by forming an RNA-induced silencing complex with 3′ untranslated regions of target mRNAs and reducing the final output of target genes at the post-transcriptional level. miR-219 and miR-338 is highly enriched in differentiating OLs, and overexpression of miR-219 or miR-338 is sufficient to accelerate OPC differentiation in culture and promote precocious expression of OL lineage markers in the developing chick neural tube and mouse CNS (Zhao et al., 2010). miR-219 expression likely permits or promotes OL differentiation by suppressing of multiple differentiation brakes, such as PDGFRα, Hes5, Sox6, Zfp238 and FoxJ3 (Dugas et al., 2010; Zhao et al., 2010). miR23 restrains the expression of lamin B1, of which the overexpression causes severe myelin loss (Lin and Fu, 2009). Furthermore, miR-23a overexpression *in vivo* enhances both OL differentiation and myelin formation by modulating the PTEN/Akt/mTOR signaling axis (Lin et al., 2013). On the other hand, a series of miRNAs are required to maintain OPCs in an immature, proliferating state. OPC-enriched miRNAs, miR-214 and miR-199a-5p, prevent precocious differentiation by inhibiting expression of Mobp and C11Orf/Myrf in OPCs, respectively (Letzen et al., 2010). miR-17-92 clusters promotes OPC proliferation by influencing Akt signaling, and targeted inactivation of the miR-17–92 cluster in post-mitotic oligodendrocytes leads to a reduction in oligodendrocyte number *in vivo*(Budde et al., 2010). In aggregates, multiple miRNAs act

combinatorically to modulate the activities of transcription factors and signaling networks posttranscriptionally and thereby regulate OL fate specification and differentiation.

Long noncoding RNAs (lncRNAs) lncRNAs are emerging as important regulators of diverse biological processes. The expression and function of lncRNAs in CNS cell types have not begun until recently. *OLMALINC* is identified as a primate-specific lincRNA that is highly expressed in the white matter of the human frontal cortex and knockdown of OLMALINC in human oligodendrocyte cell lines upregulates inhibitors of OL differentiation (Mills et al., 2015). LncRNAs are also implicated in the differentiation of OPCs from NSCs. *Lnc-OPC*, an OPC-specific lncRNA, is essential for OPC cell fate determination (Dong et al., 2015).

DNA methylation DNA methylation is an important epigenetic regulatory mechanism during the nervous system development. DNA methyltransferases and ten-eleven translocation enzymes (TETs) are dynamically expressed in the oligodendrocyte lineage cells, suggesting that DNA methylation and hydroxymethylation are essential for oligodendrocyte differentiation (Zhang et al., 2014; Zhao et al., 2014). Indeed, TET1, TET2, and TET3 are necessary for oligodendrocyte differentiation *in vitro.* Genetic ablation of Dnmt1 in OPCs results in severe hypomyelination of the CNS associated with aberrant alternative splicing events and activation of an ER stress response, suggesting that DNA methylation acts as a regulator of the OPC state and subsequent transition into differentiating oligodendrocytes.

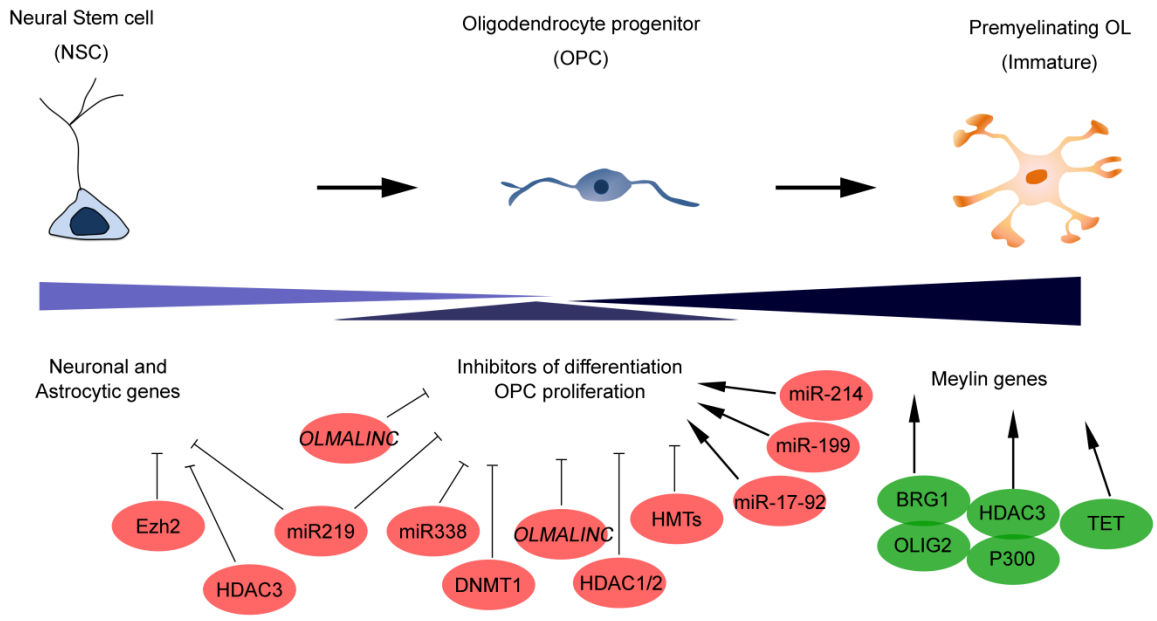

Figure 1-4 Epigenetic control of oligodendrocyte progenitor cell differentiation. The differentiation process includes three subsequent stages: repression of alternative lineage choice genes, suppression of genes inhibiting differentiation, followed by activation of myelin genes. (Adapted from (Liu et al., 2016).

As described above, despite the emerging studies designated to elucidate the regulatory circuits mediated by transcription factors and histone modifications during oligodendrocyte development, the roles of epigenetic regulators including ATP-dependent chromatin remodelers and lncRNAs remain largely unexplored. Next, I will give a general review on function of CHD chromatin remodelers and lncRNAs, and their roles in transcriptional regulation in development and disease.

CHD CHROMATIN REMODELERS IN DEVELOPMENT AND DISEASE

Chromatin Remodeling and Remodelers

In the eukaryotic nucleus, the genomes are condensed and organized into complex higher-order structures by packaging of chromosomal DNA into a compact nucleoprotein structure. The basic packaging unit of DNA is the nucleosome core, formed by wrapping naked DNA around a histone octamer. Such nucleosomal packaging occludes the regulatory DNA sequences and inhibits sequence specific recognition by most of the transcription factors. To overcome nucleosomal DNA accessibility problems and enable dynamic access to packaged DNA, cells have evolved a set of specialized chromatin remodeling complexes (remodelers). These modulators utilize energy derived from ATP hydrolysis to restructure, mobilize or eject nucleosomes, thereby freeing the DNA element and allowing the binding of sequence specific regulators (Clapier and Cairns, 2009).

The catalytic subunit of all ATP-dependent chromatin-remodeling complexes consists of a conserved ATPase domain with defined flanking domains. There are currently four different subfamilies of chromatin remodeling complexes; e.g., the SWI/SNF (switching defective/sucrose nonfermenting), CHD (chromodomain helicase DNA binding), ISWI (imitation switch) and INO80 (inositol requiring 80) family. Each of these subfamilies consists of several protein members that contain multiple different subunits. While all four subfamilies share a similar ATPase domain and utilize ATP hydrolysis to alter chromatin structure, they are also specialized for particular cellular processes and biological contexts,

modulated by unique domains residing in their catalytic ATPase domain and their unique associated subunits.

Chromodomain Helicase DNA-Binding (CHD) Family of Chromatin Remodelers

The CHD (Chromodomain-Helicase-DNA binding) family of ATP-dependent chromatin remodelers is characterized by two signature sequence motifs: tandem chromodomains in the N-terminal region, and the central SNF2-like ATPase domain located in the central region (Marfella and Imbalzano, 2007; Murawska and Brehm, 2011). The common chromodomain (chromatin organization modifier) is an evolutionarily conserved sequence motif that serves as a module to mediate chromatin interactions by binding directly to DNA, RNA, and methylated histone H3 (Smith and Peterson, 2005{de la Serna, 2006 #2335). The SNF2-like ATPase domain is found in many proteins involved in a myriad of cellular processes including chromatin assembly, transcription regulation, DNA repair, DNA replication, development and differentiation (Smith and Peterson, 2005; Tsukiyama, 2002; Woodage et al., 1997).

The CHD family is divided into three subfamilies according to the presence or absence of additional structural motifs (Figure 1-5) (Murawska and Brehm, 2011). The first subfamily contains CHD1 and CHD2, which has a C-terminal DNA-binding domain that preferentially binds to AT-rich DNA motifs (Figure 1-5) (Delmas et al., 1993; Marfella and Imbalzano, 2007; Stokes and Perry, 1995). The second subfamily includes CHD3 and CHD4 (also referred to as Mi-2α and Mi-2β, respectively). These proteins lack the DNA-binding

domain, yet, instead, they possess paired N-terminal PHD Zn-finger-like domains, which are involved in chromatin remodeling by the recognition and binding of methylated histone peptides (Eberharter et al., 2004; Ragvin et al., 2004). Subfamily III, which comprises CHD5 to CHD9, is defined by additional C-terminal motifs, like SANT or BRK domains. SANT (switching-defective protein 3, adaptor 2, nuclear receptor co-repressor, transcription factor IIIB) domains are demonstrated to interact primarily with unmodified histone tails and couple histone binding to enzyme catalysis (Aasland et al., 1996; Boyer et al., 2004).

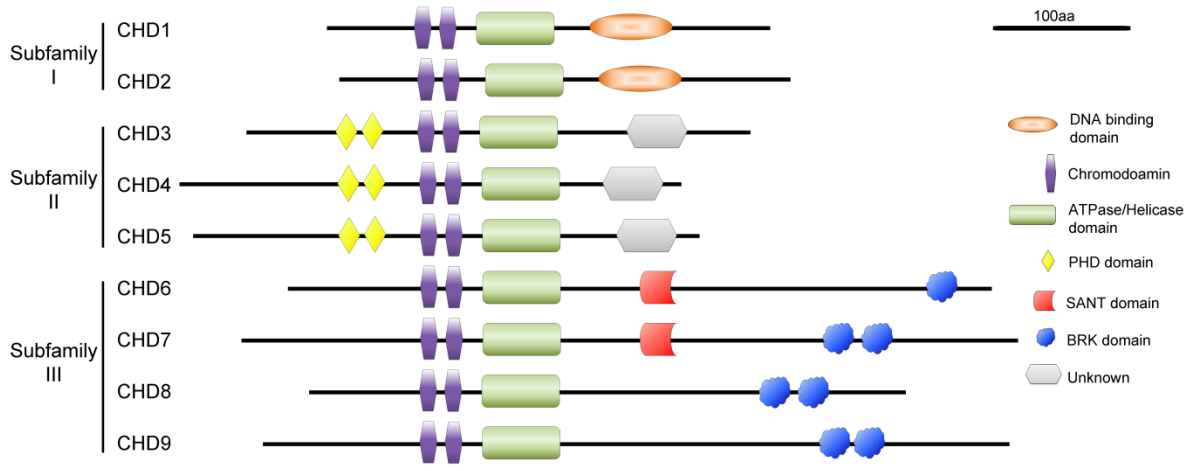

Figure 1-5 Schematic representation of structural domains of human CHD family of proteins. Subfamily I members (CHD1-2) are characterized by tandem chromodomains, a SNF2-like ATPase domain, and a DNA binding domain. Subfamily II members (CHD3-5) manifest additional paired PHD (Plant homeo domain) Zn-finger-like domains followed by the chromodomains. Subfamily III members (CHD6-9) are characterized by the presence of additional C-terminal SANT domain followed by two BRK domains.

In line with the functional structure domains present in CHD family, CHD remodelers can organize chromatin and eject nucleosomes, setting up a dynamic flux of assembly/disassembly, and thereby, influence transcriptional repression or activation. Different CHD remodelers are involved in multiple phases of the transcription cycle, including transcription initiation, transcription elongation, RNA processing and splicing, and transcription termination (Figure 1-6)(Murawska and Brehm, 2011).

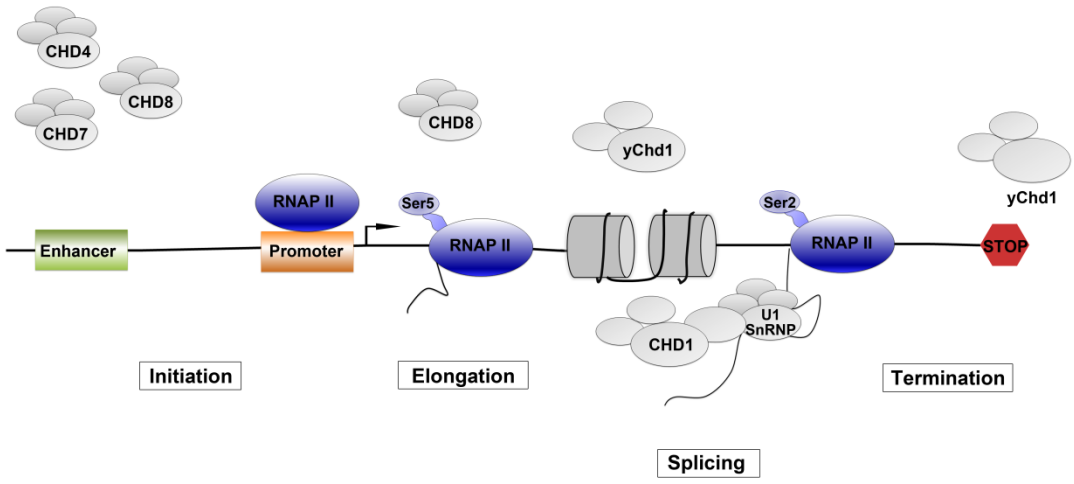

Figure 1-6 CHD remodelers at various steps of transcription cycle. Schematic representation of different CHD remodelers at various stages of transcription, including initiation, elongation, termination.

CHD remodelers, such as CHD1, have been reported to regulate nucleosome structure and density at promoters and, thereby, enable transcription initiation (Figure 2-2). Depletion of CHD1 (or its *Schizosaccharomyces pombe* orthologues Hrp1 and Hrp3) results in a genome wide increase in histone H3 density at promoters and a global loss of gene

transcription, suggesting that Chd1 is required to deplete nucleosomes, which in turn may stimulate transcription initiation (Walfridsson et al., 2007). Other CHD proteins appear to create nucleosome-depleted enhancers to facilitate the binding of transcription factors and the RNAP II machinery. CHD7 has been demonstrated to bind H3K4me1/2/3 peptides via its chromodomains and occupy DNase I hypersensitive sites enriched for H3K4me1, a hallmark of active enhancers. Similarly, CHD8 cooperates with AR in enhancer binding and loss of CHD8 abrogates AR binding and gene activation (Menon et al., 2010). Mi-2β (CHD4) has also been implicated in facilitating the recruitment of the transcription factor HEB and the histone acetyltransferase p300 to the CD4 enhancer element during T cell development (Menon et al., 2010).

Nucleosomes represent a barrier to transcription elongation. Nucleosomes ahead of elongating RNAP II are partially disassembled or displaced and then reassembled when RNAP II has passed through. CHD has been implicated in transcription elongation, likely through depositing new nucleosomes in the wake of elongating RNAP II at actively transcribed regions. In drosophila, all four CHD members colocalize with RNAPII to sites of active transcription on polytene chromosomes(Clapier and Cairns, 2009). Drospphila CHD1 (dCHD1) colocalizes with elongating RNAPII and has the capacity to assemble nucleosomes *in vitro*. Yeast studies provide strong support, as yChd1 physically interacts with elongation factors, including the FACT and PAF complexes, and associates with the transcribed body but not with promoters of active genes(Clapier and Cairns, 2009; Krogan et al., 2002; Simic et al., 2003).

CHD remodelers have also been involved in RNA splicing regulation. hCHD1 functionally associate with spliceosomal U2snRNP complex and depletion of CHD1 decreases splicing rate *in vitro* and *in vivo*(Sims et al., 2007). Similarly, dMi-2 might be involved directly in RNA processing and defective dMi-2 function compromised the splicing of the hsp83 transcripts in Drosophila larva.

CHD dysfunction in cancer and developmental disorders

Increasing evidence has linked genomic lesions such as mutations, deletions, translocations and copy number variations (CNVs), in CHD family members to human disease syndromes {Li, 2014 #2369}. Recent studies have revealed that a number of CHD proteins are potent tumor suppressors and their deficiencies contribute to development of a variety of cancers (Table 1-1). CHD5 was identified as a tumor suppressor gene mapping to human 1p36, a genomic region frequently deleted in a broad range of cancers including neural, epithelial and hematopoietic malignancies and functionally Chd5 controls proliferation, apoptosis, and senescence via the p19(Arf)/p53 pathway (Bagchi et al., 2007). Frameshift mutations of CHD7 and CHD8 frequently occur in cancers of the stomach and colon, indicating a tumor-suppressive role for Chd7 and Chd8 (Kim et al., 2011). Increasing evidence also supports for a role of CHD4 perturbation in serous tumors and other cancers. Somatic missense mutations in *CHD4* as well as copy number gain and loss of the region of human chromosome 12 that harbors CHD4 are found in serous carcinomas (Le Gallo et al., 2012; Zhao et al., 2013).

Similarly, genomic studies identified *CHD6* mutations in colorectal cancer and bladder cancer.

Table 1-1 Overview of the dysfunction of CHD proteins in human cancer.

Gene	Function	Abnormalities in Cancer	Cancer Types
CHD5	Tumor suppressor	Frequent deletions Compromised expression Promoter hypermethylation Mutation and/or deletion	neuroblastoma , glioma, breast cancer, lung cancer, ovarian cancer, gastric cancer, gallbladder carcinoma , colorectal cancer, hepatocellular carcinoma, melanoma, leukemia and laryngeal squamous cell carcinoma(Li and Mills, 2014)
CHD1	Tumor suppressor	Splice site mutations intragenic Breakpoints Focal deletions/mutations	prostate cancer(Huang et al., 2012)
CHD8	Tumor suppressor	Frameshift mutations Compromised expression	gastric cancer, colorectal cancer(Tahara et al., 2014)
CHD4		Copy number gain and loss of the region of human chromosome 12 that harbors *CHD4* Somatic (missense) mutations	serous endometrial tumor(Le Gallo et al., 2012), serous carcinoma(Zhao et al., 2013)
CHD6		Missense mutations gains of chromosomal region that encompasses *CHD6*	colorectal cancer(Ali Hassan et al., 2014), bladder cancer(Gui et al., 2011)
CHD7		Rearrangements (*PVT1-CHD7* fusion) Mutations	pancreatic cancer(Colbert et al., 2014) lung cancer(Pleasance et al., 2010) colorectal cancer(Tahara et al., 2014)

In addition to dysfunctions in cancers, CHD proteins play important roles in the development of multicellular organisms. Table 1-2 gives an overview of all human CHD family members and their possible or known functions in humans or other species as well as their existing mutant models. For instance, disruption in genes encoding CHD chromatin remodelers such as *CHD2*, *CHD7* and *CHD8* play important roles in the pathogenesis of autism spectrum disorders (Neale et al., 2012). Similarly, *CHD2* is identified as a risk gene for epileptic encephalopathy (Carvill et al., 2013), and CHD4-6 perturbation may contribute to intellectual disability and other neurological dysfunction (Kaminsky et al., 2011).

Table 1-2 Overview of the dysfunction of CHD proteins in developmental disorders.

Gene	Mutants phenotype
CHD1	Maintenance of mouse embryonic stem cell(Gaspar-Maia et al., 2009) Chd1-null embryos arrest at the peri-implantation stage in mice (E6.5) (Guzman-Ayala et al., 2015)
CHD2	Chd2-null mutants display growth delay and perinatal lethality, and Chd2 heterozygotes showed gross kidney abnormalities (Marfella et al., 2006)
CHD4	Chd4 null mutants display embryonic lethality before implantation with complete penetrance (O'Shaughnessy-Kirwan et al., 2015) Conditional null leads to Spleen and thymus hypoplasia(Williams et al., 2004) and hypomyelination in PNS (Hung et al., 2012)
CHD6	*Chd6* Exon 12 −/− mice lack coordination and are ataxic (Lathrop et al., 2010)
CHD5	Male Chd5 KO mice have deregulated spermatogenesis, characterized by immature sloughing of spermatids, spermiation failure, disorganization of the spermatogenic cycle and abnormal head morphology in elongating spermatids (Zhuang et al., 2014)

CHD7	Chd7 null mouse embryo dies at E10.5. Heterozygous mice shows head bobbing and circling, behavior due to inner ear defect, heart malformations, cleft palate, choanala atresia and genital anomalies (Bergman et al., 2010; Bosman et al., 2005) Chd7 is required for adult neurogenesis and control multipotent neural crest formation (Bajpai et al., 2010; Feng et al., 2013)
CHD8	Chd8 knockout mice show early embryonic lethality and growth retardation (Nishiyama et al., 2004). Chd8 haploinsufficiency results in autistic-like phenotypes in mice (Katayama et al., 2016).

CHD7 Mutation and CHARGE Syndrome

CHARGE syndrome is a multiple anomaly disorder named by its constellation of birth defects including ocular coloboma, congenital heart defects, choanal atresia, retardation of growth and development, genital hypoplasia and ear anomalies associated with deafness (Sanlaville and Verloes, 2007; Vissers et al., 2004). Additional symptoms including hyposmia, cleft lip/palate, and tracheoesophageal fistula are also reported, leading to a high variability in the clinical presentation of CHARGE syndrome patients (Zentner et al., 2010). The life expectancy of patients with CHARGE syndrome also varies widely, from five days to approximately 46 years (Zentner et al., 2010). 60-90% of the individuals diagnosed with CHARGE Syndrome have *de novo* heterozygous mutations in *CHD7*. The human CHD7 gene, located on chromosome 8q12.1, comprises 188kb of DNA and contains 38 exons. Human CHD7 proteins comprises 2997 amino acids and is highly evolutionary highly

conserved among species, with orthologs described in *Xenopus*, mouse, chicken, zebrafish, *C.elegans*, *Drosophila* and yeast (Robert P. Erickson 2004). Nonsense, deletion, missense and splicing site mutations have all been reported and presumably to result in *CHD7* haploinsufficiency. Human *CHD7* mutations are distributed throughout the coding sequence and no mutation hotspots have been observed (Sanlaville and Verloes, 2007).

Despite the major clinical features described above, CNS anomalies are also reported in CHARGE patients (Blake et al., 1998). Unilateral and bilateral hypoplasia of the olfactory bulb and/or arhinencephaly are most commonly reported in CHARGE (Asakura et al., 2008; Sanlaville et al., 2006) Other defects, including agenesis of the corpus callosum, cerebellar hypoplasia, delayed brain myelination, hydrocephaly, and atrophy of the cerebral cortex have also been reported (Jongmans et al., 2006).

CHD7 Mutant Mice: Models of Charge Syndrome

Several mouse models of CHARGE syndrome have been established to explore molecular basis for the diverse clinical manifestations of CHARGE syndrome. The first Chd7 mutant mice ($Chd7^{Whi/+}$) were identified by ethylnitrosourea (ENU) mutagenesis, and carry a heterozygous nonsense mutation in exon 11 (2918G→A leading to W973X). $Chd7^{Whi/+}$ mice were viable, with phenotypes that include head bobbing, circling behaviors, disrupted lateral semicircular canals, hyperactivity, reduced postnatal growth, variable cleft palate, choanal atresia, cardiac septal defects, hemorrhage, prenatal death, genital abnormalities, keratoconjunctivitis sicca (dry eye), and olfactory defects(Bosman et al., 2005).Heterozygous

loss of function $Chd7^{Gt/+}$ mice generated with gene-trap technology have phenotypic features similar to those generated by ENU mutagenesis (Hurd et al., 2007), further supporting for vestibular dysfunction as a consequence of Chd7 mutation. $Chd7^{Gt/+}$ mice also display severe inner ear defects**,** olfactory bulb hypoplasia, defective neural stem cell proliferation(Layman et al., 2009).Consistent with the neurological defects observed in $Chd7^{Gt/+}$ mice, conditional depletion of Chd7 in adult neural stem cells leads to a reduction of neuronal differentiation and aberrant dendritic development of newborn neurons. CHD7 stimulates the expression of Sox4 and Sox11 genes via remodeling their promoters to an open chromatin state (Feng et al., 2013). In addition, CHD7 also function as a transcriptional cofactor of the essential NSC regulator Sox2 to regulate genes that are mutated in human syndromes (Engelen et al., 2011). Despite the extensive studies of Chd7 function in the development of multiple organs that are affected in CHARGE Syndrome, mechanisms underlying the CNS phenotypes, especially CNS myelination, remain poorly understood.

LONG NON-CODING RNAS IN DEVELOPMENT AND DISEASE

A large portion (~75%) of the mammalian genome is transcriptionally active despite the fact that only a small fraction of them (< 2%) encodes proteins (Djebali et al., 2012). Both human and mouse genomes encode thousands of long noncoding RNAs (lncRNAs) , which are operationally defined as transcripts of greater than 200 nucleotides that function by means other than coding for proteins; lncRNAs are typically transcribed by RNA polymerase II and

are frequently spliced and polyadenylated (Rinn and Chang, 2012). In contrast to mRNAs, lncRNAs tend to be expressed at lower levels and are predominantly localized in the nucleus (Derrien et al., 2012).

lncRNAs in development

In recent years, lncRNAs have emerged as an important layer in the epigenetic and transcriptional regulatory circuits that control spatial and temporal gene expression. lncRNAs exhibit exquisite cell- and tissue-specific expression and thereby are capable to transduce higher-order spatial information. During epidermal differentiation, ANCR suppresses the differentiation pathway in the epidermis and maintain the stem cell compartment (Kretz et al., 2012), while a different lncRNA termed terminal differentiation-induced noncoding RNA (TINCR) promotes epidermal differentiation (Kretz et al., 2013). Similarly, multiple lncRNAs have also been implicated in the development of mesodermal tissues (Figure 1-7). One example is the heart-specific lncRNA *Braveheart*, which is a key factor involved in cardiac lineage commitment. Knockdown of *Braveheart* resulted in a severe reduction in the number of spontaneous beating cardiomyocytes formed during embryoid body differentiation (Klattenhoff et al., 2013) (Figure 1-7).

Transcription and alternative splicing of lncRNAs in the brain appear to be the most complex among all organs (Mercer et al., 2010). Notably, lncRNAs are widely expressed and exhibit precisely regulated expression patterns in mammalian nervous system. 40% (equivalent to 4,000–20,000 lncRNA genes) of annotated lncRNAs are expressed specifically

in the brain (Derrien et al., 2012). An early example of lncRNAs controlling neural cell fates involves the Evf2 lncRNA and the Dlx5/6 genomic locus (Bond et al., 2009). Evf2 is transcribed antisense to Dlx6, and controls GABAergic interneuron activity by regulating the cellular levels of the Dlx5 and Dlx6 transcription factors (Bond et al., 2009). Six3os and Dlx1os are identified as two adult SVZ-enriched lnRNAs (Ramos et al., 2013). Depletion of Six3os lncRNA leads to fewer Tuj1 and more OLIG2 positive cells, whereas depletion of Dlx1as specifically affected the number of Tuj1-positive cells (Figure 1-7) (Ramos et al., 2013). In addition, systematic loss-of-function studies have identified dozens of lncRNAs that are necessary for establishing pluripotency or driving neural lineage entry (Guttman et al., 2011). For example, TUNA, a highly conserved lncRNA in fish and human, is required for the maintenance of pluripotency. TUNA depletion in zebrafish led to altered neurodevelopment and impaired locomotor response (Lin et al., 2014).

Overall, lncRNAs exert critical functions in adult tissue stem cells and regulate cell-fate choice and stem/progenitor cell turnover.

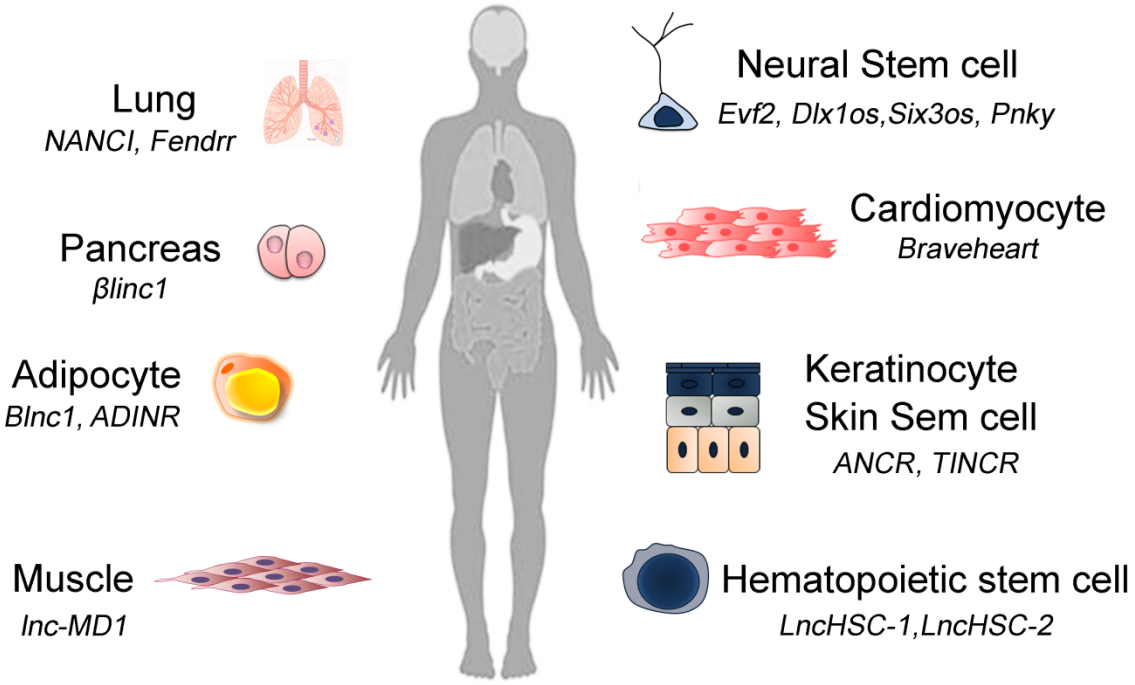

Figure 1-7 lncRNAs Control Differentiation and Self-Renewal. (Adapted from (Flynn and Chang, 2014)).

Mechanisms of lncRNA-Dependent Transcriptional Regulation

In general, transcriptional regulation by lncRNAs could work either *in cis*, within the same genomic locus, or *in trans*, affecting gene transcription in a different locus or even on different chromosomes. Extensive studies of lncRNA function have implicated lncRNAs as transcriptional regulators through both epigenetic regulations of chromatin structure and RNA-transcription factor interactions. Several mechanistic themes of lncRNAs function have emerged and are discussed below (Figure 1-8):

Scaffolds: lncRNAs can serve as adaptors to bring two or more proteins into discrete complexes (Spitale et al., 2011) (Figure 1-8). A prime example of lncRNA scaffolds involves HOTAIR, which can simultaneously bind both PRC2 and LSD–CoREST complex via specific domains of RNA structure (Tsai et al., 2010). Additional examples include the lncRNA *Rmrp*, the gene mutated in patients with cartilage-hair hypoplasia. *Rmrp* is involved in the assembly of DDX5-RORγt complex and mediated the regulation of RORγt transcription program in Th17 cells (Huang et al., 2015).

Decoys: lncRNAs can act as a "molecular sink" for RNA-binding proteins and thereby titrate away its protein target. For example, the lncRNA Gas5 (Growth arrest–specific 5) in involved in glucocorticoid resistance; Gas5 binds to the DNA-binding domain of the glucocorticoid receptor (GR) by acting as a decoy "glucocorticoid response element (GRE)", thus, competing with DNA GREs for binding to the GR (Kino et al., 2010).

Guides: many lncRNA can function as guides and are individually required for the proper localization or recruitment of transcription machinery or chromatin-modifying complexes. As an example, the lateral mesoderm-specific lncRNA *Fendrr* serves as a guide to localize PRC2 complex to the Pitx2 promoter; as a consequence, depletion of Fendrr in vivo led to a de-suppression of Pitx2 expression with an decreased occupancy of PRC2 at its promoter (Grote et al., 2013).

Chromatin Architecture: lncRNA also controls chromatin structure, including nucleosome positioning and chromosome looping. For example, multiple 17B-oestradiol (E2)-induced eRNA transcripts were found to interact with cohesin *in vitro* and to induce

looping interactions between their enhancer elements and the promoters of nearby target genes (Li et al., 2013). Another example involves a trans-regulatory lncRNA *Firre*. RNA-chromatin immunoprecipitation analyses indicate that *Firre* transcripts were localized across five distinct trans-chromosomal loci, which reside in spatial proximity to the *Firre* genomic locus and genetic deletion of the Firre locus resulted in loss of colocalization of these trans-chromosomal interacting loci, suggesting a model in which lncRNAs such as Firre can interface with and modulate nuclear architecture across chromosomes (Hacisuleyman et al., 2014).

mRNA processing: lncRNAs can act at various steps of mRNA processing and stability control. Several lncRNAs like MALAT1 can affect alternative splicing through interactions with splicing factors (Tripathi et al., 2010). Another classes of lncRNAs, natural antisense lncRNAs may affect the alternative splicing of their overlapping transcripts by virtue of masking splice sites through base complementarity. For example, Zeb2 antisense lncRNA overlaps with the 5′ splice site in the intron of Zeb2 and it therefore binds to Zeb2 pre-mRNA and prevents splicing of the Zeb2 5′-UTR (Beltran et al., 2008).

mRNA stability control: lncRNAs have also been implicated in both positive and negative regulation of mRNA stability. For instance, epidermal differentiation regulatory lncRNA TINCR is demonstrated to interact with the staufen1 (STAU1) protein and thereby mediate stabilization of differentiation mRNAs (Kretz et al., 2013).

miRNA sponges: lncRNAs also can act as decoys to attenuate miRNA-mediated regulation through sequestration of proteins or RNA-dependent effectors. Examples include

the muscle-specific lncRNA LINCMD1. LINCMD1 is shown to bind and sequester miR-133, thereby protecting protecting their target RNAs from repression (Cesana et al., 2011).

Over all, lncRNAs are demonstrated to regulate all aspects of gene expression, including transcription, processing and post-transcriptional control pathways. Despite the emerging evidence supporting the essential roles for lncRNAs in diverse developmental processes, complete biological inference of lncRNA function still remains a challenging task.

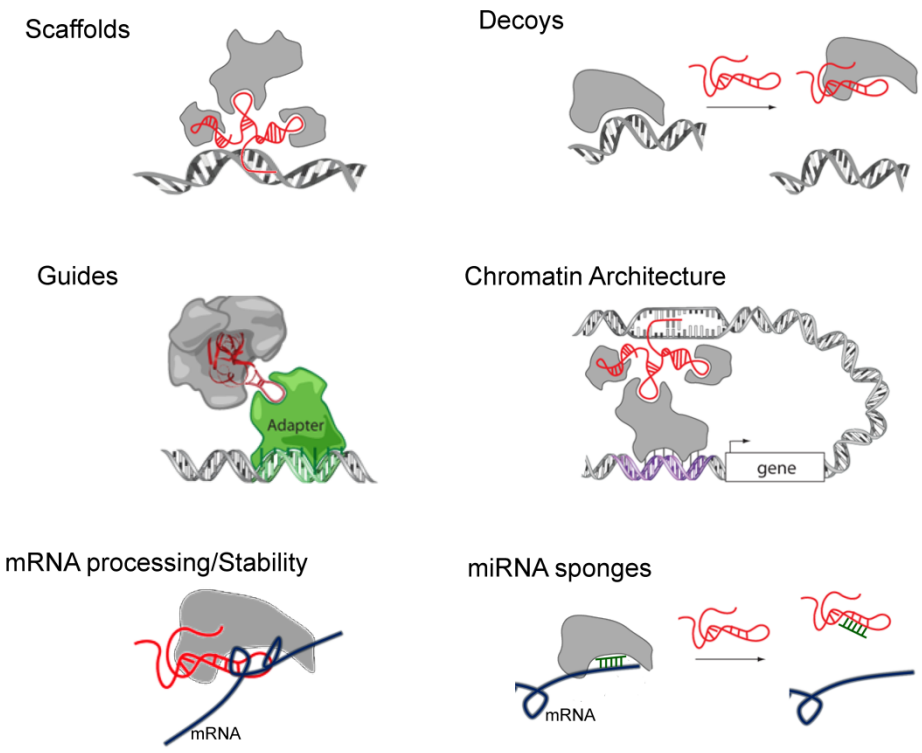

Figure 1-8 Models of lncRNA mechanisms of action. lncRNAs can function as scaffolds to bring two or more proteins into a complex, or as decoys that titrate away a protein target, or as guides to recruit proteins such as chromatin modifying enzymes or transcription machinery, or as mediators of chromosome looping and subdomain, or as regulators of

mRNA splicing and stability control, or as miRNA sponges. (Adapted from (Rinn and Chang, 2012)).

CHAPTER TWO

CHD7 IS REQUIRED FOR CNS MYELINATION AND REMYELINATION

INTRODUCTION

As introduced in Chapter 1, chromatin remodeling control is essential to orchestrate cell growth and differentiation, and to maintain proper cell identity (Ho and Crabtree, 2010; Luna-Zurita and Bruneau, 2013). Mutations in chromatin-modifying enzymes have been implicated in the pathogenesis of various human diseases, manifesting in growth/developmental defects, neurological disorders and tumorigenesis (Brookes and Shi, 2014; Jakovcevski and Akbarian, 2012). One class of chromatin-modifying enzymes, the chromodomain helicase DNA-binding (CHD) family of SNF2H-like ATP-dependent nucleosome remodeling enzymes, has emerged as an important regulator of multiple biological processes(Martin, 2010). Mutations in CHD7 are the major cause of human CHARGE syndrome (Coloboma of the eye, Heart defects, Atresia of the choanae, severe Retardation of growth/development, Genital abnormalities and Ear abnormalities), an autosomal dominant disorder characterized by a non-random association of multiple birth defects impairing normal development(Bergman et al., 2014; Martin, 2010). CHD7 modulates chromatin configurations to control cell-type specific transcriptional machinery, thereby controlling temporal and spatial gene expression 8–11 (Bajpai et al., 2010; Engelen et al., 2011; Schnetz et al., 2010). Most CHARGE patients exhibit some degree of intellectual disability, and many present with structural abnormalities of the corpus callosum

and cerebellar vermis(Martin, 2010; Yu et al., 2013a). Recent reports of white matter defects in the brain of patients with CHARGE syndrome (Gregory et al., 2013; Liu et al., 2014), suggest a possible role for CHD7 in myelination in the central nervous system (CNS).

Oligodendrocytes (OLs) produce myelin sheaths that electrically insulate axons and promote rapid propagation of action potentials in the CNS. Differentiation of OL precursor cells (OPCs) into mature OLs requires precise coordination between epigenetic programming and transcriptional regulation. Nuclear reorganization has been implicated in the temporal and spatial regulation of gene expression during oligodendrocyte differentiation process (Nielsen et al., 2002). Recently, the SWI/SNF chromatin-remodeling enzyme Smarca4 (Brg1) has been demonstrated to complex with a pioneer transcription factor Olig2 to target active enhancer elements to initiate the differentiation of OL lineage cells (Yu et al., 2013b).

Herein, we identify Chd7 as a downstream target of Brg1 and Olig2. We find that expression of Chd7 is highly enriched in OL lineage cells, with a peak of expression in differentiating OLs. Inactivation of Chd7 causes defects in OL differentiation and myelination while sparing OPC formation. We further show that Chd7 is required for OL remyelination after demyelinating injury. By genome-wide mapping of Chd7 targeting sites and co-immunoprecipitation, we demonstrate that Chd7 complexes with Sox10 and directly activates a distinct set of critical regulators for OL differentiation. Moreover, our studies identify the osteoblast-differentiation factor Osterix/Sp7 as an OL-specific Chd7 downstream target in the CNS, and demonstrate a critical requirement of Osterix for OL differentiation. Collectively, these data provide evidence that the chromatin remodeler Chd7 interacts with

Sox10 to bridge Brg1/Olig2 activity during OL differentiation and controls the onset of OL myelination and remyelination via directly activating myelinogenic programs.

RESULTS

OL-enriched Chd7 is a direct target of Brg1 and Olig2 complex

We have previously shown that Brg1 and Olig2 co-occupancy in the genome establishes a transcriptional program to initiate OPC differentiation (Yu et al., 2013b). We integrated transcriptome profiling of the spinal cord from Brg1cKO mutants ($Brg1^{flox/flox}$;$Olig1\text{-}Cre^{+/-}$) by gene-chip microarray (Yu et al., 2013b)and genome-wide Brg1/Olig2 occupancy at multiple phases of OL differentiation and identified Chd7 as a candidate target gene of Brg1/Olig2. Brg1 and Olig2 bound strongly at multiple sites both around the promoter region and within the *Chd7* gene locus, accompanied by the presence of an activated histone acetylation mark H3K27Ac in OPCs and early differentiating immature OLs (iOLs) (Figure 2-1A). Expression of Chd7 was substantially downregulated in Brg1cKO mice (Figure 2-1B). Consistently, the number Chd7-expressing cells appeared to be markedly reduced in the Brg1cKO spinal cord at postnatal day 14 (P14) (Figure 2-1C). These observations suggest that Chd7 is a downstream target of Brg1 and Olig2.

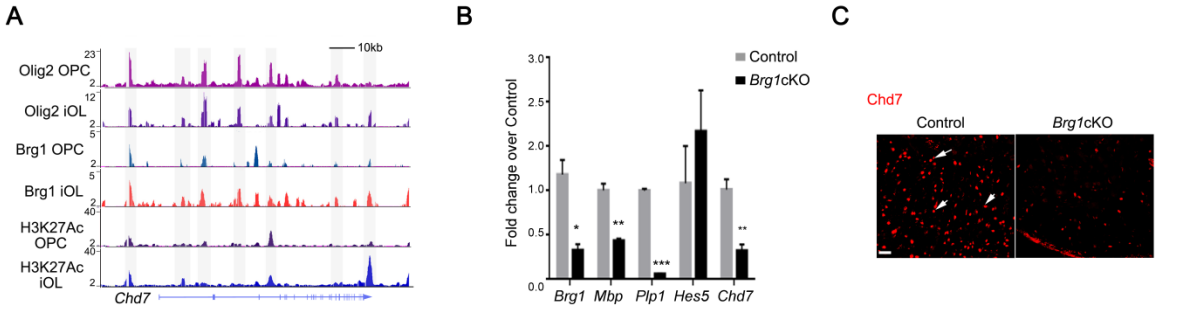

Figure 2-1 Identification of chromatin remodeler Chd7 as a direct target of the Brg1 and Olig2 complex (A) Track view of ChIP-Seq density profile for Olig2, Brg1 and H3K27Ac centered at the Chd7 locus in OPCs and OLs. (B) qRT-PCR analysis of myelination-associated genes and Chd7 in spinal cords from control and Brg1cKO animals at P14. The data are presented as mean ± s.e.m. (n = 3 mice; *P < 0.05, **P < 0.01 and ***P < 0.001; two-tailed unpaired Student's t test). (C) Immunostaining showing Chd7 expression in spinal cords of control ($Brg1^{loxP/+}$; $Olig1\text{-}Cre^{+/-}$) and Brg1cKO animals at P14. Arrows indicate Chd7+ cells. Scale bars represent 50 μm.

To further characterize Chd7-expressing cell types in the developing cortex, we co-immunostained Chd7 with cell type–specific markers, including Olig2 for the OL lineage, CC1 for OLs, glial fibrillary acidic protein (GFAP) and glutamine synthetase (GS) for astrocytes, and a pan-neuronal marker NeuN. Chd7 was detected in most Olig2-positive cells (Figure 2-2A). The majority of Chd7+ cells in the OL lineage were CC1+ differentiated OLs in the corpus callosum, optic nerve and spinal cord at P14 (Figure 2-2B-E). Intense Chd7 expression was detected in OLs, but at a lower level in PDGFRα+ OPCs (Figure 2-2F) in the P14 cortex. Similarly, in culture, Chd7 appeared to be more robustly expressed in MBP+ (myelin basic protein) mature OLs than in PDGFRα+ OPCs (Figure 2-2J), suggesting a potential role of Chd7 at the OL differentiation onset. In contrast, we did not observe Chd7 expression in GFAP+ or GS+ astrocytes in the corpus callosum (Figure 2-2G,H). In addition,

Chd7 was hardly detectable in NeuN+ neurons in the cortex at P24 (Figure 2-2I). These data reveal that Chd7 is highly enriched in differentiating OLs in the developing CNS.

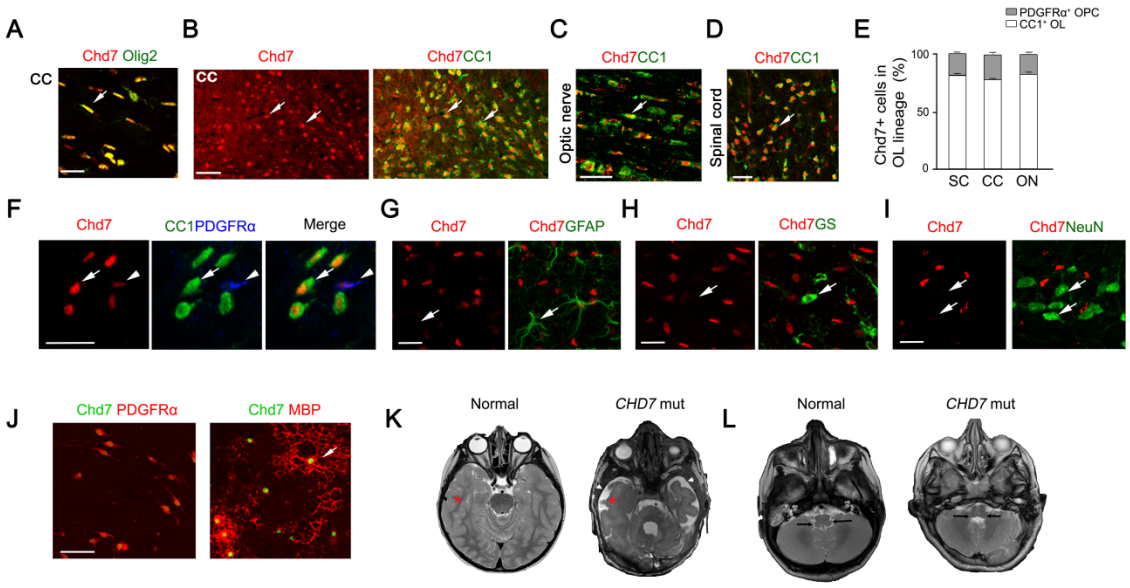

Figure 2-2 Chd7 is specifically enriched in oligodendrocytes. (A) Co-immunolabeling of Chd7 and Olig2 on the corpus callosum (CC) of wild-type brain at P7. Scale bar represents 20 μm. (B) Co-immunolabeling of Chd7 and CC1 in the CC of P14 mice. Arrows indicate co-labeled cells. Scale bar represents 50 μm. (C,D) Immunolabeling of Chd7 and CC1 on longitudinal sections of optic nerves (C) and coronal sections of the spinal white matter (D) at P14. Arrows indicate colabeled cells. Scale bars represent 25 μm (C) and 50 μm (D). (E) The percentage of CC1 or PDGFRα+ cells among total Chd7+ cells in the cortex (Ctx), spinal cord (SC) and optic nerve (ON) from P14 wild-type mice (n = 3 mice). The data are presented as mean ± s.e.m. (F) Immunostaining showing expression of CC1, PDGFRα and Chd7 in the cortical section of P14 mice. Arrows and arrowheads indicate CC1+ Chd7hi OLs and PDGFRα+ Chd7low OPCs, respectively. Scale bar represents 30 μm. (G-I) Immunostaining for Chd7 and GFAP (arrows in j) in the P24 cortex, glutamine synthetase (GS) (arrows in k) in the P7 cortex and NeuN (arrows in l) in the P24 cortex. Arrows indicate GFAP+ astrocyte. Scale bars represent 25 μm (G) and 20 μm (H,I). (J) Immunolabeling of Chd7 with PDGFRα in OPCs (left) or with MBP in OLs (right) in vitro. Scale bars represent 50 μm. (K-L) Representative T2-weighted MRI scans of cortices (K) and brainstem/cerebellar regions (L) in a control subject and a 3-year-old boy with CHARGE

syndrome carrying a CHD7 nonsense truncation mutation (7252C>T). In n, asterisks indicate the white matter, and arrowheads indicate cerebrospinal fluid–filled fluid space. Arrows in o indicate white matter structures in the brainstem and cerebellum region that are dysmorphic in the patient.

To explore the potential function of Chd7 in human CNS myelination, we examined the white matter of a cohort of 17 patients with CHARGE syndrome carrying CHD7 mutations. Magnetic resonance imaging (MRI) scans revealed severe cerebral white matter defects in 47% (8 of 17) of the CHARGE patients. Compared with the age-matched normal brain, the brains of these patients exhibited volumetric loss of cerebral white matter (Figure 2-2K) and dysmorphic features in the white matter regions of the brainstem and cerebellum (Figure 2-2L) that are commonly seen in patients with CHARGE syndrome (Gregory et al., 2013), indicating that white matter defects are a prominent feature of CHARGE syndrome with CHD7 mutations. These observations, together with Chd7 expression in the OL lineage, raise the possibility that CHD7 may be functionally required for CNS myelination in humans.

Chd7 is required for proper myelination in the CNS

To investigate the function of Chd7 in CNS myelination in vivo, we selectively ablated Chd7 in OL lineage cells by breeding the floxed Chd7 allele with mice carrying an OL-lineage expressing Olig1-Cre line (Fig. 2-3A). Chd7 expression was substantially reduced in the corpus callosum of the Chd7 conditional knockout mice ($Chd7^{loxP/loxP}$;$Olig1\text{-}Cre^{+/-}$, Chd7cKO) at P14, suggesting that the floxed Chd7 allele was effectively recombined in the Chd7cKO brain as compared with the control ($Chd7^{loxP/+}$;$Olig1\text{-}Cre^{+/-}$) (Figure 2-3B).

Chd7cKO animals were born at the expected Mendelian frequency and were of normal body size and weight. Similarly, expression of Mbp and Plp1 (proteolipid protein 1) mRNAs was visibly diminished in both the spinal cord and corpus callosum of Chd7cKO mice at neonatal and perinatal stages (Figure 2-3C,D). Similarly, the numbers of CC1+ OLs in Chd7cKO cortices were significantly decreased (Figure 2-3E,F). Consistently, cerebral white matter volume assessed by total MBP+ area in the corpus callosum was significantly reduced in developing Chd7cKO mice (Figure 2-3G,H). These observations suggest that Chd7 is required for the onset of OL differentiation in the CNS.

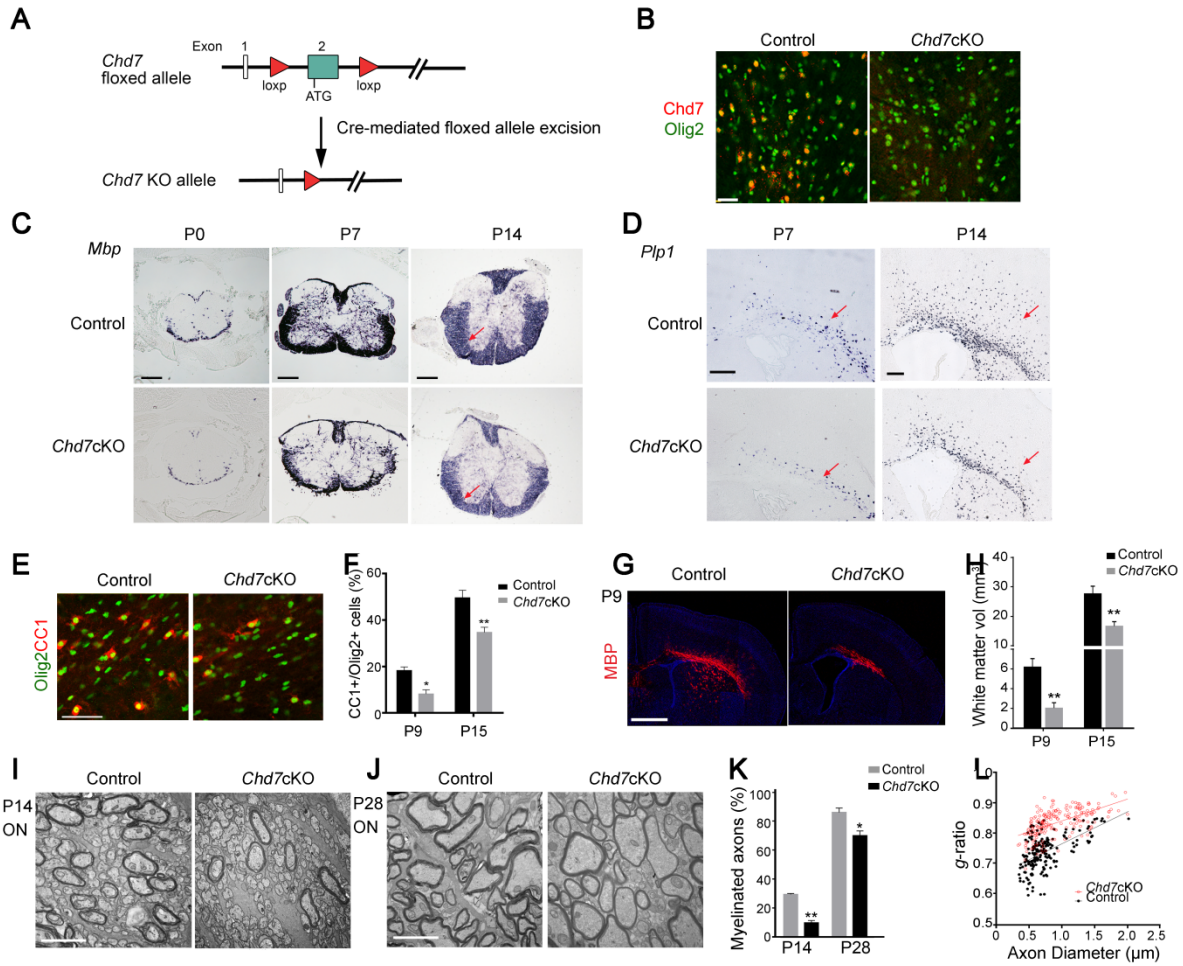

Figure 2-3 Chd7 is required for proper CNS myelination. (A) Diagram depicting Cre-mediated excision of the floxed Chd7 exon 2. (B) Immunolabeling of Chd7 and Olig2 in the corpus callosum of P14 brain from control and Chd7cKO mice. Scale bars represent 40 μm. (C) mRNA expression of *Mbp* in the spinal cord of control and Chd7cKO mice at P0, P7 and P14. Scale bars represent 100 μm. Arrows point to the spinal white matter region. (D) mRNA expression of *Plp* in P7 and P14 brain sections from control and Chd7cKO mice. Scale bars represent 100 μm. Arrows point to the white matter. (E) Immunostaining for CC1 and Olig2 in the corpus callosum from control and Chd7cKO mice at P7. Scale bars represent 100 μm. (F) Quantification of CC1+ OLs as a percentage of total Olig2+ cells in the corpus callosum of control and Chd7cKO at indicated ages. The data are presented as mean ± s.e.m. (P9, $n = 3$ control and 2 mutant mice; P15, $n = 4$ controls and 4 mutants; $^{*}P < 0.05$, $^{**}P < 0.01$ and $^{***}P < 0.001$.; two-tailed unpaired Student's t test). (G) Immunolabeling of MBP on coronal brain sections from control and Chd7cKO mice at P9. Nuclei were counterstained with 4,6-diamidino-2-phenylindole (DAPI; blue). Scale bars represent 1 mm. (H) Quantification of total cerebral white matter volume (MBP+) of control and Chd7cKO mice at P9 and P15. The data are presented as mean ± s.e.m. (P9, $n = 3$ control and 3 mutant mice, $^{*}P < 0.05$, $^{**}P < 0.01$ and $^{***}P < 0.001$.; two-tailed unpaired Student's t test). (I,J) Electron micrographs of transverse optic nerve sections from P14 (I) and P28 (J) control and Chd7cKO mice. Scale bars represent 4 μm. (k) Quantification of myelinated axons as a percentage of total axons. The data are presented as mean ± s.e.m. (P14, $n = 3$ control and 3 mutant mice, $P = 0.0017$, $t = 10.73$; P28, $n = 4$ controls and 4 mutants, $P = 0.0217$, $t = 3.656$; two-tailed unpaired Student's t test). (l) Quantification of myelin sheath thickness (*g*-ratio) in control and Chd7cKO optic nerves ($P < 0.0001$; control, g-ratio = 0.7227 ± 0.007414, $n = 196$ axons from 3 control optic nerves; Chd7cKO, *g*-ratio = 0.8325 ± 0.003235, $n = 202$ axons from 3 Chd7cKO optic nerves; two-tailed unpaired Student's t test).

Consistent with the reduction in mature OLs, ultrastructural analysis of optic nerves revealed compromised axonal ensheathment, with a markedly reduced number of myelinated axons in Chd7cKO animals at P14 (Figure 2-3J,K). At P28, the number of myelinating axons increased, but was still less than the control (Figure 2-3J,K). Notably, the thickness of myelin sheaths measured by g-ratio (the ratio between the diameter of the axon itself and the axon

plus its myelin sheath), was substantially thinner in Chd7cKO optic nerves than in controls (Figure 2-3J,L). Notably, this hypomyelination effect appeared to be transient, as the number of CC1+ OLs gradually increased during development and finally caught up in the spinal cord of adult mice (Figure 2-4A,B). By P60, the degree of myelination was essentially indistinguishable in the spinal cord between control and Chd7cKO mice (Figure 2-4C,D). Thus, these observations indicate that Chd7 loss causes a markedly delay in CNS myelination and that increased numbers of differentiated OLs may account for the myelination recovery in adult Chd7cKO animals.

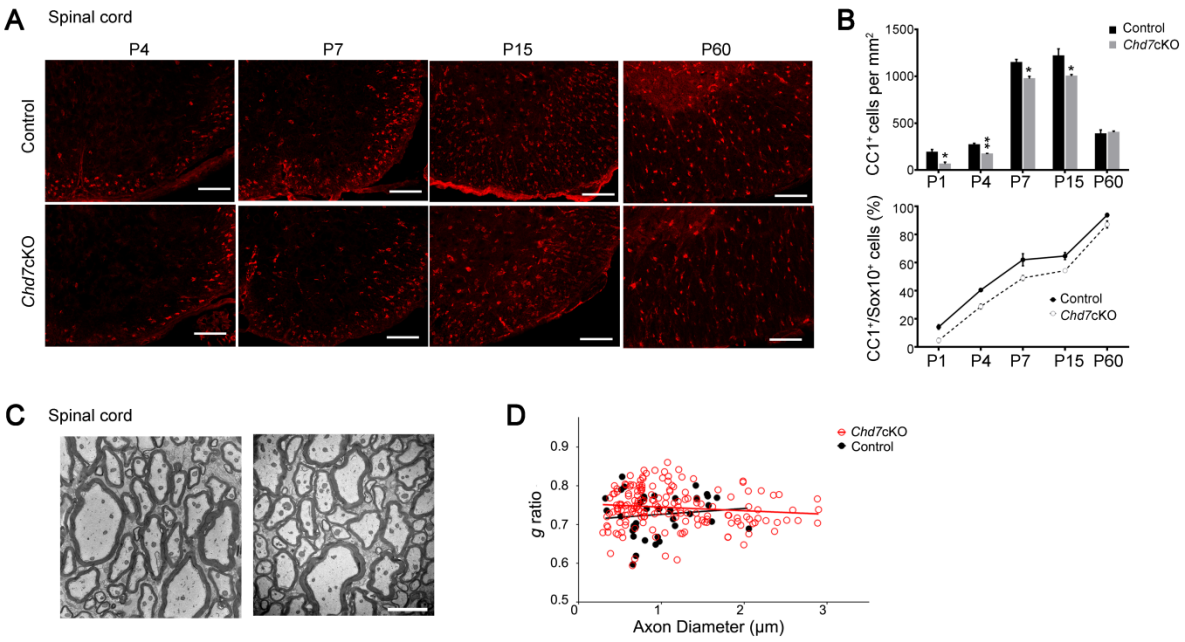

Figure 2-4 OL number and myelination is recovered in adult Chd7 mutant mice. (A) Immunolabeling of CC1 on transverse spinal cord sections from Chd7cKO and control mice at postnatal days 4, 7, 15 and 60. Scale bar, 100 μm. (B) Quantification of CC1+ cells density (top) and CC1+ cell proportion among total Sox10+ cells (bottom) in the white matter region of spinal cords from Chd7cKO and control mice at P1, P4, P7, P15 and P60 (mean ± SEM, n

= 3*$P < 0.05$, **$P < 0.01$ and ***$P < 0.001$; unpaired two-tailed Student's t test; bottom panels, F(1, 19) = 56.75; Two-way ANOVA test). (C) Representative electron microscopy images for P60 spinal cord of control and Chd7cKO mice. Scale bar, 2 μm. (D) Quantification of myelin thickness determined by g-ratio. n = 3 animals of each genotype. No statistical difference of g-ratio between control and mutants.

Chd7 regulates the transition from OPC to OL

Given the possibility that the dysmyelinating phenotype in Chd7cKO mice could be a result of a failure to generate OPCs, we assessed OPC development in the brain. Expression of the OPC marker PDGFRα was comparable between control and Chd7cKO cortices at P7 and P14 (Figure 2-5A). Quantification of PDGFRα+ cells at postnatal stages (P0, P7 and P21) indicated that deletion of Chd7 did not alter OPC formation (Figure 2-5B). Supporting this, we found similar OPC proliferation rates (percentage of Ki67+ proliferative OPCs; Figure 2-5C,D) and survival (absence of activated Caspase 3) between Chd7cKO and control mice. Collectively, our observations demonstrate that Chd7 deletion does not alter OPC generation and expansion.

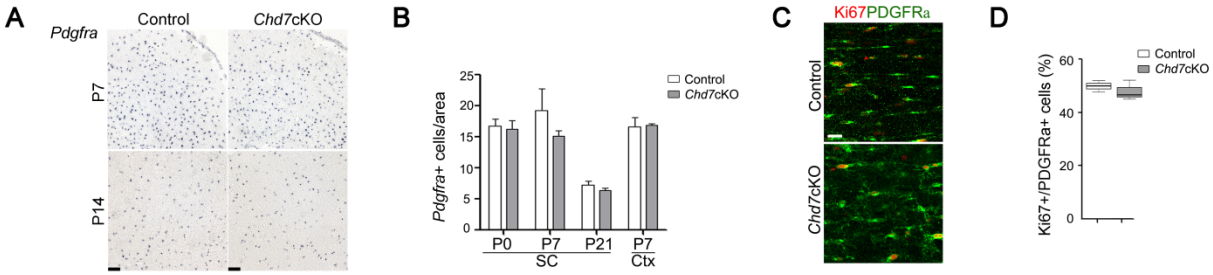

Figure 2-5 Chd7 deletion does not affect OPC development. (A) In situ hybridization for Pdgfrα on forebrain sections of control and Chd7cKO mice at P7 and P14, as indicated. Scale bars represent 100 μm. (B) Quantification of the number of Pdgfrα+ cells per area (0.04

mm2) in the cortex (Ctx) and spinal cord (SC) of control and Chd7cKO. The data are presented as mean ± s.e.m. (P0 SC, *n* = 4 control and 3 mutant mice,; P7 SC, *n* = 3 controls and 3 mutants,; P21 SC, *n* = 4 controls and 3 mutants; P7 Ctx, *n* = 3 controls and 3 mutants; two-tailed unpaired Student's t test). (C) Immunostaining for Ki67 and PDGFRα in the corpus callosum from P7 control and Chd7cKO mice. Scale bars represent 20 μm. (D) Quantification of Ki67+ cells as a percentage of PDGFRα+ OPCs in the corpus callosum of P7 control and Chd7cKO mice (*n* = 3 control and 3 mutant animals; Whiskers show the minimum and maximum, boxes extend from the first to the third quartiles with cross lines at the medians; two-tailed unpaired Student's t test).

To further determine whether defects in OL differentiation are a cell-autonomous effect of Chd7 ablation, we purified OPCs from the neonatal cortex of Chd7loxP/loxP pups, transduced them with adenoviral vectors expressing either eGFP as a control (Ade-GFP) or Cre-IRES-eGFP (Ade-Cre-GFP), and analyzed their ability to differentiate in vitro after withdrawal of the mitogens PDGFAA and NT3. Chd7$^{loxP/loxP}$ OPCs transduced with Ade-GFP or wild-type OPCs transduced with Ade-Cre-GFP were able to differentiate into mature MBP+ OLs. Chd7$^{loxP/loxP}$ cells transduced with Ade-Cre-GFP, however, essentially failed to differentiate into MBP+ OLs (Figure 2-6A,B), suggesting that Chd7-deleted OPCs are intrinsically defective in maturation.

To examine the effects of inactivation of Chd7 on OPC differentiation during postnatal development in a time-controlled manner, we generated OPC-inducible *Chd7* mutants by breeding Chd7$^{loxP/loxP}$ mice with *PDGFRα-CreERT* mice, which express OPC-specific tamoxifen-inducible Cre (Kang et al., 2010) and a *Rosa26tdTomato* reporter. Tamoxifen administration in *PDGFRα-CreERT*:*Chd7*$^{loxP/loxP}$ mutants (*Chd7*-iKO) pups at P3 induced effective recombination of both *Chd7* and *Rosa26* loci, with approximately 90% of

PDGFRα+ OPCs expressing tdTomato and not Chd7 after 11 d post-induction (Figure 2-6C). Loss of Chd7 in OPCs led to a marked (~76%) reduction in differentiating OLs (CC1high-expressing cells) in the cortical regions of *Chd7*-iKO mice compared with control littermates (*PDGFRα-CreERT*:*Chd7*$^{loxP/+}$) (Figure 2-6D,F). Similarly, expression of myelin oligodendrocyte glycoprotein (MOG) in mature OLs was reduced compared with robust expression in controls (Figure 2-6E,F). Collectively, these observations indicate that the primary role of Chd7 lies in the genesis of differentiated OLs from OPCs rather than OPC generation and expansion.

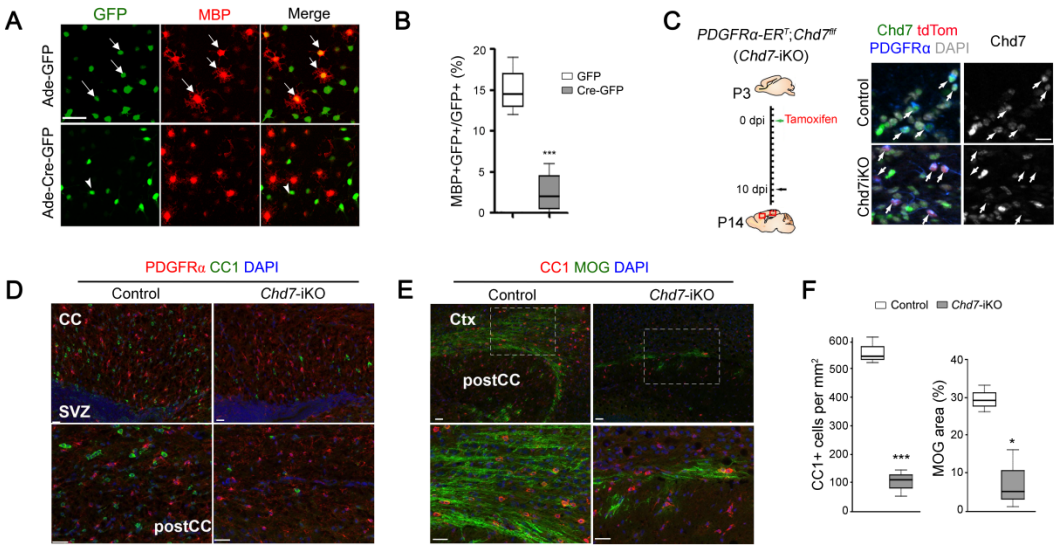

Figure 2-6 Chd7 deletion impairs OPC differentiation in a cell-autonomous manner. (A) Immunolabeling of MBP after 2 d of differentiation in Chd7$^{loxP/loxP}$ OPCs transduced with control GFP- or Cre-GFP–expressing adenoviruses. Arrows and arrowheads indicate the GFP or Cre-GFP virus transduced cells, respectively. Scale bars represent 50 μm. (B) Quantification of MBP+ OLs as a percentage of total GFP+ cells after 2 d of differentiation (n = 4 independent experiments, ***P < 0.001; Whiskers show the minimum and maximum, boxes extend from the first to the third quartiles with cross lines at the medians; two-tailed

unpaired Student's t test). (C) Left, diagram showing tamoxifen (TAM) administration to Chd7-iKO mice from P3 to P10 followed by tissue collection at P14. Right, immunolabeling for Chd7, PDGFRα and tdTomato on the corpus callosum of wild-type and Chd7-iKO;Rosa26Tom mice. Nuclei are counterstained with DAPI. Scale bars represent 20 μm. (D,E) Immunolabeling for CC1 and PDGFRα (D) or MOG (E) on sagittal corpus callosum (CC) sections of TAM-treated control and Chd7-iKO mice at P14. Ctx, Cortex; SVZ, subventricular zone. Scale bars represent 20 μm. Boxed areas in upper panels are shown at a high magnification in corresponding lower panels. (F) Quantification of CC1+ OL density (left) and percentage of MOG+ area (right) in the corpus callosum of TAM-treated control and Chd7-iKO mice at P14 (n = 3 controls and 3 Chd7-iKO animals; *$P < 0.05$, ***$P < 0.001$; Whiskers show the minimum and maximum, boxes extend from the first to the third quartiles with cross lines at the medians; two-tailed unpaired Student's t test).

Chd7 is critical for OL remyelination after demyelination

Given that myelination was normal in adult Chd7cKO animals, that is, the numbers of myelinated axons and myelin morphology were comparable between Chd7cKO and control mice (Figure 2-4); we assessed the function of Chd7 in the remyelination process following lysolecithin-induced demyelination. Local injection of lysolecithin in the white matter induces rapid myelin breakdown followed by myelin regeneration through an OPC recruitment phase at 7 d post-lesion (Dpl 7) and a remyelinating phase at Dpl 14 (Franklin, 2002). In normal adult spinal white matter, expression of Chd7 was hardly detectable; however, Chd7 was re-expressed following demyelination induced by lysolecithin beginning at Dpl 7 (Figure 2-7A) and the number of Chd7+ cells increased substantially at Dpl 14 in the lesion (Figure 2-7B). Chd7 was mainly expressed in Sox10+ OLs and was predominantly confined to CC1+ differentiating OLs at Dpl 14 (Figure 2-7C).

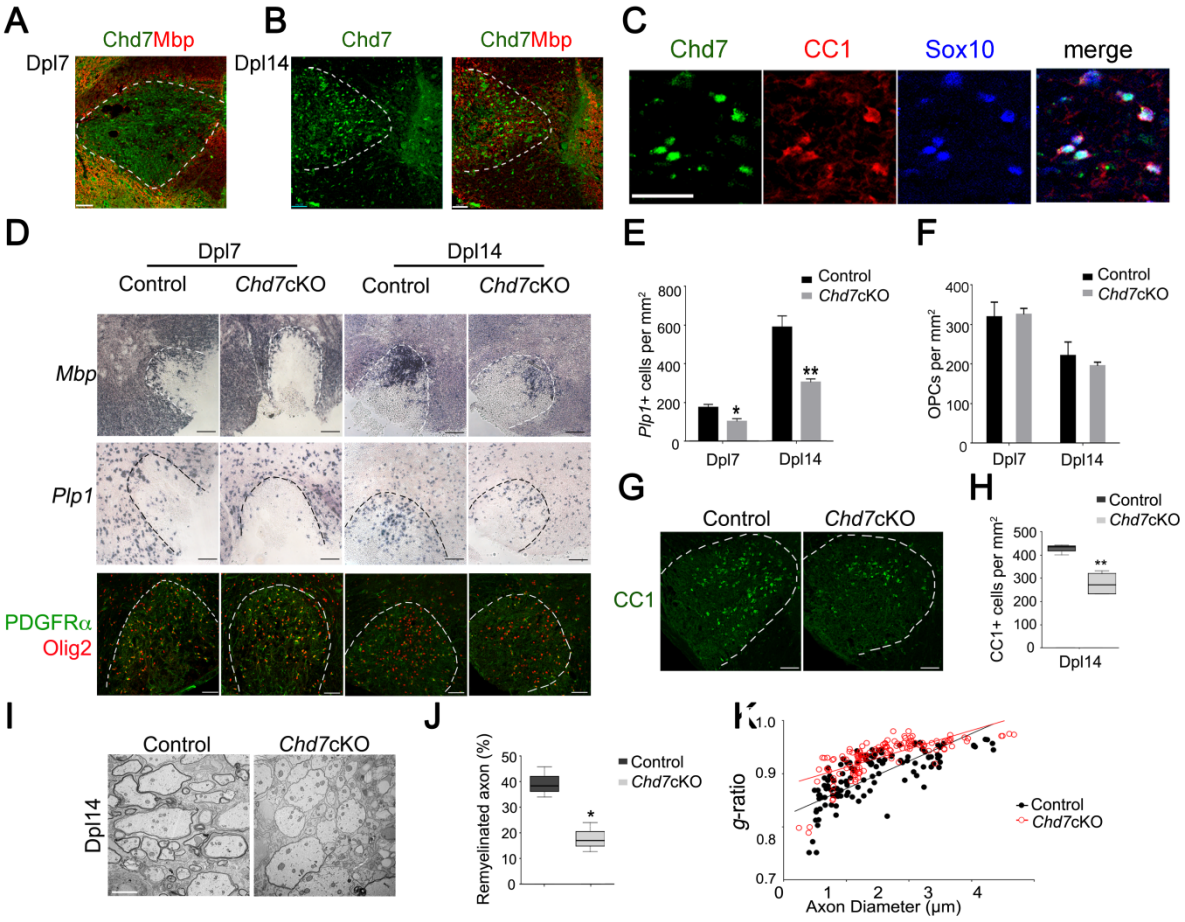

Figure 2-7 Chd7 is required for timely CNS remyelination. (A,B) Immunostaining showing Chd7 and MBP at Dpl 7 and 14 in spinal cord LPC lesions from 8-week-old mice. Scale bars represent 50 μm. (C) Immunostaining showing Chd7, CC1 and Sox10 at Dpl 14 in spinal cord LPC lesions. Scale bar represents 50 μm. (D) In situ hybridization for Mbp and Plp and immunolabeling for PDGFRα and Olig2 in spinal LPC lesions of control and Chd7cKO mutants at Dpl 7 and 14. Scale bars represent 100 μm. (E,F) Quantification of Plp1+ OLs and PDGFRα+ OPCs in LPC lesion sites at Dpl 7 and 14. The data are presented as mean ± s.e.m. (Plp1 at Dpl 7, $n = 4$ controls and 4 mutant animals, $^{*}P < 0.05$, $^{**}P < 0.01$ and $^{***}P < 0.001$; two-tailed unpaired Student's t test). (G) Immunostaining for CC1 in LPC lesions from control and Chd7cKO spinal cords at Dpl 14. Scale bars represent 100 μm. (H) Quantification of CC1+ OLs in LPC lesion sites at Dpl 14 ($n = 4$ controls and 4 mutant animals, $^{**}P < 0.01$; Whiskers show the minimum and maximum, boxes extend from the first to the third quartiles with cross lines at the medians; two-tailed unpaired Student's t test). (I) Electron microscopy images of LPC lesions from control and Chd7cKO spinal cords at Dpl 14. Scale bars represent 2 μm. (J) The percentage of remyelinated axons in LPC-

induced lesions of control and Chd7cKO spinal cords at Dpl 14 (n = 4 controls and 4 mutant animals, *P < 0.05; Whiskers show the minimum and maximum, boxes extend from the first to the third quartiles with cross lines at the medians; two-tailed unpaired Student's t test). (K) The myelin g-ratio in LPC-induced lesions of control and Chd7cKO mutants at Dpl 14 (control, g-ratio = 0.8943 ± 0.005128, n = 128 remyelinated axons from 4 control mice; Chd7cKO, g-ratio = 0.9330 ± 0.003088, n = 126 remyelinated axons from 4 mutant mice; P < 0.0001; two-tailed unpaired Student's t test).

To determine the potential role of Chd7 in OL regeneration, we examined the re-appearance of myelin genes and OLs in the lesion during remyelination in control and Chd7cKO mice. At Dpl 7 and Dpl 14, Mbp and Plp1 expression and the number of Plp1+ differentiating OLs (Figure 2-7D,E) were substantially reduced in Chd7cKO compared with control lesions. In addition, the number of CC1+ OLs in Chd7cKO mice during remyelination was markedly reduced (Figure 2-7G,H). In contrast, loss of Chd7 did not appear to impair the recruitment of PDGFRα+ OPCs (Figure 2-7 D) and the number of OPCs in the lesion was comparable between control and Chd7cKO mice (Figure 2-7 D,F). Notably, far fewer myelinated axons were detected in the lesions of Chd7cKO mice than in controls (Figure 2-7I). The percentage of myelinating axons and the thickness of newly generated myelin sheaths around axons assessed by g-ratios at Dpl 14 were substantially reduced in Chd7cKO mutants (Figure 2-7J,K). Similar results of reduction in OL regeneration were obtained for remyelination in the adult corpus callosum of Chd7cKO mice (Figure 2-8). Altogether, these observations indicate that Chd7 has a crucial role in OL remyelination in the context of white matter injury.

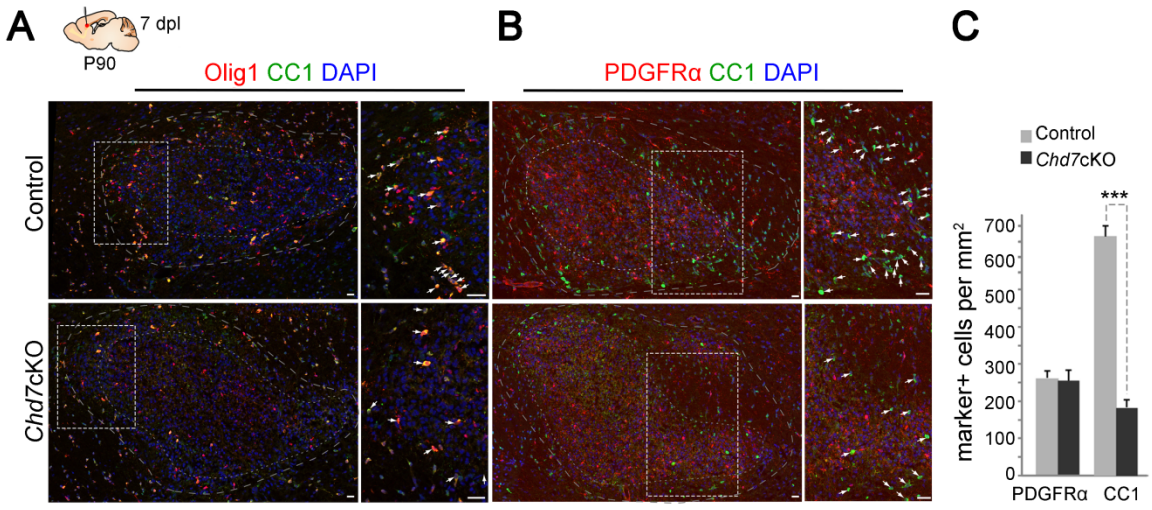

Figure 2-8 Chd7 is required for brain remyelination. (A,B) Immunofluorescence staining of representative lesions in the corpus callosum from adult (P90) LPC-injected Chd7cKO and control littermates at dpl 7 stained for CC1 (green) & Olig1 (A) or PDGFR ✔ (B) & CC1 (green). Right panels are higher magnification of boxed insets in left panels. Arrows indicate new OLs (CC1high/Olig1high cells) in the remyelinating area. Internal dotted line represents the border of lesion core (almost devoid of OLs) and external dotted line the remyelinating border area. Scale bar, 20 μm. (C) Quantification of PDGFRα+ cell (OPCs) and CC1 high-expressing cells (differentiating OLs) in LPC lesion sites at dpl 7 (mean ± SEM, $n = 3$; ***$P < 0.001$; n, number of animals; unpaired two-tailed Student's t test).

Chd7 regulates transcriptional programs for OL maturation

To investigate the underlying molecular mechanisms of dysmyelination in Chd7-deficient animals, we performed transcriptome profiling and analyzed global gene expression patterns in Chd7cKO and control spinal cords at P8. We identified genes altered in Chd7cKO pups that were either upregulated (n = 256) or downregulated (n = 545) relative to controls (fold change ≥ 1.5, P < 0.05; Figure 2-9A). Among those, a cohort of myelin structural genes and

critical myelination regulators, including *Myrf/Gm98* and *Sox10* (Emery et al., 2009; Finzsch et al., 2008), were downregulated in the Chd7cKO spinal cord (Figure 2-9A B), consistent with deficient myelin formation phenotype. Similarly, quantitative real-time PCR (qRT-PCR) analysis confirmed a marked reduction in myelination-promoting genes, such as *Myrf* and *Sox10*, and an increase in differentiation inhibitors, including *Id2/4* and *Hes1* (Figure 2-9C). Gene ontology (GO) analysis further revealed that the genes downregulated in Chd7-deficient mice are enriched for those that function in cytoskeletal organization and lipid metabolism in addition to myelination (Figure 2-9D). Congruent with physiological and morphological features of OLs *in vivo*, cytoskeleton and lipid metabolism pathways are highly active when OLs acquire complex morphology and assemble myelin sheaths around axons (Swiss et al., 2011). Consistently, analysis of the potential gene regulatory network revealed dysregulation in the genes involved in actin assembly and lipid homeostasis, and in OL lineage-enriched genes in Chd7 mutants (Figure 2-9E). Those alterations were further confirmed by qRT-PCR analysis of Chd7cKO spinal cords (Figure 2-9F,G). Together, these data suggest that Chd7 manages a gene regulatory network that controls OL differentiation and myelination.

Chd7 selectively targets enhancers of myeliogenic genes

RNA-seq analysis does not establish whether a given regulated transcript is a direct Chd7 target. To identify Chd7 direct target genes, we used chromatin-immunoprecipitation and sequencing (ChIP-Seq) to assess Chd7 genome-wide occupancy in maturing OLs (mOL), which were differentiated from OPCs after 3 d of triiodothyronine (T3) exposure. Chd7 peak

density was enriched within ±5-kb elements proximal to transcriptional start sites (Figure 2-10A,B). Chd7-occupied regions exhibited features of the active chromatin status, characterized by a bimodal distribution of H3K27Ac around Chd7 peaks and co-occupancy of Olig2 (Figure 2-10A,C,D), an OL transcription factor that has been shown to target functional enhancers. Notably, among Chd7 target genes that were differentially expressed following Chd7 deletion, the majority (~84%) was downregulated (Figure 2-10E,F), suggesting that Chd7 predominantly functions as a transcriptional activator for promoting the OL differentiation program.

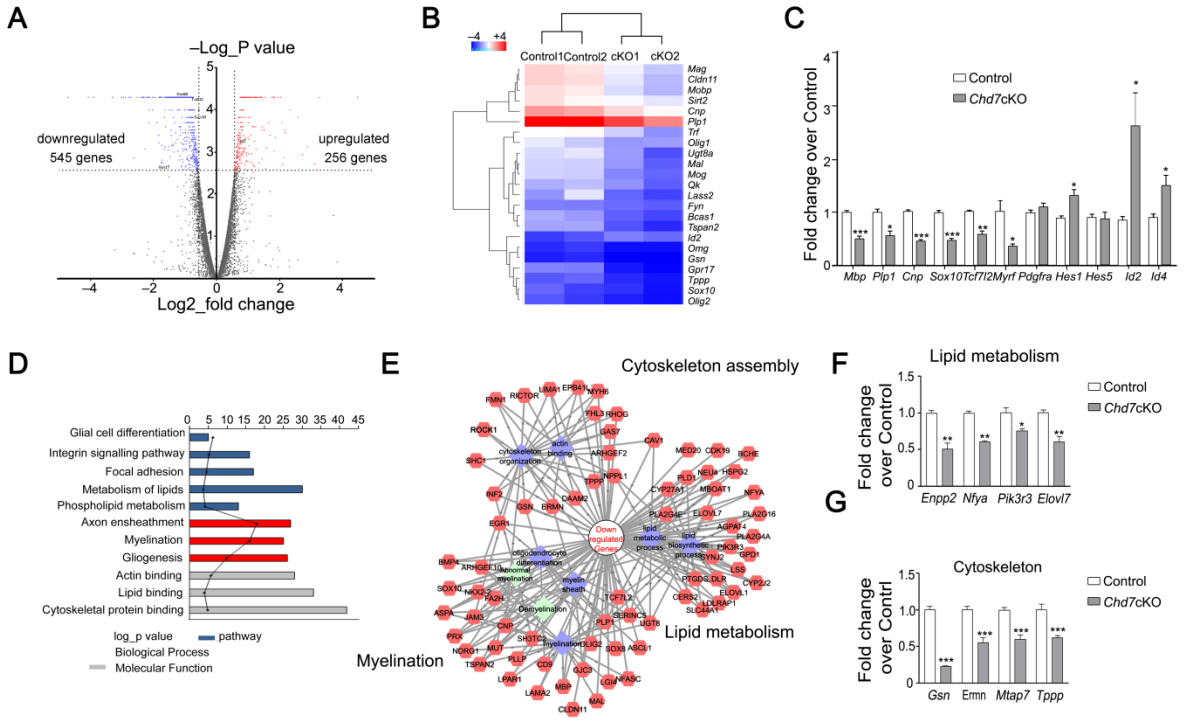

Figure 2-9 Chd7 controls the core myelinogenic regulatory network. (A) Volcano plots depict gene expression changes between control and Chd7cKO spinal cord at P8. Significantly differential transcripts were highlighted in color and totaled in each direction (false discovery rate < 0.05). (B) Heat map representing the expression of OL differentiation–related genes in control and Chd7cKO spinal cords from two independent

animals. (C) qRT-PCR analysis of myelination-associated genes in P8 control and Chd7cKO spinal cords. The data are presented as mean ± s.e.m. (n = 3 controls and 3 mutant tissues; *Mbp*, $*P < 0.05$, $**P < 0.01$ and $***P < 0.001$; two-tailed unpaired Student's t test). (D) The gene ontology (GO) analysis of the significantly downregulated genes between control and Chd7cKO. (E) Protein-protein interaction networks among downregulated genes in Chd7cKO are plotted using a ToppGene suite. (F,G) qRT-PCR validation of selected genes involved in lipid metabolism (F) and cytoskeleton organization in control versus Chd7cKO spinal cords at P8 (G). The data are presented as mean ± s.e.m. (n = 3 controls and 3 mutant tissues; $*P < 0.05$, $**P < 0.01$ and $***P < 0.001$; two-tailed unpaired Student's t test).

Gene ontology analyses revealed a strong association between Chd7-targeted loci with several regulatory arms of pathways and modules related to OL maturation (Figure 2-10G). Among Chd7-targeted genes were those encoding molecules involved in transcriptional control of myelinogenesis (*Sox10*, *Myrf*, *Olig1*, *Zfp191* and *Sip1/Zeb2*), lipid metabolism and cytoskeleton assembly, as well as key myelin components (*Mbp*, *Ugt8*, *Plp1* and *Cnp*; Figure 2-10H) When comparing Chd7 binding with those in embryonic stem cells (ESCs) (Schnetz et al., 2010) or neural stem cells (NSCs) (Engelen et al., 2011), the binding sites of Chd7 in OLs minimally overlapped with those in ESCs or in NSCs (Figure 2-10I), suggesting a unique role of Chd7 in OL differentiation. Accordingly, Chd7 target genes were generally expressed at relatively high levels in the OL lineage compared with other cell types (Figure 2-10J). This significant correlation between Chd7 occupancy and elevated myelination-associated gene expression further suggests that Chd7 selectively activates specific gene sets for OL differentiation. Collectively, our data suggest that that the chromatin remodeler Chd7 selectively target the distal enhancer elements of a subset of genes that are unique for oligodendrocyte differentiation.

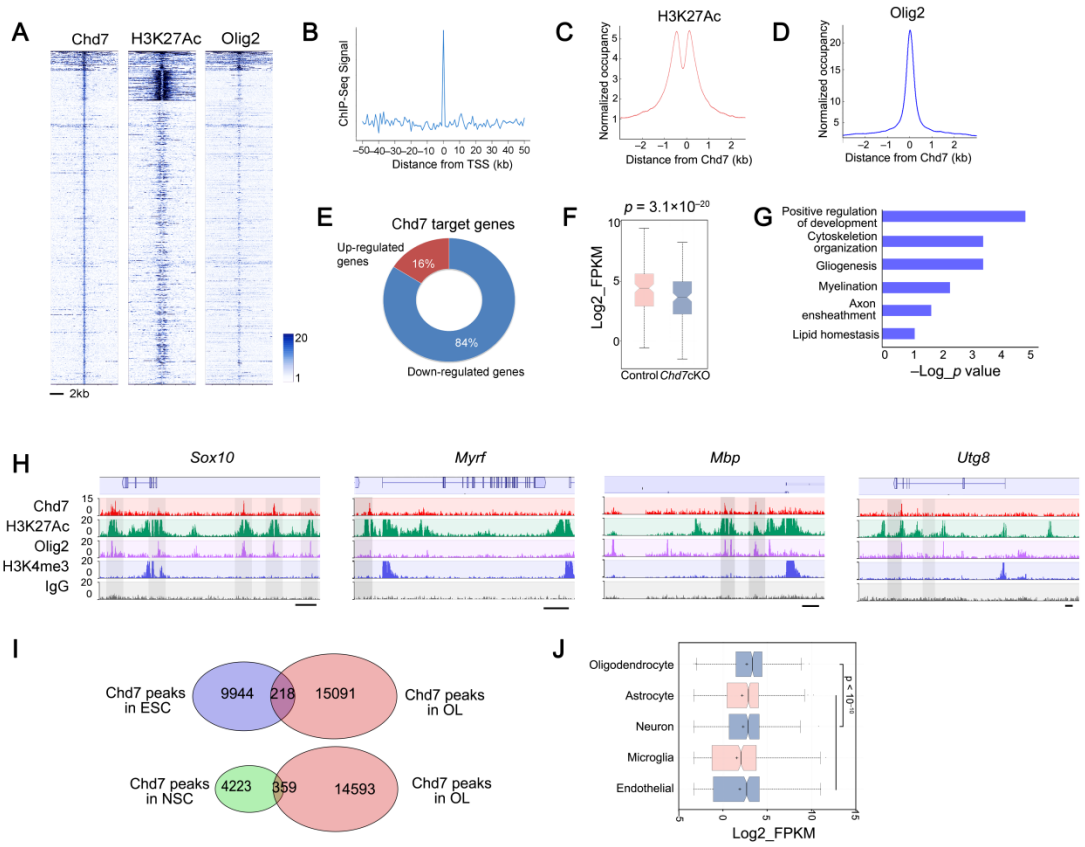

Figure 2-10 Chd7 Targets Lineage-Specific Regulators during OL Differentiation. (A) ChIP-seq density heat maps for Chd7, H3K27Ac and Olig2 within ±5 kb of the Chd7 peak center. (B) Histogram showing the distribution of ChIP-seq peaks relative to the transcriptional start site (TSS). (C,D) Average H3K27Ac and Olig2 ChIP-seq enrichment profiles around the central position of Chd7 binding regions. (E) Pie chart showing relative percentage of Chd7 target genes that were significantly upregulated or downregulated in Chd7cKO. (F) Box plots for mRNA levels of Chd7 targeted genes in control and Chd7cKO mutants. Whiskers show the minimum and maximum, boxes extend from the first to the third quartiles with notches at the medians (n = 144 genes with Chd7 occupancy within 5 kb of TSS; Mann-Whitney-Wilcoxon rank test). (G) Representative GO functional categories for Chd7 targeted genes. (H) ChIP-seq showing Chd7 enrichment at selected gene loci (Sox10, Myrf, Mbp and Ugt8). Tracks represent sequence tag enrichments for Chd7, H3K27Ac, Olig2, Brg1, H3K4me3 and IgG. Genome scale bars represent 5 kb. (I) Venn diagram showing minimal overlaps of Chd7 genome-occupancy in OLs and ESCs or NSCs,

respectively. (J) Box plot representing Chd7 target gene expression values in log2 FPKM in OLs, astrocytes, neurons, microglial and endothelial cells. Higher expression of Chd7 target genes were observed in OLs. Whiskers show minimum and maximum, box limits are first and third quartile and crosses show average. (n = 704, P < 10–10; n, number of genes with Chd7 occupancy within 5Kb from TSS; Mann–Whitney–Wilcoxon rank test).

Chd7 interacts with Sox10 to activate myelination program

As an ATP-dependent nucleosome-remodeling factor, Chd7 requires additional transcriptional cofactors to target and activate gene expression. To investigate whether any specific DNA sequence motifs were enriched at Chd7 binding sites, we used the *de novo* DNA motif–discovery program MEME(Bailey et al., 2006)to identify consensus-sequence motifs associated with Chd7 targeted sites. This analysis revealed that Chd7 binding sites with the consensus binding motif C(T/A)TTG(T/A)(T/A) for Sox10 (MEME motif score E = 5.7×10^{-97}; Figure 2-11A), a transcription factor required for terminal differentiation of the OL lineage(Lopez-Anido et al., 2015), were most overrepresented. To determine whether Chd7 and Sox10 colocalization result from a direct interaction between these two proteins or unrelated occupancy, we performed co-immunoprecipitation by expressing Sox10 and Chd7 in 293T cells or by pulling-down endogenous Sox10 using a Chd7 antibody in an oligodendroglial cell line, Oli-neu, under differentiating conditions (Schuster et al., 2002). We found that Chd7 formed a complex with Sox10 in the 293T cells transfected with Sox10 and Chd7 and differentiating Oli-neu cells (Figure 2-11B,C), suggesting that Chd7 and Sox10 targeting to these sites occurred through a physical complex of these proteins. To determine whether Sox10 and Chd7 co-occupied the same regulatory elements in mOLs, we then charted genome-wide occupancy of Sox10 in mOL using ChIP-seq. We found that

approximately 40% of Chd7 peaks overlapped with those of Sox10 in mOL (Figure 2-11D,E).

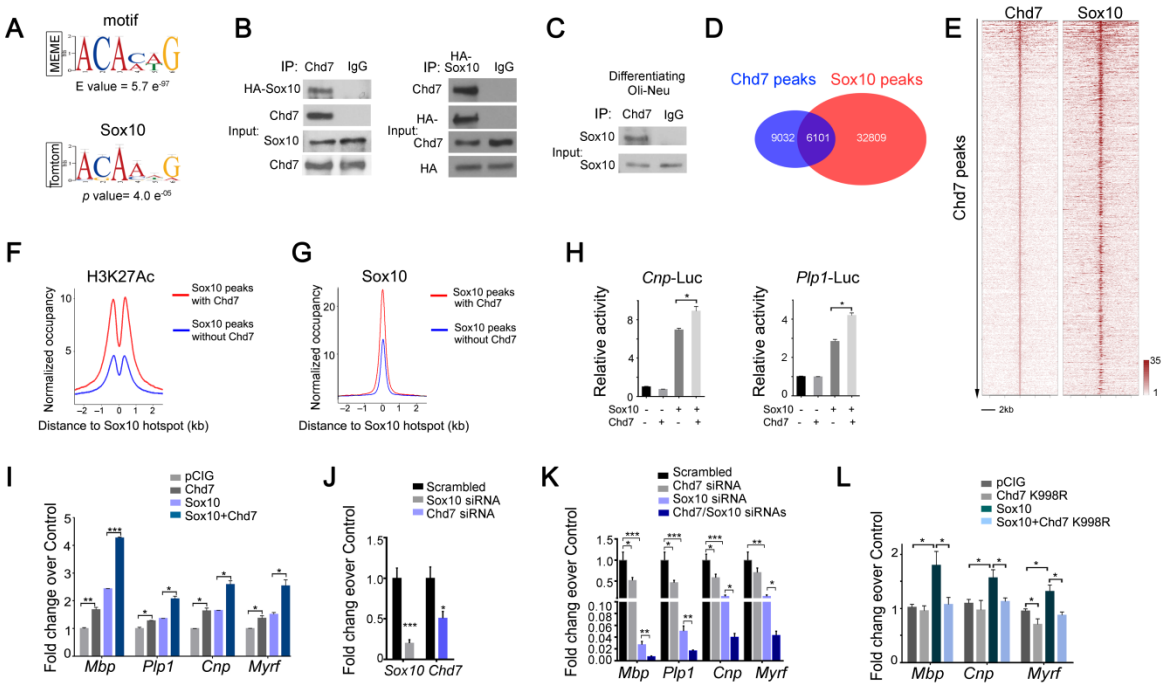

Figure 2-11 Chd7 interacts with Sox10 to activate myelination program. (A) MEME analysis of the most highly represented de novo motif in the Chd7 cistrome in OLs. Sox10 binding motif was identified as the most significant matching binding site. Letter size indicates nucleotide frequency (presented as bits) at each position (horizontal axis). (B,C) Co-immunoprecipitation of HA-Sox10 with Chd7 from transiently transfected 293T cells (B) or endogenous Sox10 with Chd7 in differentiating Oli-Neu cells (C). (D) Venn diagrams depicting overlap between Chd7 and Sox10 occupancy in OLs. (E) Heatmap of Sox10 and Chd7 signal at all Chd7-binding sites. 2 kb upstream and downstream of the anchor sites are plotted. (F,G) ChIP reads density plots for levels of H3K27Ac and Sox10 at loci targeted by Sox10 only and co-targeted by Sox10/Chd7. (H) Luciferase activity of *Cnp* (left) and *Plp1* (right) promoter–driven reporters in 293T cells co-transfected with Chd7, Sox10 or both. The data are presented as mean ± s.e.m. (*Cnp*-Luc, $n = 3$ independent experiments, $^*P < 0.05$; *Plp1*-Luc, $n = 4$ independent experiments, $^*P < 0.05$; pairwise comparison for Sox10 compared with Sox10 + Chd7). (I) qRT-PCR analyses of differentiating markers *Mbp*, *Plp1*, *Cnp* and *Myrf* in Oli-Neu cells transduced with Sox10, Chd7 or both under proliferation

condition. The data are presented as mean ± s.e.m. (n = 3 biological replicates; *P < 0.05, **P < 0.01 and ***P < 0.001; multiple comparisons with t test). (J) qPCR validation of knockdown efficiency of Sox10 and Chd7 in primary rat OPCs under differentiation conditions. The data are presented as mean ± s.e.m. n = 5 biological replicates; *P < 0.05, ***P < 0.001; two-tailed unpaired Student's t test. (K) qRT-PCR analyses of OL-differentiation associated genes following treatments with scrambled (n = 3), Sox10 (n = 5), Chd7 (n = 5), and both Sox10 and Chd7 siRNAs (n = 5), respectively. Data are presented as mean ± s.e.m. (n, numbers of biological replicates; *P < 0.05, **P < 0.01 and ***P < 0.001; multiple comparisons with t test). (L) qRT-PCR analyses of differentiated OL markers *Mbp*, *Cnp* and *Myrf* in Oli-Neu cells transduced with Sox10, Chd7 K998R mutant form or both under proliferation condition. The data are presented as mean ± s.e.m. (n = 4 independent experiments; *P < 0.05, **P < 0.01 and ***P < 0.001.

Intriguely, Chd7 and Sox10 co-occupied sites were highly enriched with the activating histone mark H3K27ac as compared with the Sox10 loci without Chd7 colocalization (Figure 2-11F). Moreover, Sox10 binding exhibited a preference for Chd7-occupied sites (Figure 2-11G), indicating that Chd7 occupancy defines enhancer elements, favoring Sox10 recruitment with a more accessible chromatin state associated with gene activation. Consistently, a combination of Chd7 and Sox10 overexpression enhances the activity of Cnp and Plp1 promoter reporters (Figure 2-11H) and promotes expression of OL differentiation genes to a greater degree than when they were expressed individually in Oli-neu cells (Figure 2-11I). Reduction of both Chd7 and Sox10 by siRNA-mediated knockdown caused much stronger inhibition in the expression of myelination-related genes than individual Chd7 or Sox10 downregulation during OPC differentiation (Figure 2-11J,K), raising the possibility of genetic interaction and cooperativity between Chd7 and Sox10 in the control of OL differentiation. Notably, Sox10-mediated activation of myelin-associated genes was inhibited by the presence of an ATPase-defective mutant variant of *Chd7*

(*Chd7*K998R)(Bajpai et al., 2010) (Figure 2-11L), suggesting an inhibitory effect of the *Chd7*^{K998R} mutant on Sox10 function. Together, these findings suggest that Chd7 and Sox10 have cooperative functions in activating the transcriptional program for OL differentiation.

Osterix and Creb3l2 are Chd7 targets for OL maturation

The observation that Chd7 transcriptionally activates an OL-specific gene network prompted us to search for Chd7-driven candidate genes that contribute to OL differentiation. By integrating Chd7 genome occupancy and transcriptome profiling, and considering genes downregulated in the *Chd7*cKO and occupied by Chd7 as candidate targets, we identified a cohort of potential transcriptional regulators that have yet to be characterized in OL development, including *Osterix* (*Sp7*), *Creb3l2*, *Zfp365*, *Zfp167* and *Sorbs3*. Notably, *Osterix* encodes a zinc finger–containing transcription factor that is essential for osteoblast differentiation and bone formation(Nakashima et al., 2002), and *Creb3l2* encodes cAMP-responsive element binding protein 3–like 2, a basic leucine zipper (bZIP) transcription factor, which is critical for chondrogenesis(Saito et al., 2009). We chose *Osterix* and *Creb3l2* for further characterization because malformations of the temporal bone are also a common feature in CHARGE syndrome (Amiel et al., 2001; Friedmann et al., 2012). Chd7 targets the proximal elements of both gene loci around transcription start sites marked by H3K4me3 as well as distal enhancer elements marked by H3K27Ac (Figure 2-12A). Expression of *Osterix* and *Creb3l2* was essentially diminished in the spinal cord of *Chd7*cKO animals (Figure 2-12B) while Chd7 overexpression induced *Osterix* and *Creb3l2* expression in OPCs under

both proliferation- and differentiation-promoting conditions (Figure 2-12C). Collectively, these data suggest that Chd7 directly activates *Osterix* and *Creb3l2* in the OL lineage.

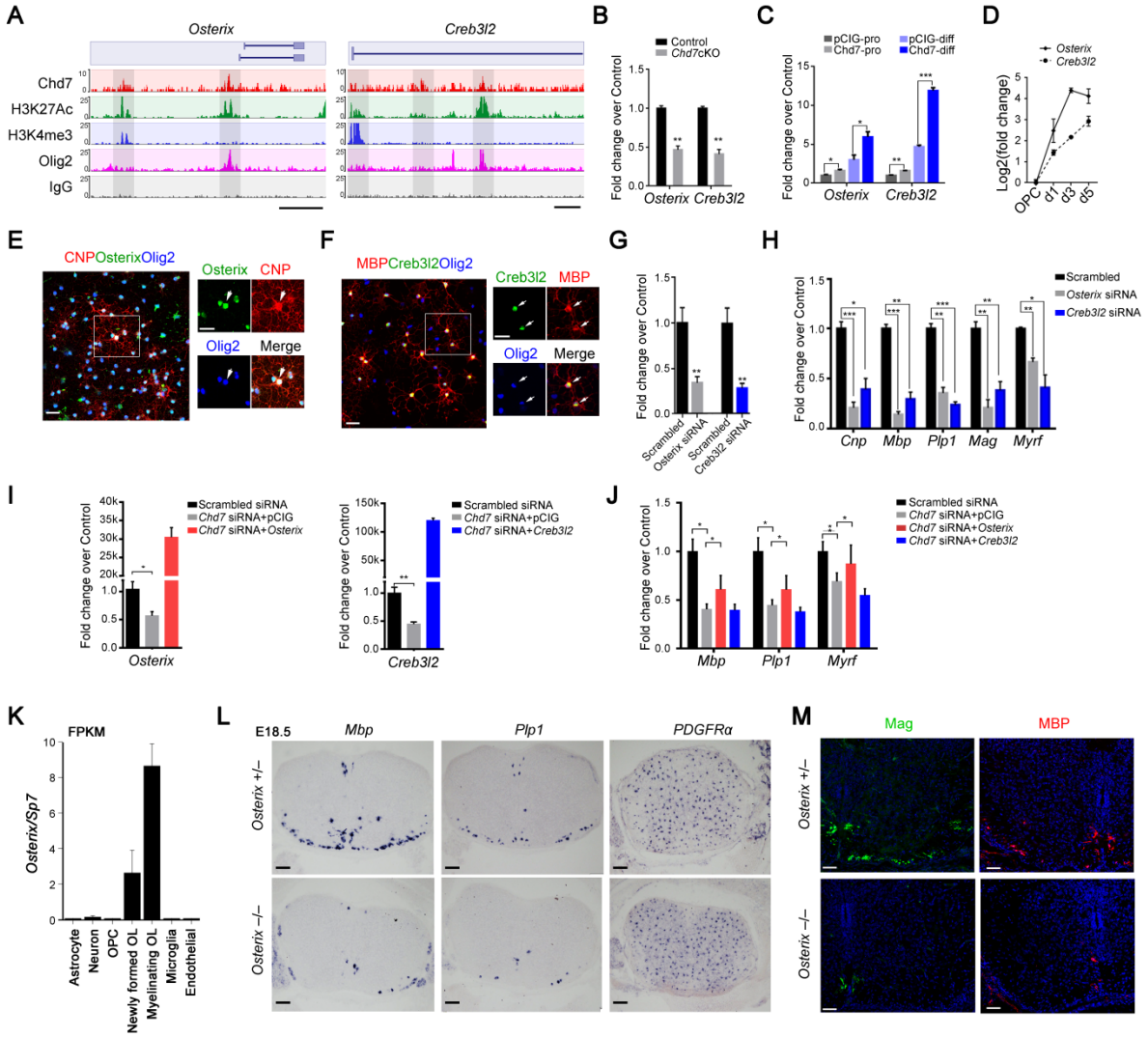

Figure 2-12 *Osterix* and *Creb3l2* are direct Chd7 transcriptional targets and required for proper OL differentiation. (A) ChIP-seq tracks for Chd7, H3K27Ac, Olig2, H3K4me3 and IgG at *Osterix* (left) and *Creb3l2* (right) loci. Genome scale bars represent 5 kb. (B) qRT-PCR analyses of *Osterix* and *Creb3l2* in P8 control and *Chd7*cKO spinal cords. The data are presented as mean ± s.e.m. (n = 3 controls and 3 mutant tissues; $^{**}P < 0.01$; two-tailed unpaired Student's t test). (C) qRT-PCR analyses of *Osterix* and *Creb3l2* in control

and Chd7-overexpressing Oli-Neu cells under proliferation (pro) or differentiation (diff) conditions spinal cords. The data are presented as mean ± s.e.m. (n = 3 biological replicates; *P < 0.05, **P < 0.01 and ***P < 0.001; two-tailed unpaired Student's t test). (D) qRT-PCR analyses of *Osterix* and *Creb3l2* expression during OL differentiation. The data are presented as mean ± s.e.m. (n = 3 biological replicates). (E,F) Immunolabeling of Osterix or Creb3l2, CNP or MBP and Olig2 in primary mouse OLs. Scale bars represent 50 μm. Boxed area (scale bars represent 25 μm) is shown at a high magnification at right. Arrows indicate the colabeling cells. (G) qPCR validation of knockdown efficiency of *Osterix* and *Creb3l2* in primary rat OLs. The data are presented as mean ± s.e.m. (n = 3 independent experiments, **P < 0.01; two-tailed unpaired Student's t test). (H) qRT-PCR analyses of OL differentiation–associated genes following treatments with scrambled, *Osterix* or *Creb3l2* siRNAs. The data are presented as mean ± s.e.m. (n = 3 independent experiments; *P < 0.05, **P < 0.01 and ***P < 0.001; two-tailed unpaired Student's t test). (I) qRT-PCR analysis of *Osterix* (left) and *Creb3l2* (right) expression in OPCs transfected with siRNAs against *Chd7* with control vector or vectors overexpressing *Osterix* and *Creb3l2*, respectively. The data are presented as mean ± s.e.m. (*Osterix*, n = 4 independent experiments, *Creb3l2*, n = 5 independent experiments, *P < 0.05, **P < 0.01; two-tailed unpaired Student's t test). (J) qRT-PCR analysis of differentiation-associated genes (*Mbp*, *Plp1*, and *Myrf*) in OPCs transfected with siRNAs against Chd7 with control vector or vectors overexpressing *Osterix* and *Creb3l2*, respectively. The data are presented as mean ± s.e.m. (n = 3 (scrambled siRNA), 3 (Chd7 siRNA + pCIG), 4 (Chd7 siRNA + *Osterix*), 4 (Chd7 siRNA + *Creb3l2*); n, numbers of biological replicates; *P < 0.05; multiple comparisons with t test. (K) RNA abundance represented as FPKM in indicated neural cell types. Data are presented as mean ± s.e.m. n = 2 biological replicates. (l) RNA *in situ* hybridization for *Mbp, Plp1* and *PDGFR*α on transverse spinal cord sections from *Osterix*+/− and *Osterix*−/− mice at E18.5. Scale bars represent 100 μm. (m) Immunolabeling for Mag and MBP on transverse spinal cord sections from *Osterix*+/− and *Osterix*−/− mice at E18.5. Scale bars represent 50 μm.

Consistent with the Chd7 expression pattern, *Osterix* and *Creb3l2* expression levels increased substantially as OPCs differentiated into mature OLs (Figure 2-12D). Similarly, we detected intense Osterix and Creb3l2 protein expression in cultured differentiating OLs bearing complex myelin processes (Figure 2-12E,F). To evaluate the role of these OL-enriched genes in OL differentiation, we knocked down endogenous *Osterix* and *Creb3l2*

expression in OPCs using RNA interference (Figure 2-12G). Downregulation of *Osterix* and *Creb3l2* inhibited expression of myelination genes including Cnp, Mbp, Plp1, Mag and Myrf (Figure 2-12H). Notably, exogenous overexpression of *Osterix*, but not *Creb3l2*, restored, at least partially, the defects in expression of myelination-associated genes caused by *Chd7* knockdown in OPCs (Figure 2-12I,J), pointing to the possibility that Osterix may mediate Chd7 function in OL differentiation.

Osterix is uniquely expressed in the OL lineage in the CNS, particularly in newly formed OL, according to neural cell–type transcriptome database (Zhang et al., 2014)(Figure 2-12K). To further determine the role of *Osterix* in OL development *in vivo*, we examined the expression of markers for mature OLs and OPCs in *Osterix*-null animals, which die at birth. At embryonic day 18.5 (E18.5), the last collectable stage for Osterix-null embryos, expression of Mbp and Plp1 was markedly diminished in the spinal cord, whereas the number of *PDGFR*α-expressing OPCs was comparable to that of control littermates (Figure 2-12L)**.** Consistently, expression of MAG and MBP assayed by immunostaining was markedly reduced as compared with the control (Figure 2-12M). These observations indicate that the Chd7 downstream regulator Osterix, an OL-enriched transcriptional regulator, is required for the onset of OL differentiation.

DISCUSSION

Epigenetics and chromatin remodeling are increasingly appreciated to play critical roles in development and human diseases. We demonstrate here that loss-of-function in Chd7 leads to defects in CNS myelination and remyelination. The dysmyelinating phenotype in our

mouse model resembles some of the features observed in CHARGE syndrome with proven CHD7 mutations, including delayed myelination and white matter defects (Figure 2-2K,L)(Gregory et al., 2013; Liu et al., 2014).

Our data suggest that Chd7 regulates OPC differentiation in a cell-autonomous manner. Deletion of Chd7 does not appear to affect the developmental transition from Olig+ progenitors to PDGFRα+ OPCs, but blocks proper transitioning from OPC to OL. Consistently, temporal specific Chd7 deletion in PDGFRα+ OPCs leads to a failure of OPCs to differentiate. In addition, our studies using a LPC-induced demyelinating animal model further demonstrate that Chd7 is critical for remyelination, and is therefore an important determinant of effective myelin repair.

The genome-wide, base-resolution mapping of the Chd7 targeted cistrome here reveals that Chd7 selectively targets the enhancers of myelinogenic factors encompassing Myrf, Nkx2.2, Sip1 and Olig1, and activates a transcriptional program for OL differentiation, consistent with the Chd7 function as a transcriptional rheostat to regulate, or fine-tune gene expression levels (Schnetz et al., 2010). We further identify a cohort of previously uncharacterized Chd7-targets in OL such as the bone formation regulators Osterix and Creb3l2, and demonstrate that these transcriptional factors are also critical for oligodendroglial maturation. Despite its critical role in osteoblast lineage differentiation 31, Osterix is expressed predominantly in maturing OLs in the CNS. We find that Osterix positively regulates OL differentiation in vitro and in vivo. It is worth noting that Osterix regulates expression of osteopontin, which is associated with multiple sclerosis pathogenesis (Braitch and Constantinescu, 2010; Comi et al., 2012). Since malformations of the temporal

bone are a common feature in CHARGE syndrome (Amiel et al., 2001; Friedmann et al., 2012), it is possible that regulation of Osterix by Chd7 may also contribute to temporal bone defects in CHARGE patients. These observations suggest that Chd7-controlled gene regulatory networks for OL differentiation may serve as an important intracellular cue to control the myelination process in the CNS and other seemingly unrelated malformations of other organs in CHARGE patients.

Chd7 interacts with Sox10 to regulate myelinogenic program

As an ATP-dependent nucleosome-remodeling factor, Chd7 requires additional transcriptional cofactors to target and activate gene expression. Our studies identify Sox10 as an important co-activator of Chd7 for target gene transcription during OL differentiation. Interestingly, mutations in Sox10 and Chd7 are both reported in Kallmann syndrome, a congenital disorder that exhibits hypogonadotropic hypogonadism and anosmia, features also frequently present in CHARGE syndrome (Jongmans et al., 2009). The clinical relevance between Sox10 and Chd7 mutations in these human diseases indicate a potential convergent role in developmental and pathogenic processes. Although the interaction of Chd7 with Sox10 provided the mechanistic basis for the role of Chd7 in myelinogenesis, the Chd7 mutant phenotype in mice seems less severe than that caused by deletion of Sox10 (Finzsch et al., 2008). These observations suggest that Chd7 may function as an important accessory factor that quantitatively enhances the OL differentiation and myelination program that can proceed in its absence, but at a lower level. Alternative possible explanation could be redundancy with other CHD family proteins, such as CHD8, which is also highly expressed

in oligodendrocytes (data not shown) and has been implicated in CHARGE syndrome pathogenesis through binding with Chd7 (Batsukh et al., 2010).

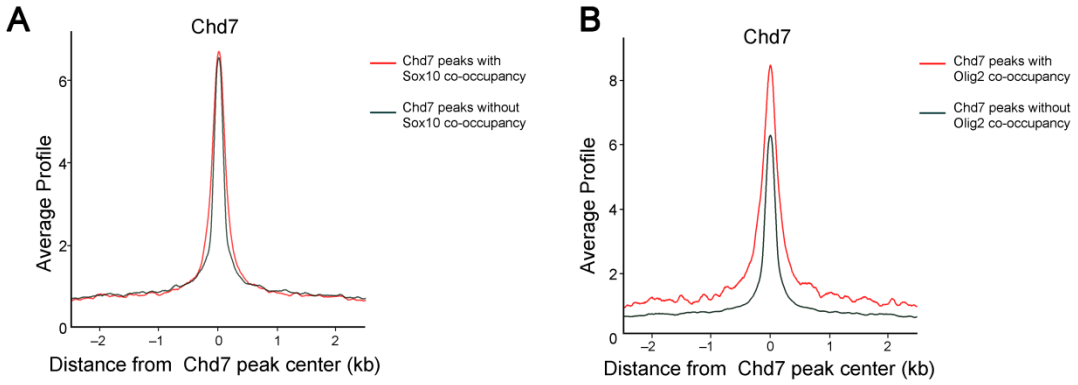

Figure 2-13 Genome occupancy of Chd7 with Sox10 and Olig2.(A) Aggregate plot of the average tag density of Chd7 binding sites at regions occupied by: Chd7 and Sox10 (red), and Chd7 only (green). (B) Aggregate plot of the average tag density of Chd7 binding sites at regions occupied by: Chd7 and Olig2 (red), and Chd7 only (green).

How Chd7 is temporally and spatially targeted to specific sites in chromatin remains to be determined. Recruitment of pioneer transcription factors by DNA consensus motifs clustered on regulatory elements could prime chromatin, which, in turn, recruits remodeling factors for activating downstream target gene expression (Voss and Hager, 2014; Zaret and Carroll, 2011). In line with this, Olig2 has been shown to act as a prepatterning factor that directs the recruitment of Brg1 to OL lineage-specific regulatory elements during the transition from OPC to immature OL 22 (Yu et al., 2013b). Different from this, our analysis of the Chd7 and Sox10 binding cistrome indicates that Sox10 preferentially occupies Chd7-targeted elements, while the frequency of Chd7 occupancy is comparable between elements

with or without Sox10 targeting (Figure 2-13). Since Sox10 occupancy in genomic loci increases gradually over the course of OPC maturation (Zhao et al., 2016), it seems likely that Chd7 is targeted to the chromatin first and then recruits Sox10. Intriguingly, Olig2 and Chd7 genome-wide binding cistromes indicate that Olig2 might possibly be prerequisite in the recruitment of Chd7 to regulatory elements (Figure 2-13B). Therefore, a potential sequential recruitment of priming factors such as Olig2, chromatin remodeling machinery such as Brg1 and Chd7, following by late phase regulators such as Sox10 may occur during OL lineage progression (Figure 2-14).

Implications for human diseases

Our study reports dysmorphic white matter in a significant portion of CHARGE patients with proven CHD7 mutations. The critical role for Chd7 in CNS myelination discovered here through OL lineage-specific mutagenesis implies that mutations in CHD7 may contribute to myelination and white matter defects seen in patients with CHARGE syndrome. A significant proportion of CHARGE patients develop growth retardation or delay, ranging from mild to severe. Given that white matter abnormalities caused by CHD7 mutations appear more severe in some of CHARGE patients compared with those in Chd7cKO mice; it is possible that altered expression or activity of Chd7 in other neural cell types such as neurons or neural stem cells (Micucci et al., 2014) may also contribute to the human phenotype. Nonetheless, our studies show that Chd7 is highly enriched in differentiating OLs and critical for CNS myelination and remyelination. These observations suggest that dysmyelination caused by CHD7 mutations might contribute, at least partially, to developmental white matter defects seen in CHARGE patients (Liu et al., 2014). Whilst

heterozygous Chd7 knockout mutants in the OL lineage are phenotypically normal, depletion of Chd7 expression in mice causes a myelination deficiency, indicating that a minimum threshold level of Chd7 expression is necessary for myelinogenesis. The phenotypic variation between the CHD7 haploinsufficient human mutants and heterozygous knockout mice could be due to a differential sensitivity to gene dosage across species or dominant negative effects of human mutant proteins.

Our studies further provide multiple lines of functional genomics data that shed light on the molecular basis whereby Chd7 directly regulates not only a network of genes essential for OL myelination, but also genes associated with development and morphogenesis of multiple organs including craniofacial, eye and ear structures that are affected in CHARGE patients 5. Examples include genes involved in the developmental processes of craniofacial and bone development such as *Osterix*, *Creb3l2*, *Col2a*, *Fgfr1/2* and *Rarg* (Nakashima et al., 2002; Sahlman et al., 2001), eye development such as *Pax6*, *Mitf* and *Rarg* (Bharti et al., 2012; Graw, 2010), and ear development such as *Ddr1*, *Prkra*, *Foxg1*, *Fgfr1/2* and *Rarg* (Meyer zum Gottesberge et al., 2008; Pauley et al., 2006; Schimmang, 2013).Notably, retinoic acid receptor gamma (Rarg) acts as a direct target of Chd7 in OLs, consistent with recent reports that Chd7 regulates the expression of Rarg (Micucci et al., 2014). Since Rarg signaling serves as a positive regulator of OL myelination and remyelination (Huang et al., 2011), its downregulation in Chd7 mutants may also contribute to CNS myelination defects in CHARGE syndrome. Together, our findings indicate that Chd7 serves as a nodal point of the regulatory network for the development of a diverse array of lineages spanning OLs and other cell types including osteoblasts, encompassing the phenotypes in CHARGE patients.

Our unbiased genome-wide target gene analysis could provide a molecular framework to identify signaling pathways and molecules as therapeutic targets for promoting myelin regeneration in patients with demyelinating diseases and CHARGE syndrome.

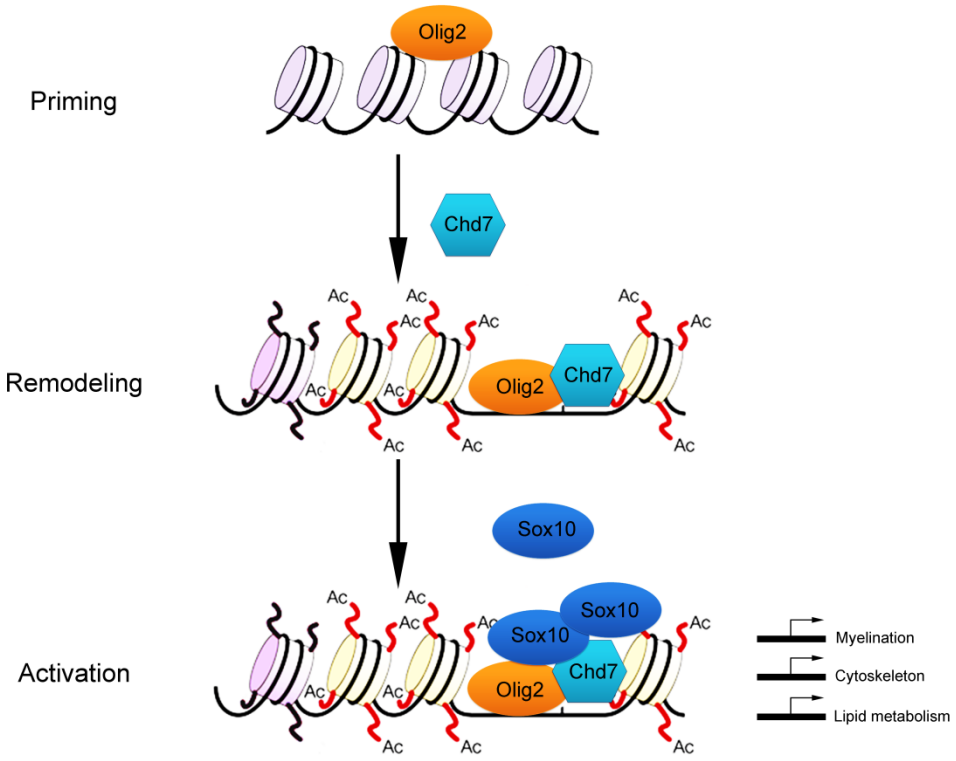

Figure 2-14 Scheme of Chd7/Sox10-mediated chromatin remodeling and myeliogenic gene program activation. The pioneer factor Olig2 recognizes and binds its cognate site in condensed chromatin (Priming), and further brings in chromatin remodeling factor to prime the enhancer for subsequent activation (Remodeling). Later phase transcription factors such as Sox10 are subsequently recruited and collaboratively active pathways that are required for oligodendrocyte differentiation and CNS myelination.

CHAPTER THREE

RECONSTRUCTION OF THE LNCRNA GENOMIC LANDSCAPE IN OLIGODENDROCYTES

INTRODUCTION

Myelination in the central nervous system (CNS) by oligodendrocytes (OLs) is required for rapid propagation of action potentials. At present, the factors that promote the initiation of OPC differentiation and overcome the block for successful remyelination in demyelinating diseases are poorly defined. OL lineage development can be orchestrated by extrinsic and intrinsic cues and coordination of genetic and epigenetic regulators, including transcription factors, chromatin remodelers and small non-coding RNAs, that activate the myelinogenic program while suppressing differentiation inhibitory pathways (Emery and Lu, 2015; Zuchero and Barres, 2013).

lncRNAs have been implicated in regulation of both normal development (Grote et al., 2013; Guttman et al., 2011; Kretz et al., 2013) and disease processes across different cell types and tissues(Gupta et al., 2010; Hu et al., 2014; Hung and Chang, 2010; Ulitsky and Bartel, 2013). Recent work points to the critical role of lncRNAs in transcriptional and post-transcriptional control of gene expression, the formation of complexes with epigenetic regulatory machinery, and chromosomal architecture organization (Hacisuleyman et al., 2014; Kretz et al., 2013; Ng et al., 2012; Yang et al., 2011). Dysregulation of lncRNAs has

been associated with human disorders caused by chromosomal deletions and translocations (Batista and Chang, 2013; Yang et al., 2014).

Whether lncRNAs are responsible for OL myelination in a temporally specific manner during development and remyelination is unknown. Although studies have shown expression of lncRNAs during CNS development (Mercer et al., 2010; Ramos et al., 2013)and in OPCs (Dong et al., 2015), a mechanistic understanding of the functions of lncRNAs in myelinogenesis in the CNS remains elusive. At present, diverse and bi-directionally transcribed lncRNAs based on genomic localization have not been fully categorized in the OL lineage. Identification and characterization of lncRNAs during OL lineage progression are critical to our understanding of the mechanisms of myelinogenesis and myelin repair.

Herein, we provide the first all-inclusive lncRNA annotation and mapping in mouse OLs at different stages. We profiled dynamic lncRNA expression during OL lineage differentiation by utilizing paired-ended next-generation sequencing of RNA and de novo transcriptome reconstruction. Through gene co-expression network analysis, we defined a group of lncRNAs that are tightly associated with OL differentiation. Our gain- and loss-of-function studies in vitro indicate that those OL-enriched lncRNAs are required for proper OPC. Collectively, our study provides a comprehensive mapping of lncRNAs in the OL lineage and demonstrates a critical role of lncRNA-mediated regulation for OL differentiation.

RESULTS

Comprehensive de novo mapping of lncRNAs during OL lineage progression

To gain insights into the functions for lncRNAs during OL development, we first set out to create an all-inclusive high-quality catalog of such transcripts using an ab initio transcriptome reconstruction pipeline (Trapnell et al., 2010; Trimarchi et al., 2014) that incorporates evidence of RNA transcripts from a collection of high-throughput RNA sequencing datasets (paired-end stranded-specific, 80-90 million reads/sample) from primary mouse OPCs and OLs that were differentiated with triiodothyronine (T3) for 1 day (iOL, immature OL) and 3 days (mOL, maturing OL) (Figure 3-1A). To identify putative lncRNA genes, we selected transcripts that were longer than 200 nucleotides and multiexonic and that did not overlap with protein-coding genes on the same strand. We then removed transcripts with coding-potential assessment (CPAT) scores higher than 0.44, which has been shown to identify noncoding RNAs (Wang et al., 2013). The high stringency annotation revealed 2392 lncRNA transcripts derived from 1342 unique gene loci (Figure 3-1A). Of these loci, 42% were not found in the Ensembl database (Figure 3-1B). Approximately 75% of lncRNAs detected here are intergenic, 6% are located within the introns of well-defined mRNA or lncRNA genes, and 19% are antisense to a known gene (Figure 3-1C,D). The oligodendrocytic lncRNAs identified had very little protein-coding potential as measured by the CPAT algorithm (Figure 3-1 E). As observed previously among data from various cell types (Cabili et al., 2011), lncRNA exons were less conserved than protein-coding exons as shown by PhastCons scores (Figure 3-1F), and their average expression levels were lower than those of protein-coding genes in OL lineage cells (Figure 3-1G).

We next examined the expression patterns of oligodendrocytic lncRNAs over a diverse panel of cell types including neurons, astrocytes, microglia(Zhang et al., 2014), neuronal tissues, and other somatic tissues(Yue et al., 2014). We scored the specificity of each gene by its average fractional expression level in OL lineage cells and found greater tissue specificity (Ts) of lncRNAs than protein-coding genes (Figure 3-1H,I), which corroborates the notion that lncRNA expression is highly cell-type specific (Guttman et al., 2009).

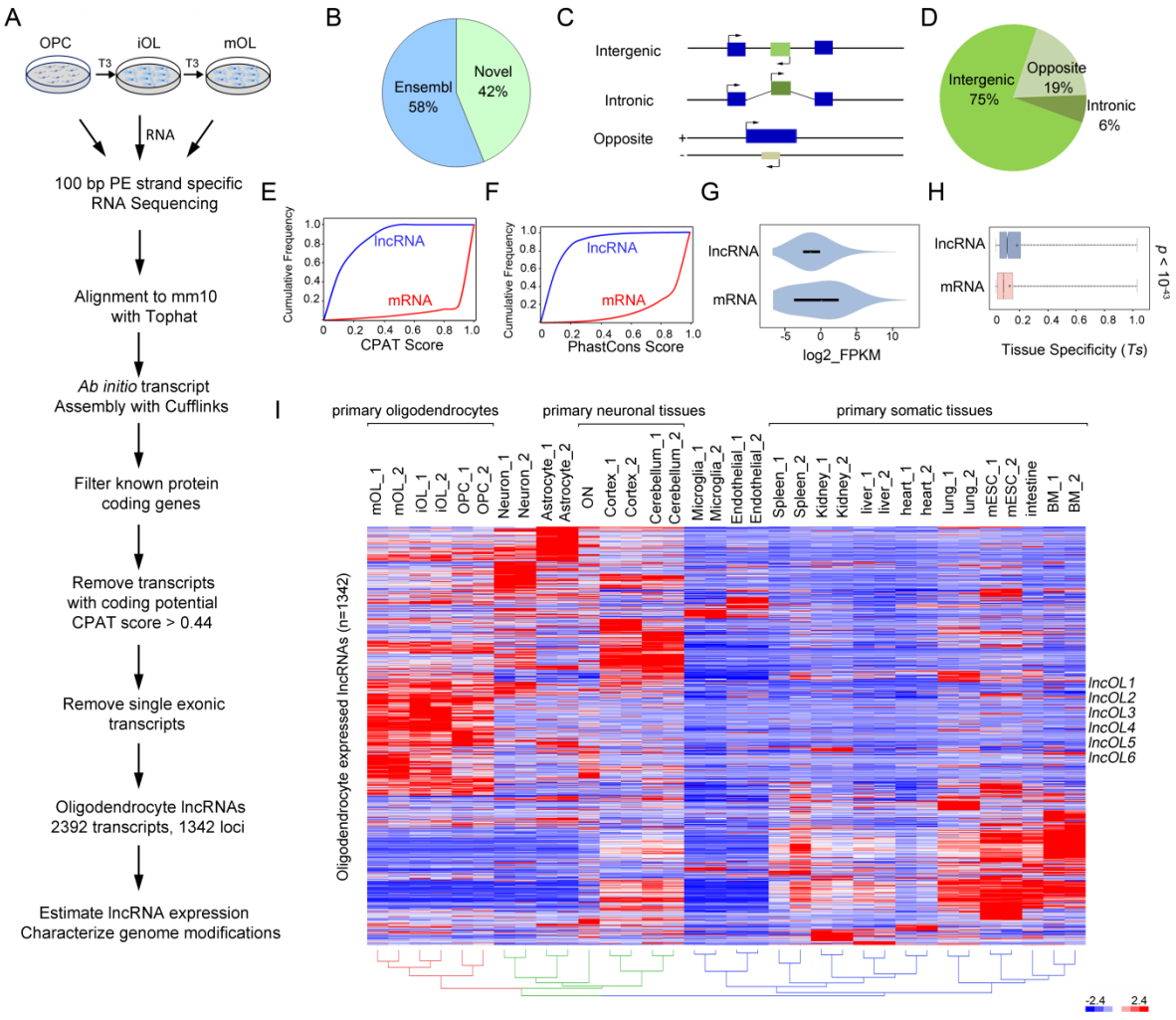

Figure 3-1 *de novo* mapping of lncRNAs transcriptome in OL lineage cells. (A) A schematic illustration of the procedure adopted to discover lncRNAs in primary mouse OPCs and OLS. (B) Venn diagram showing the fractions of lncRNA genes that were previously annotated and newly identified in OL lineage cells. (C) Three lncRNA categories classified based on relationships with protein-coding neighbors. (D) Pie charts of numbers of lncRNAs in each category for all lncRNAs annotated in this study. (E) Cumulative frequency plot of coding potential CPAT scores for mRNA (red) and lncRNA (blue) genes. (F) Cumulative frequency plot of PhastCons conservation scores for mRNA (red) and lncRNA (blue) genes. (G) Violin plot of log2 maximum expression values (FPKM) for mRNA and lncRNA genes. Whiskers show the minimum and maximum, boxes extend from the first to the third quartiles with cross lines at the medians. Unpaired Student's t test with Welch's corrections. (H) Box plot of tissue specificity index (Ts Score) for mRNA (red) and lncRNA (blue) genes. Ts scores are calculated by analysis of fractional expression in OLs across all the tissues examined. Whiskers show the minimum and maximum, boxes extend from the first to the third quartiles with cross lines at the medians. Unpaired Student's t-test with Welch's corrections. (I) A heatmap representation of all OL-expressing lncRNAs across OL lineage cells at different stages, primary neuronal cell types and tissues, and various other somatic tissues.

lncRNAs are dynamically regulated and expressed during OL lineage progression

To further characterize the lncRNA expression pattern obtained from our RNA-seq analysis, we analyzed transcription start site (TSS) regions for the presence of histone modifications. In agreement with previous reports (Casero et al., 2015; Trimarchi et al., 2014), a large majority of the promoters in the identified lncRNAs were associated activating histone marks H3K4me3 and H3K27ac in mouse cortical cells (Lu et al., 2016b) (Figure 3-2A). More importantly, whereas lncRNAs evolve rapidly and often lack orthologues in other species (Diederichs, 2014), we found that a significant portion of lncRNAs is also present in the syntenic loci of rat OL lineage cells, evident by the enrichment of H3K4me3 and H3K27ac in conserved genomic regions (Figure 3-2B,C), suggesting that these lncRNAs play a

functionally conserved role during OL development. In addition, genomic occupancy by Sox10, an OL differentiation regulator (Lopez-Anido et al., 2015), was detected at many putative lncRNA promoters in rat OLs (Figure 3-2B,C), suggesting that Sox10 transcriptionally regulates these lncRNAs.

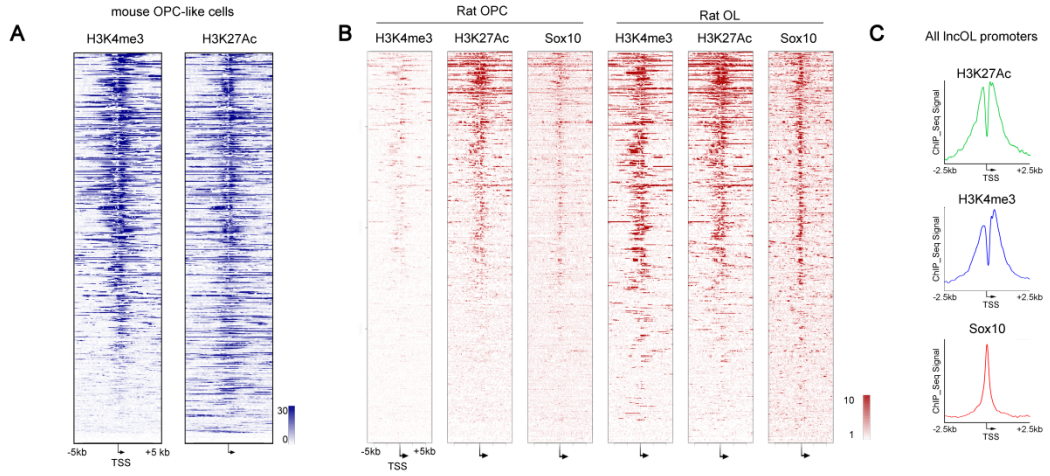

Figure 3-2 TSSs of lncRNAs are conserved and show active chromatin profiles. (A) Heatmap representation of ChIP-seq signal density for H3K4me3 and H3K27ac centered on annotated lncRNA TSSs (± 5 kb). ChIP data were from mouse OPC-like cells(Lu et al., 2016b). (B) Heatmap representation of ChIP-seq signal density for H3K4me3, H3K27ac, and Sox10 for 5 kb centered on predicted lncRNA TSSs in primary rat OPCs and OLs. (C) Histogram depicting ChIP-seq signal density on all predicted lncRNA promoters for H3K27ac, H3K4me3, and Sox10 in primary rat OLs.

To investigate the dynamics of lncRNA expression during OL differentiation, we profiled their expression over the course of OPC differentiation and maturation. These analyses yielded a subset of lncRNAs that displayed differential expression between differentiating OLs and OPCs (Figure 3-3A). Notably, a large fraction of lncRNAs was dramatically upregulated as OPCs differentiated (Figure 3-3A). To determine the lncRNAs expression

pattern during regeneration, we then characterized the temporal changes in lncRNA expression after contusive spinal cord injury in mice (Chen et al., 2013). The spinal cord injury resulted in an acute loss of OLs followed by OPC recruitment and differentiation (Franklin, 2002). Similar to dynamic changes of OL-associated genes, expression of a large fraction of oligodendrocyte-enriched lncRNAs such as lncOL1 was reduced at 2 days post lesion (*dpl*) with a small group reactivated at 7 *dpl* during the regeneration process (Figure 3-3 B). These data suggest a potential importance of lncRNAs for OL regeneration, diminishing during OL loss and conversely increasing during differentiation.

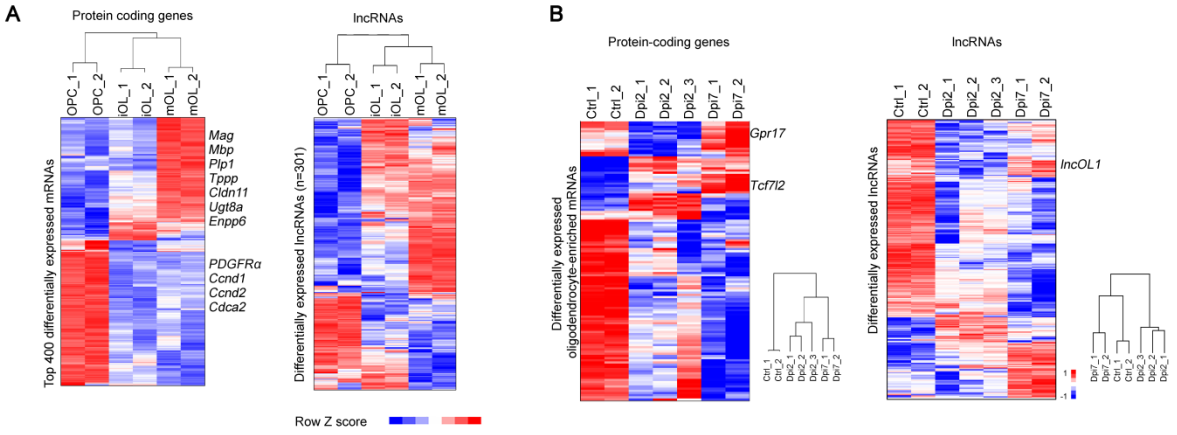

Figure 3-3 lncOLs are dynamically expressed during OL differentiation and regeneration. (A) Heatmaps showing top differentially expressed protein-coding (left) and lncRNA (right) genes during mouse OPC maturation. (B) Heatmaps showing top differentially-expressed protein-coding (left) and lncRNA (right) genes during the time course of spinal cord injury. Hierarchical sample clustering is shown at the right of the heatmap.

Co-expression networks between lncRNAs and protein-coding genes in OLs

Expression of many lncRNAs is highly correlated with that of their protein-coding neighbors, and some lncRNAs influence the expression of nearby genes (Briggs et al., 2015; Rinn and Chang, 2012). Therefore, we first assessed the proximities and Pearson correlations of neighboring pairs of lncRNAs and mRNAs. Even though some lncRNAs were transcribed proximally (within 5 kb) of the promoters of protein-coding neighbors, as a group, no obvious correlations determined by correlation coefficients were observed between the majority of lncRNAs and adjacent mRNAs in the OL lineage (data no shown), suggesting that expression of the majority of OL-enriched lncRNAs is not related to local transcriptional activity of neighboring protein-coding genes or involved in the same biological processes.

To assess the potential functions of oligodendrocytic lncRNAs, we then evaluated the co-relationship of lncRNAs and protein-coding genes using the Markov clustering algorithm (MCL), which assigns genes into modules based on their similarity in expression patterns(van Dongen and Abreu-Goodger, 2012). We identified 19 clusters contained at least 100 correlated lncRNAs and protein-coding genes (Figure 3-4A) that are associated with known biological processes including neurogenesis and neural differentiation (Figure 3-4B).

We focused on the lncRNA genes in cluster I because these genes are primarily associated with the process of neurogenesis and gliogenesis. Assessment of the Pearson correlation between lncRNA and protein-coding genes within MCL cluster I, which represents the highest lncRNA proportion, revealed that this group of lncRNAs is indeed highly correlated with the myelinogenic gene program (Figure 3-3C). In particular, lncOL1 and lncOL4 levels positively correlate with the levels of myelination-associated mRNAs such as *Mbp* and

Nkx2.2 across a panel of various cell types and tissues (Figure 3-4D), suggesting that this group of lncRNAs is likely involved in OL myelination.

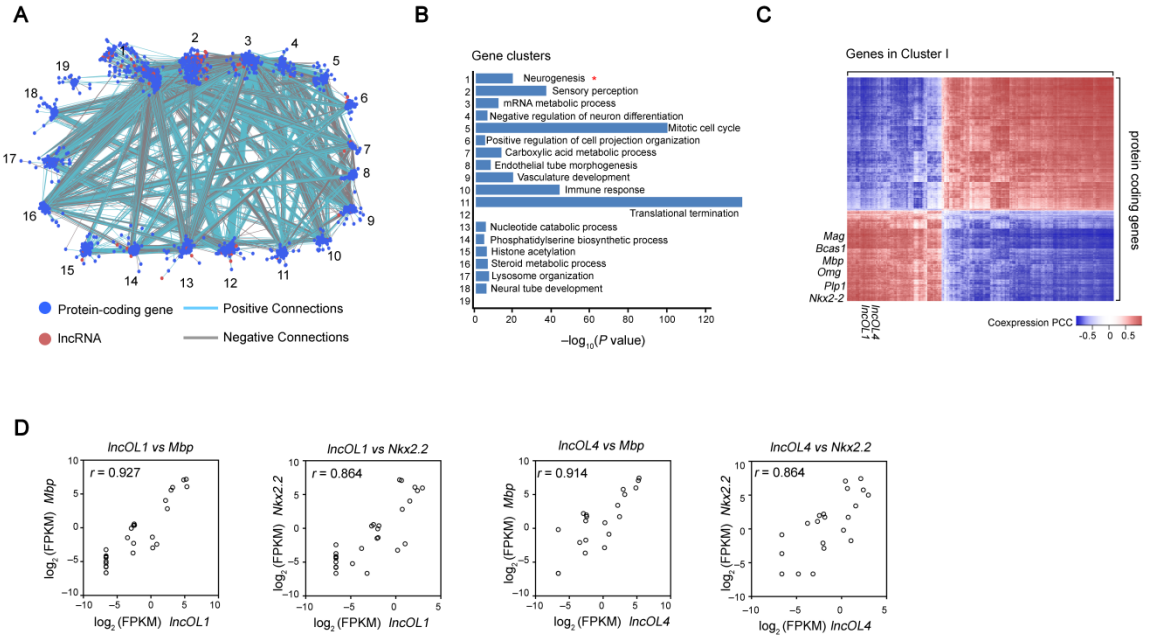

Figure 3-4 Co-expression networks between lncRNAs and protein-coding genes in OLs. (A) Cytoscape representation of the 19 largest MCL clusters in the gene co-expression network from all tissues and cells examined. (B) GO enrichment for the 19 largest MCL clusters. The most significant GO categories are displayed. (C) Heatmaps displaying Pearson correlation coefficients of lncRNA and protein coding genes in MCL cluster I. Columns and rows represent protein-coding genes and lncRNAs, respectively. Myelin-associated genes and lncOLs are highly correlated. (D) Correlations between lncRNAs and myelinogenic genes across OL lineage cells, primary neuronal cell types and tissues, and various other somatic tissues. Each dot represents the expression levels (FPKM) of lncRNA and mRNA in one sample.

Selected OL-enriched lncOLs are required for proper OL differentiation

Given that a set of OL-enriched lncOLs were identified in our lncRNA *de novo* reconstruction and network analysis, we next sought to validate and characterize the expression and function of candidate lncOLs. We selected four lncRNAs from the lncOL set for further analysis: *lncOL1* (aka *9630013A20Rik*), *lncOL2* (aka *9530059O14Rik*), lncOL3 (aka *1700047M11Rik*), three previously annotated, but poorly characterized lncRNAs, and *lncOL4* , a previously unannotated lncRNA (Figure 3-5A). *LncOL1-4* are transcribed from genomic regions associated with active histone marks including H3K4me4 and H3K27Ac (Figure 3-5A). Despite varying cellular abundance of total transcripts detected(relative level to *GAPDH*), all four lncRNAs were robustly expressed in mouse CNS tissues such as brain and spinal cord but were barely detectable in other somatic tissues (Figure 3-5b). Furthermore, concurrent with dynamic expression of OL differentiation regulators such as Tcf7l2/Tcf4 (Zhao et al., 2016) in the developing spinal cord, lncOL1-4 expression was detected at the neonatal stage P0 and peaked at the perinatal stage P14, followed by a sharp decline into adulthood, suggesting that it is involved in OL differentiate but not for myelin maintenance (Figure 3-5C). Consistently, lncOL1-4 were substantially upregulated during OPC differentiation *in vitro* (Figure 3-5D).

To determine *lncOL1-4* function in OL differentiation, we attenuated their expression in primary mouse OPCs individually using siRNAs. Knockdown of the lncOL1-*4* significantly inhibited expression of myelin genes including *Mbp, Plp1* and *Cnp* (Figure 3-5E,F), suggesting that induction of these lncRNAs is required for proper OL differentiation. Next, we investigated whether the gain-of-function of lncOL1-4 could promote OL differentiation genes induction. To ensure the proper processing and secondary structure formation, we

cloned murine lncOL1-4 into the pBI-CMV3 vector to allow transcription of lncRNAs and a GFP reporter ZsGreen1 from constitutively active bidirectional human cytomegalovirus promoters (Figure 3-5G). Forced expression of *lncOL1*, *lncOL2* and *lncOL4* significantly enhanced the induction of myelin gene expression, but *lncOL3* overexpression exhibited moderate, if any, impact on OL differentiation (Figure 3-5G). In particular, overexpression of lncOL1, the most abundant lncRNA detected in oligodendrocyte lineage cells, dramatically induced a set of differentiation signature genes (Figure 3-5G).

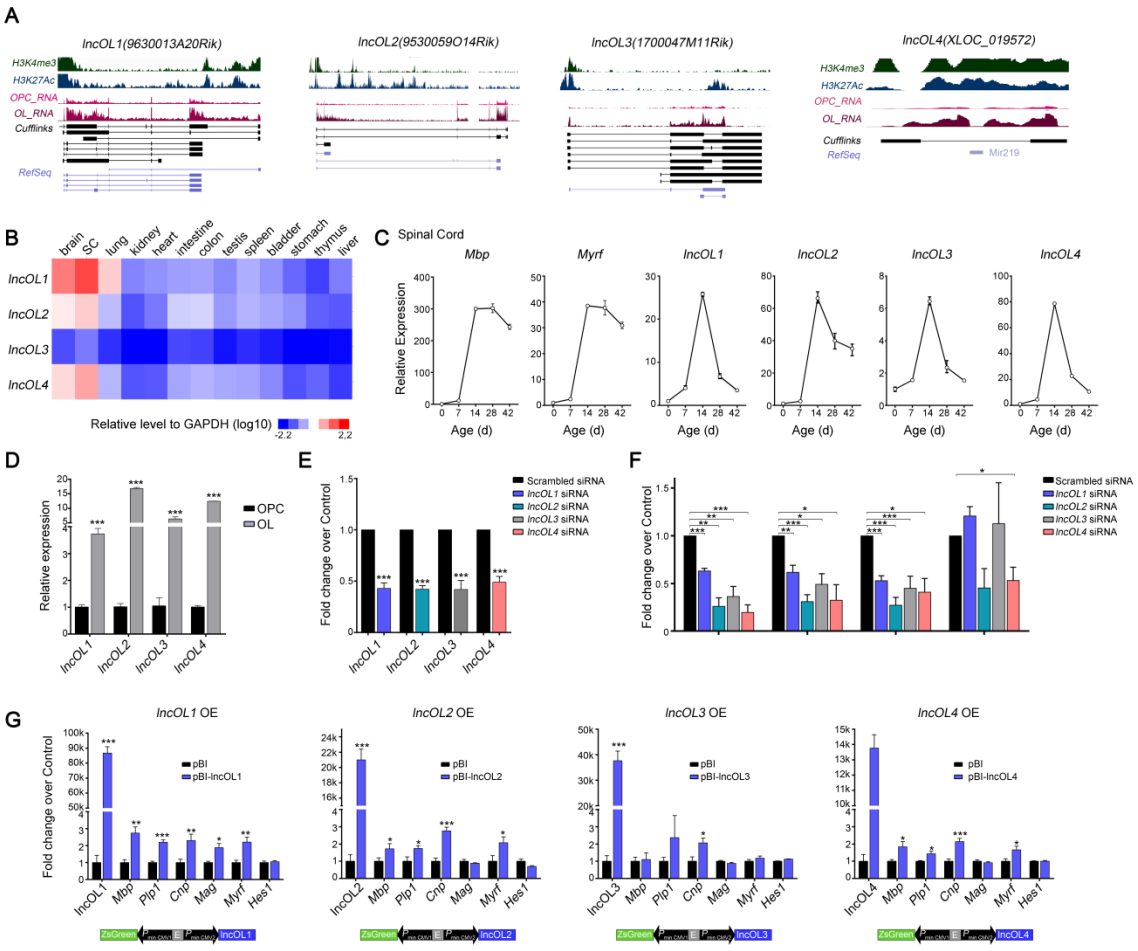

Figure 3-5 OL-enriched lncRNAs are required for OL differentiation. (A) UCSC Genome browser tracks of lncOL1-4 loci Tracks depict RNA-seq signals for OPCs and OLs along with ChIP-seq signals for H3K4me3 and H3K27ac. Bottom tracks depict de novo transcript models created from Cufflinks and RefSeq annotations. (B) qRT-PCR analyses of lncOL1-lncOL4 transcript levels in 13 murine tissue samples at postal day 14. (C) qRT-PCR analyses of lncOL1 and Mbp transcript levels in mouse spinal cords at various developmental stages. Data are presented as means ± S.E.M, n = 3 at each time point. (D) qPCR analyses for lncOL1-lncOL4 in primary mouse OPCs and OLs. Data are presented as means ± S.E.M, n = 3 at each time point; paired Student's t-test. (E) qPCR validation of efficiency of siRNA-mediated inhibition of lncRNA expression. Data are presented as means ± S.E.M; n = 4 independent experiments, **p < 0.01, *** p < 0.001; paired Student's t-test. (F) qRT-PCR analyses of OL-differentiation associated genes following treatments with scrambled or lncRNA-targeted siRNAs. Data are presented as means ± S.E.M; n = 4 independent experiments, *p < 0.05, **p < 0.01, *** p < 0.001; one-way ANOVA with post hoc Tukey's test. (G)) qRT-PCR analyses of OL-differentiation associated genes in rat OLs transduced with control or lncRNA-overexpressing vectors. Bottom is a schematic presentation of lncRNA-overexpressing vectors used in the experiments. Data are presented as means ± S.E.M; n = 4-6 independent experiments, *p < 0.05, **p < 0.01, *** p < 0.001; paired Student's t-test.

DISCUSSION

Decoding regulatory elements and factors that control OL myelination is crucial for identifying new therapeutic targets to treat demyelinating disorders. Our study presents the first integrated transcriptional map, to our knowledge, of lncRNA elements at multiple stages during OL lineage progression, and defines the association of distinct OL-expressing lncRNA clusters with corresponding protein-coding genes. Through global gene-expression profile analyses of OL lineage cells, we provide a resource that parses the lncRNA circuitry and their functional relationship with protein-coding genes in controlling OL development.

By integrative analyses of transcriptome profiling and genome-wide chromatin states, we systematically constructed and cataloged lncRNAs that are actively transcribed during OL differentiation. Previously studies only annotated lncRNAs in OPCs (Dong et al., 2015) and used the Ensembl public databases to identify glial cell differentiation from mixed neural progenitors using a microarray platform(Mercer et al., 2010). The lncRNAs annotated in the present de novo annotation not only include lncRNAs previously annotated, but also identify over 500 unique, previously un-annotated lncRNAs that are enriched during OL differentiation. In contrast to the previous studies that only polyA (+) RNAs were included, our lncRNA dataset included both poly-A (+) and poly-A (-) lncRNAs, lncRNAs transcribed from the opposite strand of mRNAs and confirmed with active histone marks in the promoter regulatory elements. lncRNA expression profiling at multiple phases during OL differentiation and regeneration after spinal cord injury revealed that transcription of lncRNAs, like mRNAs, is dynamically regulated during development and repair. Our analyses reveal tissue and temporal specificity and genetic diversity of complex lncRNAs, which allow fine-mapping the dynamic processes of OL development and demyelinating diseases.

The unmapped nature of lncRNAs and their interaction with protein-coding genes during OL lineage progression has represented a substantial obstacle to the delineation of the transcriptional and epigenetic network that regulates step-wise myelinogenesis. The temporally restricted expression patterns of lncRNAs in the OL lineage suggest that lncRNAs may control the development and function of OLs in a stage-specific manner. The reconstruction of a conserved co-expression network that links lncRNAs with protein-coding

gene expression and their functions allows identifying the potential functions of lncRNAs during OL lineage progression and remyelination.

CHAPTER FOUR

TIMELY CNS MYELINATION AND REMYELINATION IS REGULATED BY A LNCOL1/SUZ12 COMPLEX

INTRODUCTION

Mammalian genomes encode thousands of long noncoding RNAs (lncRNAs), which are identified as emerging regulators in diverse biological processes (Rinn and Chang, 2012; Schmitt and Chang, 2016). Genome-wide association and expression profiling followed by gain- and loss-of-function studies in cell-based *in vitro* systems have enabled us to uncover important roles of OL-enriched lncRNAs (lncOLs) during the transition from OPCs to OLs (Chapter 3). Yet, direct *in vivo* evidence of the functional significance of lncOLs in CNS myelination and remyelination by genetic perturbation remains elusive.

lncOL1, a CNS-enriched lncRNA, is highly induced during OL differentiation and regeneration (Chapter5). We have demonstrated that knockdown of *lncOL1 in vitro* by siRNAs inhibited myelin gene expression while enforced expression of *lncOL1* in cultured OPCs enhance the induction of differentiation genes. However, the physiological function of *lncOL1* at the tissue and organismal levels has not been investigated. To address this directly, we have established *lncOL1* knockout mice utilizing CRISPR/Cas9 technology. We found that genetic inactivation of lncOL1 causes defects in CNS myelination and remyelination following injury. Furthermore, we found that *lncOL1* interacts and recruits a suppressor of zeste 12 protein homolog (Suz12) in the polycomb repressive complex 2 (PRC2) to suppress

OL differentiation inhibitory pathways. Collectively, our study provides a comprehensive mapping of lncRNAs in the OL lineage for elucidating the transcriptional and epigenetic regulation of myelinogenesis and demonstrates a critical role of LncRNAs for OL differentiation and subsequent CNS myelination.

RESULTS

lncOL1 is an OL-restricted lncRNA that promotes OL differentiation

As deliberated in Chapter 5, our ranking of oligodendrocytic lncRNAs by their abundance, regulation during the transition from OPC to OL, and potential functions identified lncOL1 as a top candidate modulator of OL differentiation. In mouse and rat OL lineage cells, lncOL1 is located within the second intron of Pcdh17 and is actively transcribed in the direction opposite Pcdh17 (Figure 4-1A). Peaks in genomic occupancy by Sox10 and Olig2, two critical OL transcriptional regulators, were observed near the lncOL1 TSS in rat OLs. Occupancy of activating histone marks H3K4me3 and H3K27ac as well as Olig2 (Yu et al., 2013b)was markedly enhanced around the TSS of lncOL1 in differentiating OLs relative to OPCs (Figure 4-1A), suggesting greater chromatin accessibility and transcription activity at the lncOL1 promoter during OL differentiation. *lncOL1* expression is restricted to OL lineage cells as transcripts of lncOL1 were not detected in other neural cell types such as neural progenitor cells and astrocytes (Figure 4-1A).

In line with the enhancement of activating histone marks at the *lncOL1* promoter, *lncOL1* transcript levels were substantially induced during OL differentiation in culture (Figure 4-1B). In situ hybridization revealed prominent expression of lncOL1 in CNS white

matter tracts in the brains and spinal cords of mice at perinatal stages (Figure 4-1C,D). lncOL1 was expressed exclusively in a subset of $Olig2^+$ OL lineage cells (Figure 4-1E). Moreover, lncOL1 was co-expressed in cells that expressed the mature OL markers CC1 and Sip1/Zeb2 (Weng et al., 2012) (Figure 4-1E) but was only weakly detected in $PDGFR\alpha^+$ OPCs (Figure 3E). Taken together, our data indicate that lncOL1, an evolutionally conserved lncRNA, is restricted to differentiating OLs in the OL lineage.

To determine the cellular localization of lncOL1, we performed RNA fluorescence in situ hybridization (FISH) in OPCs and differentiating OLs. lncOL1 was detected both in the cytoplasm and nucleus of OPCs, but it is enriched in the nuclear fraction and formed multiple "foci" in the nucleus of differentiating OLs (Figure 4-1F). Consistent with this, fractionation of cellular components of Oli-Neu cells, an oligodendroglial cell line (Jung et al., 1995) followed by quantitative RT-PCR demonstrated that the nuclear fraction of lncOL1 was associated with chromatin (data not shown), suggesting a potential role of the lncOL1 transcript in transcriptional regulation during OL differentiation.

Given that siRNA-mediated silencing of lncOL1 significantly inhibited myelin gene expression (Figure 3-5F), we then evaluated the functional role of lncOL1 in OL maturation, we attenuated lncOL1 expression by transduction of OPCs with a lentiviral vector for expression of shRNAs designed to target lncOL1. OPCs depleted of lncOL1 exhibited a defect in differentiation into MBP^+ OLs (Figure 4-1G,H).

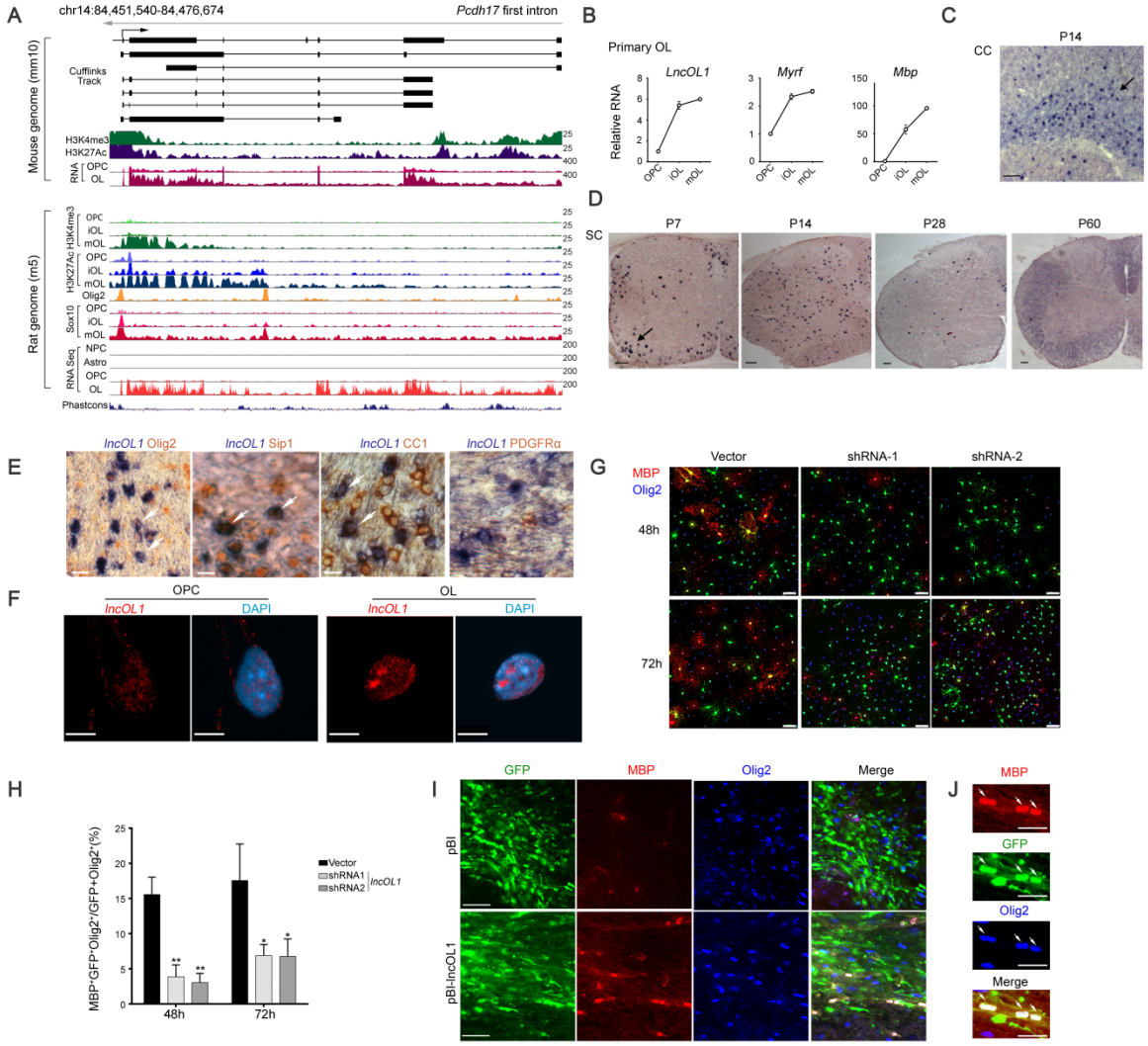

Figure 4-1 lncOL1 is a conserved oligodendrocyte-specific lncRNA that regulates OL differentiation. (A) Genome browser tracks of lncOL1 locus in primary mouse OLs (top) and its corresponding genomic locus in primary rat OLs (bottom). Top tracks depict RNA-seq signals for mouse OPCs and OLs and ChIP-seq signals for H3K4me3 and H3K27ac (Lu et al., 2016a). Bottom tracks represent RNA-seq signals for rat OPCs, OLs, astrocytes (Astro), and neural precursor cells (NPC) and ChIP-seq signals for H3K4me3, H3K27ac, Olig2 and Sox10 in primary rat OPCs and OLs. (B) qRT-PCR analyses of lncOL1, Myrf, and Mbp transcript levels in primary mouse OPCs, iOLs, and mOLs. Data are presented as means ± S.E.M, n = 3 at each time point. (C-D) In situ hybridization showing that expression of lncOL1 is enriched in white matter of brain and spinal cord at the indicated developmental time points. Arrows point to lncOL1-expressing cells. CC: corpus callosum; SC: spinal cord.

Scale bar, 100 μm. (E) In situ hybridization for lncOL1 (blue) and Immunohistochemistry for Olig2, Sip1/Zeb2, CC1 or PDGFRα (brown) at P14. Arrows indicate lncOL1$^+$ cells. Arrowheads indicate PDGFRα$^+$ OPCs without weak lncOL1 expression. Scale bar, 10 μm. (F) FISH for lncOL1 in primary OPCs and OLs differentiated for three days. Nuclei are counterstained with DAPI. Scale bar, 5 μm. (G) Immunostaining for MBP (red) and Olig2 (blue) after 48 or 72 hr of differentiation (PDGFAA and NT3 withdrawal) in control or lncOL1-shRNA transduced mouse OLs. Scale bar, 50 μm. (H) Histogram depicting quantification of the percentage of MBP$^+$ cells among GFP$^+$ transduced cells. Data are presented as means ± S.E.M; n = 3 independent experiments; *$p < 0.05$, **$p < 0.01$; one-way ANOVA with post hoc Tukey's test. (I,J) Cortical sections at E17.5, 3 days after electroporation with control (pBI-zsgreen) or lncOL1 overexpressing (pBI-lncOL1/zsgreen) vectors. Panel L shows high magnification of transduced cells co-labeled with GFP, MBP, and Olig2. Scale bars in K, 50 μm; in L, 25 μm.

Next, we investigated whether the gain-of-function of lncOL1 could promote precocious OL formation *in vivo*. Electroporation of the lncOL1-expressing vector into the cortical ventricular zone of developing embryos at E14.5 led to the precocious formation of MBP$^+$ OLs that expressed Olig2 at E17.5 (Figure 4-1I,J), at which stage no MBP$^+$ OLs are observed in the control cortex. These observations suggest that enforced expression of lncOL1 in neural progenitors induces OL differentiation in the cortex.

Loss of *lncOL1* leads to defects in OL differentiation and myelination onset in vivo

To investigate the functional requirement for lncOL1 in OL development in vivo, we generated lncOL1-knockout (KO) mice using CRISPR-Cas9 technology (Doudna and Charpentier, 2014; Shalem et al., 2015).Two pairs of single guide RNAs (sgRNAs) were designed to delete a 5.7-kb region covering the first 4 exons of lncOL1 (Figure 4-2A). Pups from the F0 generation were screened for indels and confirmed by Sanger sequencing of

potential off-target sites. A founder carrying a monoallelic deletion was chosen and backcrossed with wild-type mice for three generations. lncOL1-KO mice were born at expected Mendelian ratios from heterozygous intercrosses (Figure 4-2B). Quantitative RT-PCR confirmed the loss of transcripts of lncOL1 containing regions targeted for deletion in brain tissues of homozygous mutant mice (Figure 4-2C). Levels of transcripts containing the 3' non-deleted regions of lncOL1 were also substantially downregulated (Figure 4-2C).

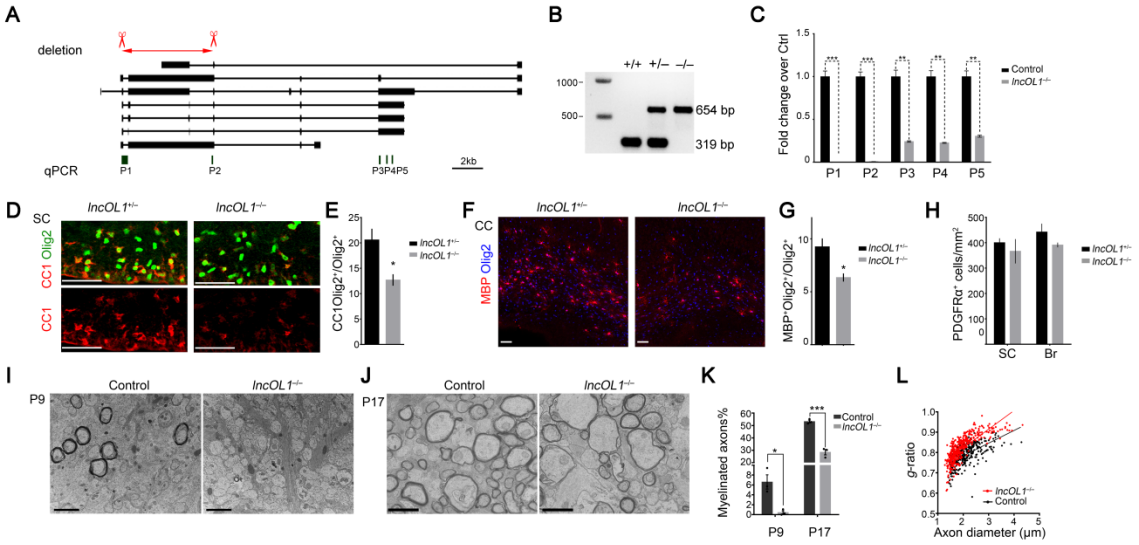

Figure 4-2 lncOL1-deficient mice exhibit defects in the onset of OL differentiation and in myelination. (A) Schematic diagram of CRISPR/Cas9-mediated knockout strategy at the lncOL1 locus. Two sgRNA recognition sites for lncOL1 deletion are demarcated in red. P1-P5 (primer pairs 1-5) are sites for primer binding for qRT-PCR amplification used for validation of knockout efficiency of different exons in lncOL1. (B) Validation of lncOL1-KO mouse lines by PCR analysis. Genomic DNA was amplified with primers selective for the wild-type allele and with primers spanning the deleted region.(C) qPCR analyses of lncOL1 transcript levels with primers indicated on the x-axis in brains from lncOL1-KO and control littermates at P12. Primers P1 and P2 are located in deleted genomic regions and P3, P4, and P5 are in genomic regions that remain in the lncOL1-KO mice. Data are presented as means ± S.E.M; n = 3 animals; **p < 0.01, ***p < 0.001; Student's t-test. (D) Coronal sections of P1 spinal cords from control and lncOL1-null animals were co-immunostained for CC1 (red)

and Olig2 (green). Scale bar, 50 μm. (E) Quantification of $CC1^+$ OLs as a percentage of total $Olig2^+$ cells in P1 control and lncOL1-KO spinal cords. Data are presented as means ± S.E.M; n =3-4 animals; * p <0.05; Student's t-test. (F) Immunofluorescence labeling for Olig2 (blue) and MBP (red) in P6 control and lncOL1-KO corpus callosum. Scale bars, 50 μm. (G) Quantification of MBP^+ OLs as a percentage of all $Olig2^+$ cells within the corpus callosum of control and lncOL1-KO mice at P6. Data are presented as means ± S.E.M; n = 4 animals; * p <0.05; Student's t-test. (H) Quantification of $PDGFR\alpha^+$ OPC density in control and lncOL1-KO brains (Br) and spinal cords (SC). Data are presented as means ± S.E.M; n = 3-4 animals. (I) Representative electron micrographs of transverse optic nerve sections from P9 control and lncOL1-KO animals. Scale bar, 2 μm. (J) Representative electron micrographs of transverse optic nerve sections from P17 control and lncOL1-KO animals. Scale bar, 2 μm. (K) Quantification of the percentage of axons myelinated at P9 and P17. Data are presented as means ± S.E.M; each data point is an average for a single animal; n = 4 animals; * p <0.05, ***p < 0.001; Student's t-test. (L) Scatter plots of g-ratios of individual fibers from lncOL1-KO (black circles) and littermate controls (red circles) at P17. Between 300 and 400 axons from three mice of each age and genotype were analyzed; ***p < 0.001.

When the developing spinal cords at P1 were analyzed, the percentage of $CC1^+$ differentiating OLs among $Olig2^+$ OL lineage cells was significantly lower in lncOL1-KO mice than in control littermates (Figure 4-2D,E). Similarly, expression of MBP, a mature OL marker, was reduced in the lncOL1-KO brain compared to controls (Figure 4-2F,G). In contrast, the total numbers of $PDGFR\alpha^+$ OPCs were comparable between control and lncOL1-KO animals (Figure 4-2H). These observations suggest that lncOL1 is required for timely OPC differentiation but not their formation. Strikingly, ultrastructural analysis of optic nerves from lncOL1-KO mice at the onset of myelination e.g. P9 showed severe defects in myelinogenesis with an absence of myelinated axons (Figure 4-2I,K). At the postnatal week two e.g. P17, the peak period of myelinogenesis, the number of myelinating axons had increased in lncOL1-KO mice relative to P9 but was still less than that in control mice

(Figure 4-2J,K). Notably, the myelin sheaths (as measured by g-ratio, the ratio of the diameter of the axon to the diameter of the axon plus its myelin sheath) were significantly thinner in lncOL1-mutant optic nerves than controls (Figure 4-2K). At adulthood, however, the number of mature OLs and degree of myelination were indistinguishable between adult lncOL1-KO and control mice (Figure 4-3). Collectively, these observations indicate that lncOL1 mainly regulates for OL differentiation and the onset of myelination, but not myelin maintenance.

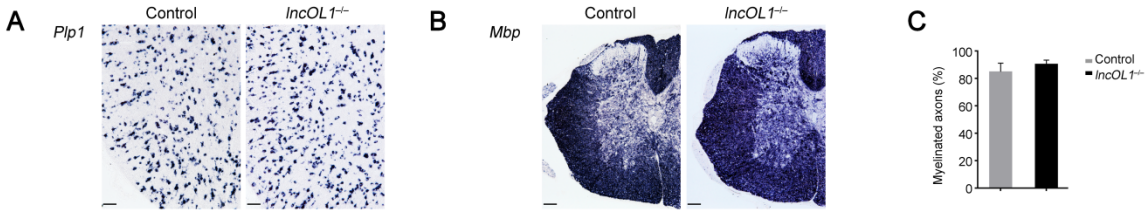

Figure 4-3 OL number and myelination recovery in adult lncOL1 mutant mice. (A, B) In situ hybridization analyses for (A) Plp1 and (B) Mbp on transverse spinal sections from wildtype and lncOL1-null mice at P60. Scale bars, 100 μm. (C) Percentages of myelinated axons in the spinal white matter regions of wildtype and lncOL1-null mice at P60. Data are presented as means ± S.E.M; n = 3 animals; Student's t-test.

To determine whether defects in OL maturation in lncOL1-KO animals are cell-autonomous due to lncOL1 deletion, we cultured OPCs isolated from control and lncOL1-KO neonates and analyzed their capacity to proliferate and to differentiate in vitro. In the presence of mitogen PDGFAA, lncOL1-KO OPCs proliferated as cells that expressed both PDGFRα and Ki67 (Figure 4-4A,B). In contrast to efficient differentiation of control OPCs into CNP^+ and MBP^+ OLs upon treatment with T3, lncOL1-KO OPCs exhibited significant deficits in their capacity to differentiate into mature OLs (Figure 4-4C,D), suggesting that the

lack of lncOL1 results in OPCs that are intrinsically defective in differentiation and maturation.

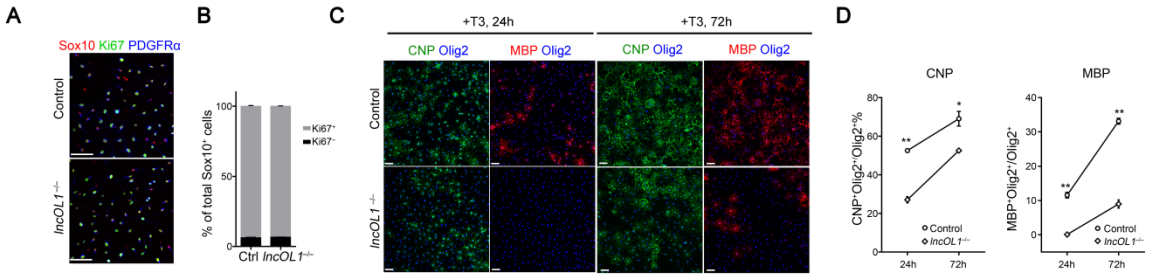

Figure 4-4 lncOL1-deficient OPCs exhibit intrinsic defects in the transition from OPCs to OLs. (A) Immunostaining for Sox10 (red), Ki67 (green), and PDGFRα (blue) on control and lncOL1-null OPCs cultured with PDGFAA and NT3. Scale bar, 50 μm. (B) Quantification of $Ki67^+$ proliferating and $Ki67^-$ non-proliferating OPCs as a percentage of total $Sox10^+$ $PDGFR\alpha^+$ OPCs derived from control or lncOL1-null mice. Data are presented as means ± S.E.M; n = 3 independent experiments. (C) Immunostaining for MBP (red), CNP (green), and Olig2 (blue) on mouse OPCs from control and lncOL1-null mice. Cells differentiated with T3 for 24 and 72 hr are shown. Scale bar, 50 μm. (D) Quantification of the proportions of CNP^+ (left) or MBP^+ (right) OLs in primary mouse OL cultures from control and lncOL1-null mice. Data are presented as means ± S.E.M; n = 2-4 independent experiments; *p <0.005, **p <0.01; one-way ANOVA with post hoc Tukey's test.

lncOL1 is required for OL remyelination after demyelination

Despite downregulation in adult CNS tissues, lncOL1 transcription was reactivated during the subacute phases of spinal cord injury (Figure 3-3). We reasoned that lncOL1 might participate in myelin repair after demyelinating injury. To test this hypothesis, we injected lysolecithin (LPC) into the white matter of adult control and lncOL1-KO mice at P60, when the numbers of myelinated axons and myelin morphology were comparable between lncOL1-KO and wild-type animals (Figure 4-3). Focal injection of LPC induces rapid myelin

breakdown followed by myelin regeneration through an OPC recruitment phase at 7 dpl and a remyelinating phase at 14 dpl (Franklin and Ffrench-Constant, 2008). In normal adult spinal white matter, expression of lncOL1 was hardly detectable; however, lncOL1 levels were increased over the course of remyelination following LPC-induced demyelination (Figure 4-5A-C).

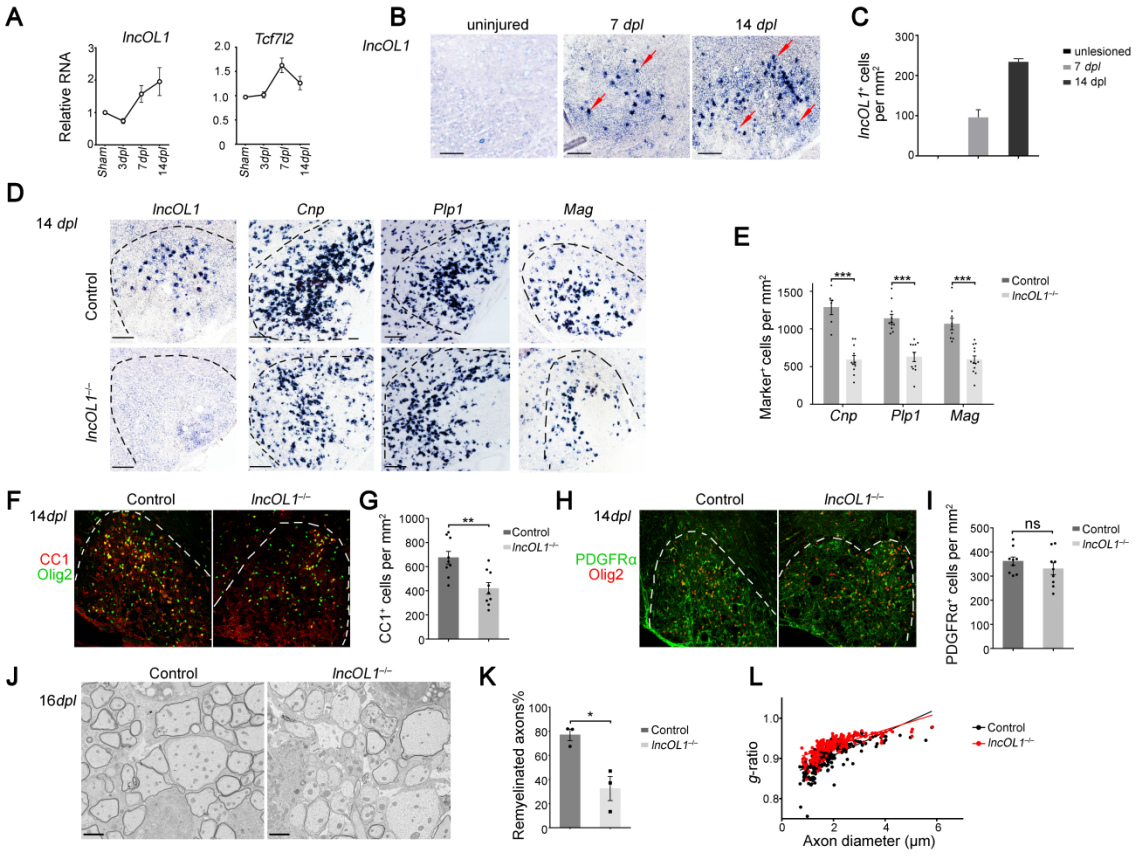

Figure 4-5 lncOL1 is required for myelin repair. (A) qRT-PCR analyses for lncOL1 and Tcf7l2 levels in spinal cord lesions at various time points post LPC-induced demyelination. Data are presented as means ± S.E.M; n = 4 animals at each time point. *dpl*, day post-lesion. (B) In situ hybridization for lncOL1 in representative spinal cord lesions from 8-week old

wildtype control mice at 7 and 14 dpl. Scale bars, 100 μm. (C) Quantification of lncOL1-expressing cells in unlesioned and lesioned regions of spinal cords of wildtype control mice at 7 and 14 dpl. Data are presented as means ± S.E.M; n = 3; Student's t-test. (D) In situ hybridization for lncOL1, Plp, Cnp, and Mag in representative spinal cord lesions from control and lncOL1-KO mice at 14 dpl. Scale bars, 100 μm. (E) Quantification of mature OLs in 14 dpl demyelinated spinal cord of lncOL1-null and control mice. Data are presented as means ± S.E.M; n = 9, ***p < 0.001; Student's t-test. (F) Immunostaining for CC1 (red) and Olig2 (green) in representative spinal cord lesions from control and lncOL1-KO mice at 14 dpl. Scale bar, 100 μm. (G) Quantification of $CC1^+$ OLs in lesions at 14 dpl. Data are presented as means ± S.E.M; n = 9, **p < 0.01; Student's t-test. (H) Immunostaining for PDGFRα (green) and Olig2 (red) in representative LPC-induced lesions from control and lncOL1-KO mice at 14 dpl. Scale bar, 100 μm. (I) Quantification of $PDGFR\alpha^+$ OPCs in lesions at 14 dpl. Data are presented as means ± S.E.M; n = 9. (J) Representative electron microscopy images of LPC-induced lesions from control and lncOL1-KO mice at 16 dpl. Scale bar, 2 μm. (K) The percentage of remyelinated axons in LPC-induced lesions of control and lncOL1-KO mice at 16 dpl. Data are presented as means ± S.E.M; n = 3, *p < 0.05; Student's t-test. (L) The myelin g-ratio in LPC-induced lesions of control and lncOL1-KO mice at 16 dpl. n = 3 animals/genotype, p < 0.001; Student's t-test.

To determine the potential role of lncOL1 in OL remyelination, we examined the re-appearance of myelin genes and OLs in the lesion during regeneration processes. At 14 dpl, we observed an increase of myelin genes *Cnp*, *Plp1*, *Mbp*, *Mag*, or $CC1^+$ OLs in control animals, whereas expression of these myelin genes and the number of $CC1^+$ OLs were substantially reduced in *lncOL1* mutants (Figure 4-5D-G). In contrast, loss of lncOL1 did not appear to impair the recruitment of $PDGFR\alpha^+$ OPCs as numbers of OPCs in lesions were comparable between control and lncOL1-null animals (Figure 4-5H,I). Ultrastructural analysis indicated that there were far fewer myelinated axons in the lesions of lncOL1-KO mice than in controls (Figure 4-5J,K). In addition, newly generated myelin sheaths around axons at 14 dpl were substantially thinner in lncOL1-KO mutants than in controls (Figure 4-

5L). Thus, these observations suggest that lncOL1 is crucial for OL remyelination, but not OPC formation, in the context of white matter injury.

lncOL1 interacts with the Suz12/PRC2 complex to control OL differentiation program

Given that nuclear lncRNAs have been shown to regulate gene expression through interactions with specific protein partners(Maass et al., 2014), we hypothesized that lncOL1 exerts its regulatory function through interaction with certain transcriptional regulators. To identify potential lncOL1-interacting proteins, we adopted a sequence-based RNA-protein interaction prediction algorithm catRAPID (Bellucci et al., 2011) and identified a cohort of candidate lncOL1 interacting partners. Among the candidates was Suz12, which is required for the enzymatic activity of polycomb repressive complex 2 (PRC2). PRC2 is an epigenetic regulator that participates in transcriptional repression by catalyzing histone H3 trimethylation (Conway et al., 2015). The canonical PRC2 complex consists of Eed, Suz12, and the histone methyltransferase Ezh2, which is required for PRC2 activity.

To test whether lncOL1 and Suz12 form a ribonucleoprotein complex, we transiently transfected HEK293T cells with plasmids expressing lncOL1 RNA and HA-tagged Suz12 and performed RNA immunoprecipitation using an anti-Suz12 antibody. lncOL1 was present in the Suz12 immunocomplex but the control, Gapdh mRNA, was not (Figure 4-6A). Furthermore, biotin-labeled full-length lncOL1 RNA, but not control RNA, robustly enriched Suz12 protein from cell lysates of 293T cells that overexpress Suz12 (Figure 4-6B), confirming the association between lncOL1 and Suz12 in a complex. More importantly, the *lncOL1*-Suz12 interaction *in vivo* was further confirmed by purifying endogenous Suz12 in primary mouse oligodendrocytes and analyzing co-purified RNA by qRT-PCR. *lncOL1* was

specifically enriched in Suz12 immunoprecipitates compared to the control RNA (Figure 4-6C). We also confirmed that *lncOL1* specifically interacted with Suz12 and other components of PRC2 complex, e.g Ezh2 and Eed, in Oli-Neu cells cultured under differentiation conditions (Figure 4-6D,E). These protein-RNA interaction studies suggest that lncOL1 and Suz12 form a complex in OLs.

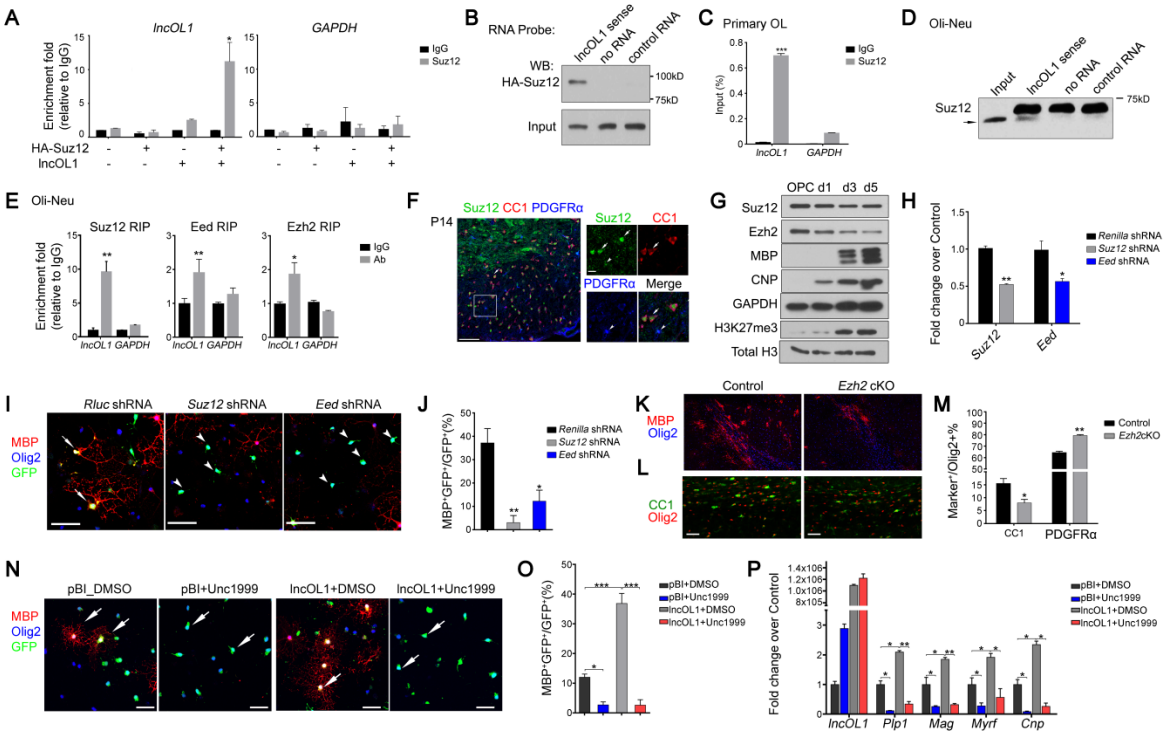

Figure 4-6 lncOL1 interacts with Suz12/PRC2 complex in OLs. (A) HEK293T cells overexpressing HA-tagged Suz12 and pBI-lncOL1 were lysed and precipitates with anti-Suz12 antibody and control IgG were analyzed using qRT-PCR for lncOL1 and Gapdh. Data are presented as mean ± S.E.M; n = 3 independent experiments. *p < 0.05; Student's t-test. (B) Immunoblot for HA-Suz12 after RNA pulldown with biotin-labeled lncOL1 RNA or biotin-labeled RNA control. Pulldown by streptavidin magnetic beads with no RNA probe or control RNA probe (OPC-expressing *Bmp4* RNA) was used as controls. (C) lncOL1 and Gapdh quantification by qRT-PCR in Suz12 immunoprecipitates from primary mouse oligodendrocytes. Data are presented as means ± S.E.M; n = 3. **$p < 0.01$; Student's *t*-test.

(D) Immunoblot for endogenous Suz12 in differentiating Oli-Neu cells after RNA pulldown with biotin-labeled lncOL1 RNA or biotin-labeled RNA control (OPC-expressing *Bmp4* RNA). Pulldown by streptavidin magnetic beads without RNA probe as a negative control. The larger band appeared as a non-specific protein associated with beads. (E) lncOL1 and Gapdh quantification by qRT-PCR in Suz12, Eed and Ezh2 immunoprecipitates from differentiating Oli-Neu cells. Data are presented as means ± S.E.M; n = 3-4 independent experiments. $^{**}p < 0.01$; Student's *t*-test. (F) P14 mouse spinal cord transverse sections immunostained for Suz12 (green), CC1 (red), and PDGFRα (blue). Scale bar, 100 μm. Boxed area is shown at higher magnification on right; scale bar, 20 μm. (G) Immunoblotting for PRC2 components (Eeh2, Suz12), MBP, CNP, H3K27me3, histone H3 total, and GAPDH in rat OPCs at 0, 1, 3, and 5 days of culture under differentiation conditions. (H) qRT-PCR analyses of Suz12 and Eed in Oli-Neu cells transduced with retroviral vectors for expression of shRNAs targeting Renilla luciferase (Rluc) as a control (Ctrl), Suz12, or Eed. * p <0.05, *** p <0.001; Student's t-test. (I) Immunostaining for MBP (red) and Olig2 (blue) after 72 hr of differentiation induced by T3 in GFP^+ mouse OPCs transduced with retroviral vectors for expression of shRNAs targeting Renilla luciferase, Suz12, or Eed. White arrows indicate control transfected MBP^+ OLs; arrowheads indicate shSuz12 or shEed transduced cells, respectively. Scale bar, 50 μm. (J) Quantification for the percentage of MBP^+ among GFP^+ transduced cells. Data are presented as means ± S.E.M; n = 3 independent experiments; *p < 0.05, **p < 0.01; one-way ANOVA with post hoc Tukey's test. (K) Immunofluorescence labeling for Olig2 (blue) and MBP (red) in P7 control and $Ezh2^{flf}$; Olig1-Cre corpus callosum. Scale bars, 100 μm. (L) Immunofluorescence labeling for Olig2 (red) and CC1 (green) in P7 control and $Ezh2^{flf}$; Olig1-Cre corpus callosum. Scale bars, 50 μm. (M) Quantification of $CC1^+$ OLs and $PDGFR\alpha^+$ OPCs as a percentage of total $Olig2^+$ cells in P7 control and Ezh2cKO corpus callosum. Data are presented as means ± S.E.M; n = 2-4 animals; * p <0.05, ** p <0.01; Student's t-test. (N) Immunostaining for MBP (red) and Olig2 (blue) after 72 hr of differentiation (PDGFAA and NT3 withdrawal). DMSO or 1μM Unc1999 were added to culture medium as indicated. Scale bar, 25 μm. (O) Histogram depicting quantification of the percentage of MBP^+ cells among GFP^+ cells. Data are presented as means ± S.E.M; n = 4 independent experiments; *p < 0.05, **p < 0.01; one-way ANOVA with post hoc Tukey's test. (P) qRT-PCR analyses of OL-differentiation associated genes in rat OLs transduced with control or lncOL1-overexpressing vectors in the absence or presence of 1μM Unc1999. Data are presented as means ± S.E.M; n = 4 independent experiments; *p < 0.05, **p < 0.01; one-way ANOVA with post hoc Tukey's test.

A Suz12-PRC2 complex is required for *lncOL1*-dependent OL differentiation

Similar to *lncOL1*, Suz12 was detected in oligodendrocyte lineage cells, marked by PDGFRα or CC1, in the spinal white matter at P14 (Figure 4-6F). Intriguely, whereas Suz12 protein levels were slightly downregulated during OPC differentiation *in vitro*, H3K27me3 levels, similar to that of *lncOL1* transcripts, substantially increased as OLs became mature (Figure 4-6G), pointing to a possible regulation between *lncOL1* and Suz12-mediated gene silencing during OL maturation. To evaluate the functional role of Suz12-PRC2 complex, we knocked down Suz12 and Eed expression in mouse OPCs using retrovirally-expressed shRNAs (Shi et al., 2013) (Figure 4-6H). Similar to the lncOL1-deficient OPCs, cells with Suz12 or Eed silencing exhibited a defect in differentiation into MBP^+ OLs compared to control OPCs upon withdrawal of mitogens (Figure 4-6I,J), indicating that PRC2 integrity is required for proper OL maturation in vitro. In addition, selective ablation of the Ezh2 floxed allele with OL lineage-expressing Olig1-Cre (*Ezh2*$^{fl/fl}$*;Olig1-Cre*$^{+/-}$) in mice led to a dramatic reduction of $CC1^+$ and MBP^+ OLs (Figure 4-6K-M), with an increase of OPC fraction within the OL lineage, as compared with heterozygous controls (*Ezh2*$^{fl/+}$*;Olig1-Cre*$^{+/-}$). Consistently, interference of Ezh1/2 enzymatic function by the small molecule inhibitor Unc1999 (Konze et al., 2013) diminished OL formation and the induction of myelin-associated genes (Mbp, Plp1, Mag, Cnp, and Myrf) (Figure 4-6N-P). More importantly, the enhancement of OL differentiation driven by ectopic lncOL1 expression was overridden by Unc1999-mediated inhibition of PCR2 activity (Figure 4-6N-P), suggesting that *lncOL1*-dependent OL differentiation requires the function of Suz12-PRC2 complex.

lncOL1 acts as a modulatory factor for Suz12 to silence the OPC gene program during OL differentiation

To investigate the mechanism underlying lncOL1 functions in OPC differentiation, we performed transcriptome profiling analysis of gene expression alteration in differentiating OLs between lncOL1-KO and control OPCs under differentiation conditions. Consistent with an impaired OL differentiation phenotype, lncOL1 deletion caused a reduction in expression of OL-enriched genes (Zhang et al., 2014) (gene Module I) and an increase in expression of OPC-enriched genes (gene Module II) (Zhang et al., 2014) (Figure 4-7A,B). Intriguingly, promoters of upregulated genes in OPC-enriched Module II exhibited low levels of active histone modifications, such as H3K27ac and H3K4me3 than those in OL-enriched Module I (Figure 4-7C), suggesting that lncOL1 antagonizes the transcriptional program that maintains OPC state while activating OL differentiation programs. Consistently, gene ontology (GO) analysis revealed that the genes downregulated in lncOL1-null OLs are associated with myelination, cytoskeletal organization, and glial cell differentiation, whereas genes upregulated in lncOL1-null cells are linked to cell growth, proliferation, and neurogenesis (Figure 4-7D,E). Furthermore, RT-PCR analysis confirmed a substantial reduction in mRNAs encoding myelin structural markers (e.g. Mbp, Plp1), regulators of lipid metabolisms (e.g. Pik3r3, Elovl1), and proteins involved in cytoskeleton organization (e.g. Gjc2, Tppp, Matp7) in lncOL1-null OLs compared to controls (Figure 4-7F). However, expression of OPC signature genes, such as Pdgfrα and Cspg4, remains unaltered in lncOL1-depeleted cells (date not shown), suggesting that lncOL1 ablation does not block but delays the transition from OPC to OL. In aggregation, these observations indicate that lncOL1

orchestrates the balance necessary between transcriptional programs to permit OL differentiation.

Given the upregulation of OPC-associated transcriptional program in the absence of lncOL1, we hypothesize that lncOL1 may cooperate with a Suz12-mediated repressive complex to silence the expression of OPC-enriched genes. To determine how lncOL1 and Suz12 regulate the changing chromatin states during OL lineage progression, we performed chromatin immunoprecipitation-sequencing (ChIP-seq) to identify Suz12 binding elements in OPCs. Strikingly, Suz12 was essentially excluded from H3K27ac-enriched enhancers and promoters (Figure 4-7G). Furthermore, expression of Suz12-targeted genes was downregulated substantially as compared to those without proximal Suz12 binding in newly formed OLs and myelinating OLs (Figure 4-7H), suggesting that Suz12 silences the transcription of OPC-enriched genes by deposition of repressive H3K27me3 marks on their enhancers and promoters.

To elucidate whether lncOL1 influences Suz12 function, we assessed the expression of Suz12 targeted genes in differentiating OLs derived from control and lncOL1-KO OPCs. Gene set enrichment analysis (GSEA) demonstrated that the levels of genes targeted by Suz12 were significantly increased in lncOL1-KO cells (Figure 4-7I), suggesting that lncOL1 loss leads to a general de-repression of Suz12-targeted genes. lncOL1-Suz12 target gene sets (genes upregulated in lncOL1-null cells with promoters occupied by Suz12) are associated with cell growth and proliferation, and their expression is enriched in OPCs (Figure 4-7J). These include Igf2 which encodes a insulin-like growth factor 2 that promotes OPC growth and proliferation(Frederick and Wood, 2004; Zhang et al., 2010), H19, which is an imprinted

lncRNA that promotes progenitor cell proliferation(Ratajczak, 2012), and Cyp1b1, which encodes cytochrome P450 family protein that enhances cell proliferation and tumorigenesis (Kwon et al., 2016; Mitsui et al., 2015) (Figure 4-7K),. These genes are highly expressed in OPCs but strongly repressed during OL maturation (Dugas et al., 2006; Zhang et al., 2014), suggesting that their expression maintains OPCs in the precursor state. Furthermore, qRT-PCR analyses indicated that expression of these genes was significantly induced in lncOL1-null OPCs and in cells in which Suz12 expression was silenced (Figure 4-7L,M). Since lncOL1 depletion had no effect on PRC2 core subunit expression (data not shown),we then asked whether the induction of Suz12 targeted genes in *lncOL1* null OLs is due to alteration of Suz12 recruitment. To test this hypothesis, we performed chromatin immunoprecipitation followed by quantitative PCR (ChIP–qPCR) for Suz12 in mouse OLs from control and *lncOL1* deficient mice. The binding of Suz12 was markedly reduced at the promoter of Igf2, H19 and Cyp1b1 in the absence of *lncOL1* (Figure 4-7N), suggesting that lncOL1 is required for Suz12 recruitment in OLs. Collectively, these observations suggest that interacts with Suz12 to promote OL differentiation by promoting the deposition of Suz12 at its targeted gene loci.

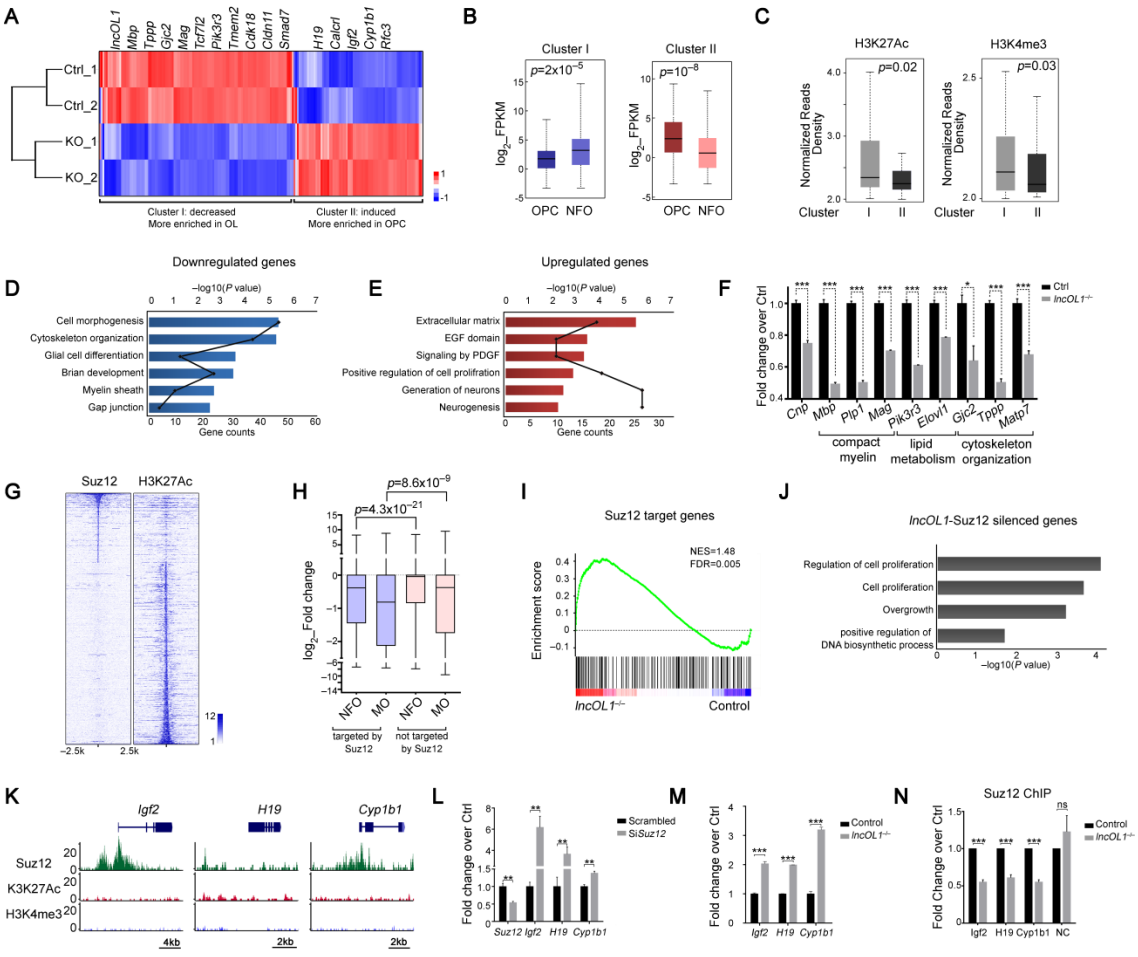

Figure 4-7 lncOL1 acts as a modulatory factor for Suz12 to regulate transcriptome dynamics during OL differentiation. (A) A heatmap showing genes differentially expressed in control and lncOL1-null OLs cultured under differentiation conditions for 24 hr. Modules I and II represent upregulated and downregulated genes compared to wildtype, respectively. Data are from two separate cultures. (B) Box plots for mRNA levels of Module I and II genes in OPCs and newly formed OLs (NFO). Whiskers show the minimum and maximum, boxes extend from the first to the third quartiles with cross lines at the medians. Significance was determined using the Mann-Whitney-Wilcoxon test. (C) Box plots comparing the levels of active histone marks H3K27ac and H3K4me3 in the gene promoters of genes downregulated (Module I) and upregulated (Module II) in lncOL1-null OL lineage cells. Whiskers show the minimum and maximum, boxes extend from the first to the third quartiles with cross lines at the medians. Significance determined using the Mann-Whitney-

Wilcoxon test. (D, E) GO biological process terms enriched among mRNA genes that show significantly decreased (D) or increased (E) expression upon lncOL1 deletion relative to control. (F) qRT-PCR analyses of genes involved in different regulatory arms of OL differentiation. Data are presented as means ± S.E.M; n = 3; *p < 0.05, ***p < 0.001; Student's t-test. (G) ChIP-seq density heatmaps for Suz12 and H3K27ac within 2.5 kb on either side of the Suz12 and H3K27ac peak centers in OPCs. The sites are ranked in descending order of Suz12 intensity. (H) Box plots for $\log_2$ fold change in expression levels of the genes targeted with or without Suz12 in newly formed OLs (NFO) and myelinating OLs (MO) (Zhang et al., 2014) compared to OPCs. Whiskers show the minimum and maximum, boxes extend from the first to the third quartiles with cross lines at the medians. Significance determined using the Mann-Whitney-Wilcoxon test. (I) Gene Signature Enrichment Analysis plot comparing the Suz12-targeted genes (top 500 genes with Suz12 binding peak within ± 50 kb around TSS) in wildtype or lncOL1-KO mouse OLs. NES, normalized enrichment score. FDR: false discovery rate. (J) GO biological process terms enriched among mRNA genes that are targeted by Suz12 with significantly higher expression levels in lncOL1-null OLs. (K) Genome browser tracks over select gene loci with ChIP-seq density mapping of Suz12, H3K27ac, and H3K4me3 from rat OLs. (L) qRT-PCR analyses of Cyp1b1, H19, and Igf2 in control and lncOL1-KO OLs. Data are presented as means ± S.E.M; n = 3 independent experiments, *** p < 0.001; Student's t-test. (M) qRT-PCR analyses of Suz12, Cyp1b1, H19, and Igf2 in primary mouse OLs treated with scrambled or Suz12-targeted siRNAs. Data are presented as means ± S.E.M; n = 5 independent experiments. ** p < 0.01; Student's t-test. (N) ChIP–qPCR analyses for Suz12 at the Igf2, H19, Cyp1b1 promoters or control genomic regions in primary mouse oligodendrocytes from control and *lncOL1*KO mice. Data are presented as means ± S.E.M; n = 3. *** p < 0.001; Student's t-test.

DISCUSSION

The functions of the vast majority of lncRNA transcripts are currently unknown. We identify that lncOL1 is an evolutionally conserved and OL-restricted lncRNA. Enforced expression of *lncOL1* induces precocious OL formation in the developing brain. Inhibition of lncOL1 by siRNA silencing in vitro and CRISPR-mediated targeting *in vivo* establish a critical role of

lncOL1 for the timely initiation of OL myelination. The dramatic impact on the onset of myelination observed upon deletion of lncOL1 is in contrast to the very subtle phenotypes of many lncRNA knockout mice during development (Nakagawa, 2016). Although myelination recovery is observed in the adult lncOL1-null mice, this may indicate the functional redundancy of other factors, which may compensate the loss of lncOL1, and therefore OL differentiation can proceed at later stages in the absence of lncOL1, but at a suboptimal level. The requirement of lncOL1 for the myelination onset is consistent with its upregulation in newly formed myelinating OLs. lncOL1 may act as transiently expressed regulator to boost the initiation of myelinogenesis while subsides when myelination falls into a steady maintenance phase in adulthood.

Epigenetic regulation plays an important role in OL development and myelination (Emery and Lu, 2015). Recent studies have shown that deposition of repressive H3K27me3 marks by the PRC2 complex increases during OL differentiation and contributes to the terminal differentiation of myelinating OLs(Liu et al., 2015; Sher et al., 2012). Our study revealed that lncOL1 directly interacts with Suz12, a core component of the PRC2 complex for H3K27 methylation. We showed that attenuating Suz12 or Eed expression in vitro impaired OL differentiation and that genetic inactivation or pharmacological inhibition of Ezh2 led to a blockage of OL maturation in vivo and in vitro, suggesting that Suz12-PRC2 is crucial for OL differentiation through transcriptional silencing of OPC-enriched gene clusters. More importantly, lncOL1-driven OL differentiation diminished by the loss of Suz12 or PRC2 activity, supporting that lncOL1 exerts its regulatory function through Suz12. Transcriptome profiling of lncOL1-null OLs indicated that lncOL1 perturbation resulted in a

derepression of Suz12 target genes in a trans-regulatory manner, suggesting that lncOL1 is required for the repressive activity of the PRC2 complex on Suz12 target gene expression.

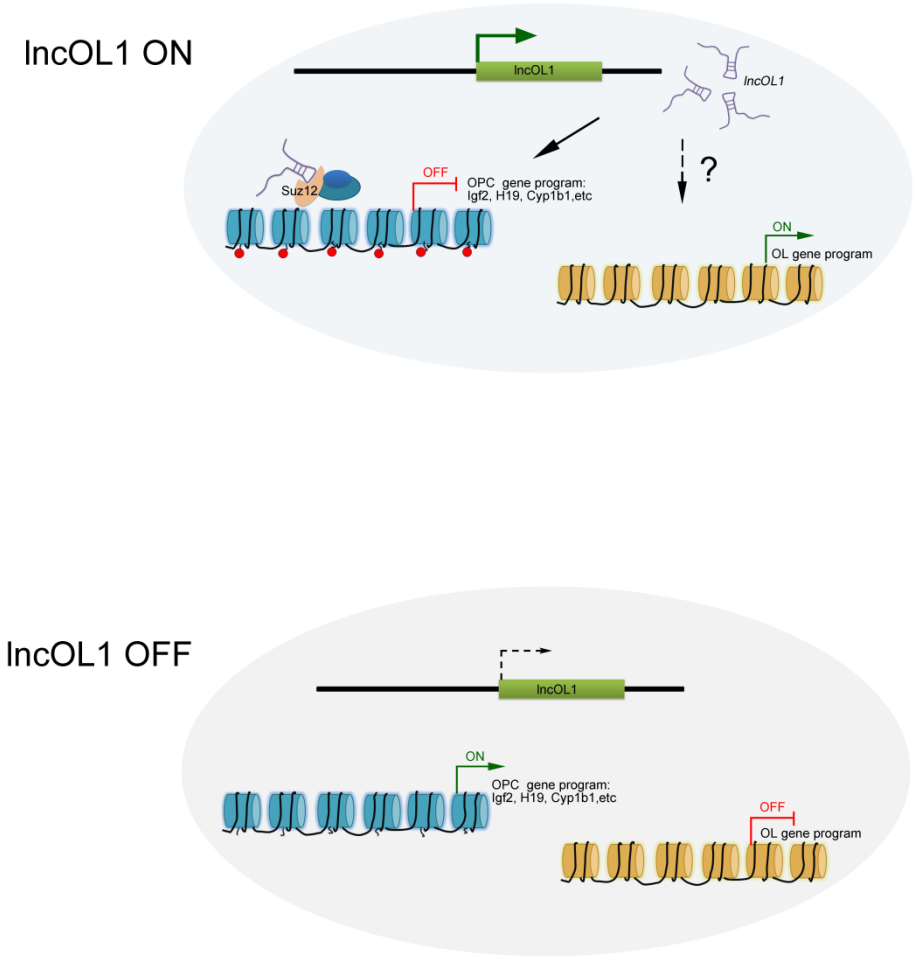

Figure 4-8 Model for the lncOL1-mediated control of OL differentiation. When *lncOL1* expression is turned on, it recruits Suz12-mediatd PRC2 complex and silences OPC gene regulatory program that antagonize their differentiation process, and thereby allow the activation of OL differentiation program. When *lncOL1* expression is off, the OPC-promoting gene program is derepressed and activated, which inhibits OL differentiation processes.

Among PRC2-associated lncRNAs, there appear to be at least two distinct functional mechanisms at play: 1) lncRNA-dependent recruitment or assembly of PRC2 core subunits and 2) modulation of PRC2 enzymatic activity directly by a nascent lncRNA transcript (Kaneko et al., 2014). We find that *lncOL1* interact with Suz12 to form a repressor complex to silence gene transcription through implementing repressive H3K27me3 marks on gene regulatory elements. This aligns with the general theme of increasing heterochromatin and gene silencing as OLs mature(Nielsen et al., 2002). Though further studies will be required to fully elucidate the mechanism behind lncOL1 function, our work suggests that lncOL1 promotes OL differentiation, in part, by modulating the recruitment of Suz12 to silence the OPC-enrichment network including Igf2 and H19 that maintain OPCs in the precursor state. Thus, the lncOL1 interaction with Suz12 forms a repressor complex to control the balance between OPC maintenance and OL differentiation (Figure 4-8), suggesting an important role of the interplay between lncRNAs and chromatin remodeling factors in OL development.

lncRNAs in myelin repair

Functional studies of lncRNAs in cardiac and liver regeneration indicate that lncRNAs, like miRNAs, likely act as fine-tuning factors that enable cells and organs to respond to stress, injury, and chronic disease (Ounzain and Pedrazzini, 2015; Xu et al., 2013). In line with this, our study demonstrates that expression of lncRNAs is dynamically regulated across remyelinating phases. In particular, we showed that lncOL1 is reactivated and required for robust OL regeneration after demyelinating injury. The crucial role of lncOL1 in the regulation of OL differentiation and remyelination highlights a therapeutic potential of

lncRNAs as a molecular therapy to enhancing myelin regeneration. Given the unique expression pattern of individual lncRNAs in the OL lineage, modulation of OL-restricted lncRNA expression will not impact other cell types and would provide unique therapeutic avenues for promoting myelin repair in demyelinating diseases with lower odds of side effects.

CHAPTER FIVE

METHODS AND MATERIALS

Animals/Subjects

All animal studies were approved by the Institutional Animal Care and Use Committees of the Cincinnati Children's Hospital Medical Center, USA, and Sorbonne Universités, UPMC University Paris 06, France. MRI images of CHARGE patients including males and females from age 2 to age 15 were evaluated by neuroradiologists and compared with age-matched controls. All human patient images were obtained with informed consent as outlined by the institutional review board at the Cincinnati Children's Hospital Medical Center. The mouse strains used in this study were generated and maintained on a mixed C57Bl/6;129Sv background and housed in a vivarium with a 12-hour light/dark cycle.

To generate Chd7cKO (*Chd7$^{f/f}$;Olig1-Cre$^{+/-}$*) and heterozygous control (*Chd7$^{f/+}$;Olig1-Cre$^{+/-}$*) mice, mice homozygous for floxed alleles of Chd7 (*Chd7$^{f/f}$*) (Hurd et al., 2010) were crossed with mice carrying Cre recombinase driven by the *Olig1* promoter (*Olig1-Cre$^{+/-}$*) (Xin et al., 2005) Generation of *Brg1*cKO mice has been described previously (Yu et al., 2013b). Briefly, *Brg1$^{f/f}$* mice (Sumi-Ichinose et al., 1997) were crossed with *Olig1-Cre* mice to generate Brg1cKO (*Brg1$^{f/f}$;Olig1-Cre$^{+/-}$*) and heterozygous control (*Brg1$^{f/+}$;Olig1-Cre$^{+/-}$*) mice. *Osterix/Sp7* mutant mice have been described previously (Nakashima et al., 2002), in which an IRES-lacZ-polyA/loxP-flanked PGK neo-bpA cassette is inserted into the second coding exon of *Osterix.* To generate Chd7 conditional inducible knockout mice, *PDGFRα-*

CreER^{T} *BAC* mice (Kang et al., 2010) and *Rosa26*^{tdTomato}reporter mice (Ai14, Jax laboratory) were crossed with *Chd7*$^{f/f}$ mice.

lncOL1 mutant mouse lines were generated using four sgRNAs. sgRNA target sequences are 5' to exon1; catatcacgctattatgcac; 5' to exon1; acttcttcgtgcagctgact; exon 4, tgaccacccattttgatctc; intron 3 and exon4 junction; gggtggtcatctcctgtgta. The sgRNA design and vector construction were described previously (Ran et al., 2013). Briefly, pairs of complementary DNA oligos with compatible overhangs were annealed and cloned into a pX458 vector that carries a U6 promoter to drive sgRNA expression and a ubiquitously expressed promoter to drive Cas9-2A-GFP expression (Addgene plasmid #43138). sgRNA editing activity was then evaluated in mouse mK4 cells (Valerius et al., 2002) by the T7E1 assay (New England Biolabs), and compared side-by-side with Tet2 sgRNA that has been shown to modify the mouse genome efficiently (Wang et al., 2013). Validated sgRNAs and Cas9 mRNA were *in vitro* transcribed using MEGAshorscript T7 kit and mMESSAGE mMACHINE T7 ULTRA kit (Life Technologies), respectively, according to manufacturer's instruction. sgRNAs and Cas9 mRNA were mixed at a concentration of 50 ng/μl each and 100 ng/μl, respectively, and injected into the cytoplasm of one-cell-stage embryos of B6D2F2 genetic background (Yang et al., 2014). Injected embryos were immediately transferred into the oviductal ampulla of pseudo-pregnant CD-1 females. Progeny was genotyped using the following primers: VS3086: 5'-actgggtattactttctggagcg-3'; VS3089: 5'-gaaatgtgggaagcagcgc-3'. Appearance of 654 bp band indicated large deletion at the *lncOL1*

locus and resulting PCR product was subjected to sequencing to detect the editing sites on genome. *lncOL1* mutant mice were back-crossed with C57/BL6 for three generations.

Mice homozygous for floxed alleles of Ezh2 ($Ezh2^{fl/fl}$) (Shen et al., 2008) were crossed with mice carrying Cre recombinase driven by the *Olig1* promoter (Olig1-$Cre^{+/-}$) (Xin et al., 2005) to generate Ezh2cKO ($Ezh2^{fl/fl}$;Olig1-$Cre^{+/-}$) and heterozygous control ($Ezh2^{fl/+}$;Olig1-$Cre^{+/-}$) mice.

Primary OPC and OL isolation and culture

Primary rat OPCs were isolated as described (Chen et al., 2007) with the minor modifications. Briefly, mixed glial cells were initially cultured in DMEM-F12 medium supplied with 15% FBS, then switched to B104 conditioned medium for 2 days before isolating OPCs by mechanical detachment in an orbital shaker. Isolated rat OPCs were grown in Sato growth medium supplemented with mitogens 10 ng/ml PDGF-AA and 20 ng/ml bFGF, and differentiated in OL Differentiation Medium (Sato medium supplemented with 15 nM triiodothyronine and 10 ng/ml ciliary neurotrophic factor). Mouse OPCs were isolated from P5-P6 cortices by immunopanning with antibodies against Ran-2, GalC and O4 sequentially as previously described (He et al., 2016).

Lentivirus/Retrovirus generation and transduction

To generate lentiviruses containing shRNAs targeting murine lncOL1, shRNAs against *lncOL1* were cloned into a lentiviral expressing vector (PLKO.3G, a gift from Dr. Luis Prada). Lentiviruses were prepared by cotransfected lentiviral expressing vectors with packaging vectors pMD2.G and psPAX2 (Addgene) into 293T cells using Polyjet

transfection reagents (SignaGen labs). 48 hours after transfection, viral supernatants were collected and filtered through a 0.45 μm filter, then concentrated by Lenti-X Concentrator (Clontech, # 631231) according to the manufacturer's instructions.

To generate retroviruses containing shRNAs against Eed and Suz12, retroviral expressing vectors were transfected into Platinum-E (Plat-E) retroviral packaging cell lines. 48 hours after transfection, viral supernatants were collected and filtered through a 0.45 μm filter, then concentrated by ultra-centrifuging at 19,400 rpm for 2 hours at 4 degree.

OPCs were infected at multiplicity of infection (MOI) of 50 (MOI was determined in human 293T cells).

Tissue processing and in situ hybridization

Mice at various developmental stages were anesthetized with ketamine/xylazine and perfused with PBS followed by 4% paraformaldehyde (PFA). Spinal cords or brains were dissected, fixed in 4% PFA overnight, dehydrated in 20% sucrose at 4°C, embedded in OCT and cryosectioned at 16μm. For tamoxifen treatment of *PDGFRα-CreER^{T}-Chd7$^{f/f}$* mice, tamoxifen (T5648) was dissolved in corn oil (Sigma, C-8267) and injected intraperitoneally at 3 mg/40 gram (body weight) per day. *In situ* hybridization was performed as previously described (Lu et al., 2002). Digoxigenin-labeled riboprobes used in the study were: murine *Mag*, *lncOL1*, *Cnp*, *Mbp, Plp/Dm-20,*and *Pdgfra.*

Immunohistochemistry and immunoblotting

Cryosections (16-μm thick) or vibratome sections (50-μm thick) were permeabilized and blocked in blocking buffer (0.3% Triton X-100 and 5% normal donkey serum in PBS) for 1 h at room temperature and overlaid with primary antibodies overnight at 4 °C. After washing with 0.4% Triton X-100 in PBS, cells or sections were incubated with secondary antibodies conjugated to Cy2, Cy3 or Cy5 (Jackson ImmunoResearch Laboratories) for 2 h at room temperature, stained in DAPI for 5 min, washed in PBS and mounted with Fluoromount-G (SouthernBiotech). Cell images were quantified in a double-blinded manner. . Antibodies used in the study were: rabbit anti-Olig2 (Millipore, AB9610), rat anti-PDGFRα (BD Bioscience, 558774), mouse anti-APC (CC1, Oncogene Research, OP80), goat anti-MBP (Santa Cruz Biotechnology, sc-13914), rabbit anti-Sip1 (Santa Cruz Biotechnology, sc-48789), mouse anti-Cnp, rabbit anti-Ki67 (Abcam, ab15580), rabbit anti-Suz12 (Cell Signaling Technology, #3737), rabbit anti-Chd7 (Abcam, AB38124, 1:600), goat anti-Osterix/Sp7 (Santa Cruz Biotechnology, sc-22538, 1:300), rabbit anti-Creb3l2 (Santa Cruz Biotechnology, sc-366044, 1:300).

For immunoblotting, whole cell lysates were prepared by using 1× Passive Lysis Buffer (Promega, Madison) supplemented with a protease inhibitor cocktail (1:200, Sigma, St. Louis, MO). After western blotting, proteins were detected with appreciate secondary antibodies by using chemiluminescence with the ECL kit (Pierce) according to the instructions of the manufacturer. Antibodies used in the study were: rabbit anti- Histone H3 (Cell Signaling Technology, #4499), rabbit anti-Ezh2 (Cell Signaling Technology, #5246),

mouse anti-H3K27me3 (Active Motif, 39155), goat anti-MBP (Santa Cruz Biotechnology, sc-13914), mouse anti-CNP (BioLegen, #836401).

Electron microscopy

Tissue processing was performed essentially as described previously (Yu et al., 2013b). Briefly, mice were deeply anesthetized with ketamine/xylazine, perfused with 0.1M cacodylate, followed by 2.5% paraformaldehyde/2.5% glutaraldehyde in 0.1 M cacodylate (pH 7.2). Spinal cords and optic nerves were dissected, postfixed in 1% OsO4, dehydrated through a graded ethanol series, infiltrated in propylene oxide and embedded in resin. Semithin sections were stained with toluidine blue and ultrathin sections were stained with lead citrate.

Stereological estimation of white matter volume

White matter area was determined by measuring the MBP immunoreactive region as previously described (Hedtjarn et al., 2005). The volumetric analysis of MBP-positive tissue was performed according to the method described previously (Roughton et al., 2013)using the following formula: $V=SA \cdot p \cdot T$, where V is the total volume, SA is the sum of the area measured, p is the inverse of the section sampling fraction, and T is the section thickness.

Lysolecithin-induced demyelinating injury

Lysolecithin-induced demyelination was carried out in the ventrolateral spinal white matter of approximately 8-week-old mice. Anesthesia was induced and maintained by peritoneal injection of a mixture of ketamine (90 mg/kg) and xylazine (10 mg/kg). After exposing the

spinal vertebrae at the level of T9-T12, meningeal tissue in the intervertebral space was cleared, and the dura was pierced with a dental needle. 0.5 µl of 1% lysolecithin (L-a-lysophosphatidylcholine) via a Hamilton syringe attached a glass micropipette was injected into the ventrolateral white matter via a stereotactic apparatus. Spinal cord tissues carrying the lesions were collected 14 dpl, which represents OL differentiation and new myelin sheath formation (at least 5 mice per control and mutant groups were used for each time point analysis). Animals were to recover in a warm chamber before being returned into their housing cages. LPC-induced injuries were conducted in a genotype-blinded manner.

In Utero Electroporation

In utero electroporation was performed on E14.5 embryos from timed pregnant wild-type CD1 (Charles River) as previously described (Zhao et al., 2010). Expressing vectors used were PBI-ZsGreen (vector control) and PBI-ZsGreen-*lncOL1*. Embryos were harvested 72 hrs after electroporation for analysis.

RNA fluorescence in situ hybridization

RNA FISH probes were labeled with Alexa Fluor 594 dye (Invitrogen, # F32954). Before the hybridization, the adherent cells on glass coverslips were fixed (10 min with 4% formaldehyde), permeabilized with 70% EtOH and dehydrated in 80%, 95%, and 100% v/v ethanol for 3 min each. Prior to the hybridization, the cells were rehydrated with wash buffer containing 10% formamide (Ambion, #AM9342) and 2× SSC (Ambion, #cat. no. AM9765) for 5 min. FISH RNA probe was denatured at 80 °C for 5min and kept on ice for 3min. Cells were incubated with denatured probes at 55 °C overnight. After hybridization, the cells were

washed in 50% formamide and 2X SSC v/v at 42 °C for 15 min three times (with the addition of DAPI in the last wash) and then in 2XSSC three times.

Cellular Fractionation and RNA Extraction

Subcellular RNA was extracted as previously described (Wang et al., 2008). Oli-neu cells were lysed in RSB-100 buffer (100 mM Tris-HCl pH 7.4, 100 mM NaCl, 2.5 mM MgCl2, 40 μg/ml digitonin) followed by centrifugation at 2,000xg for 10 min. The supernatant fraction was collected as cytosolic fraction. The cell pellet was then resuspended in RSB-100 containing 0.5% Triton X-100 (RSB-100T). After centrifugation at 2,000g for 8 min, the supernatant was collected as nuclear fraction. The resulting cell pellet was resuspended in RSB-100T and sonicated (Fisher Sonic Dismembrator, Model 300). The soluble DNA-bound RNA fraction was collected after centrifugation at 4,000g for 15 min. RNA was extracted with Trizol (Invitrogen) and treated with RNase-free DNase I (DNA-free; Ambion).

RNA Immunoprecipitation

20 million Oli-neu cells were lysed in 1 ml of lysis buffer (150 mM KCl, 25 mM Tris-HCl, pH 7.4, 5 mM EDTA, 5 mM MgCl2, 1% NP-40, 1× protease inhibitor, 0.5 mM DTT, 100 U/ml RNAseOUT) for 30 min at 4 °C. The lysate was centrifuged at 13,000 r.p.m. for 30 min and the resulting protein lysate was incubated with 8 μg of Suz12 or IgG antibody (Anti-Suz12, Abcam, ab12073; anti-Eed, Millipore, #17-10034; anti-Ezh2, Cell Signaling Technology, #4905; normal rabbit IgG, Santa Cruz, sc-2027) at 4 °C overnight. Then 45 μL of protein G Dynabeads (Life Technologies, cat. no. 10003D) that were previously washed twice in 500 μL lysis buffer were added to the lysate and antibody mix. The lysate, antibody

and beads were incubated at 4 °C for another 2 h. The beads were washed five times (5 min each) with 1 mL of lysis buffer. The RNA was extracted by addition of 1 mL of Trizol (Life Technologies, cat. no. 15596-018) to the beads. For the total input RNA, 10% of the input lysate was mixed with 1 mL of Trizol. For 1 ml of Trizol, 200 µL of chloroform was added, and the mix was centrifuged at 4 °C at 13,000 r.p.m. for 15 min. The aqueous layer was then added to 1 volume of isopropanol, 1/10 volume KOAc and 1 µL of glycoblue and kept at −20 °C for at least one hour. The samples were then centrifuged at 13,000 r.p.m. at 4 °C for 30 min. The supernatant was removed, and the pellet was washed with 1 mL of ice-cold 70% EtOH twice. The pellet was then resuspended in 20 µL of RNase-free water.

Quantitative PCR analysis

For RNA quantification, total RNA was extracted per the Trizol (Life Technologies) protocol and cDNA was generated with iScript™ cDNA Synthesis Kit (Bio-Rad). qRT-PCR was performed using the ABI Prism 7700 Sequence Detector System (Perkin-Elmer Applied Biosystems). qTR-PCR primers used to detect gene expression levels or genomic enrichment were:

Gene Symbol	Species	Experiment	Sequence
lncOL1	Mouse	RT-qPCR	*lncOL1*-f1: gtacaagaccatccagcataca *lncOL1*-r1: ccttgcatgtggctcaataaag *lncOL1*-f2: caggagatgaccacccattt *lncOL1*-f2: atcatggagcttcaggttcag *lncOL1*-f3: cattggcttcctgagacatagt *lncOL1*-r3:ggagcacacctgtgatcttatt *lncOL1*-f4: ccatcctggttgctaccatatac *lncOL1*-r4: attggtggtttggaagagagg *lncOL1*-f5: ctgcatgctccacttcagta *lncOL1*-r5: tatgcaaagccctgggtatc

lncOL2	Mouse	RT-PCR	*lncOL2*-f: cataggaggtccacagcattag *lncOL2*-r: gcttagagaagaggtggcatatc
lncOL3	Mouse	RT-qPCR	*lncOL3*-f: gtctccaggtcttggcataaa *lncOL3*-r: attcactcccatgaggaacac
lncOL4	Mouse	RT-qPCR	*lncOL4*-f: agagagacagcggagattca *lncOL4*-r: gctgcaattggtactggatttg
Plp1	Mouse/Rat	RT-qPCR	*Plp1*-f: tgctcggctgtacctgtgtacatt, *Plp1*-r: tacattctggcatcagcgcagaga
Mbp	Mouse/Rat	RT-qPCR	*Mbp*-f: tcacagaagagaccctcaca *Mbp*-r: gccgtagtgggtagttcttg
Cnp1	Mouse/Rat	RT-qPCR	*Cnp1*-f: tccacgagtgcaagacgctattca *Cnp1*-r: tgtaagcatcagcggacaccatct
H19	Mouse	RT-qPCR	*H19*-f: tgctgcaatcagaaccactac *H19*-r: ggtgctatgagtctgctctttc
Mag	Mouse/Rat	RT-qPCR	Mag-f: atcctagccacggtcatcta Mag-r: tcagccacacaccagtattc
Igf2	Mouse	RT-qPCR	Igf2-f: ccctcagcaagtgcctaaa Igf2-r: ggataccaggccaattcatagt
Gjc2	Mouse	RT-qPCR	Gjc2-f: ttgtgacaacgtctgctatga, Gjc2-r, gacagaaggtgtggagatgac;
Cyp1b1	Mouse	RT-qPCR	Cyp1b1-f: tggccctttcctcctatct Cyp1b1-r: actgacacaacctgcgtatc
GAPDH	Mouse/Rat	RT-qPCR	Gapdh-f: tgccaaatatgatgacatcaagaa Gapdh-r: ggagtgggtgtcgctgttg.
Chd7	Mouse	RT-qPCR	*Chd7-f*: gcctctcatcacgtacagca *Chd7-r*: ggatgggggatttgtcctac
Elovl1	Mouse	RT-qPCR	*Elovl1*-f: gaaagggctggacacttactt *Elovl1*-r: cctcttcagtgtgaggagaaag
Creb3l2	Mouse	RT-qPCR	*Creb3l2*-f: aagaatacatggacagcctgg *Creb3l2*-r: ttccccatcaccaaagtctg
Osterix	Mouse	RT-qPCR	*Osterix*-f: ccacccattgccagtaatct *Osterix*-r:ggagccatagtgagcttcttc

Igf2 promoter	Mouse	ChIP-qPCR	Igf2-f: gagacagagtgaacgtgaaagg Igf2-r: tcgcctacccaagtggatta
H19 promoter	Mouse	ChIP-qPCR	H19-f: gactgcgatgtacgagacttc H19-r: atcaacaaggtcggcttactc
Cyp1b1 promoter	Mouse	ChIP-qPCR	Cyp1b1-f: tgctcagagtagtgaccgaa Cyp1b1-r: ctgaatggagagagtgccatc

Pulldown with biotinylated RNA

RNA pull-down assay was performed essentially as previously reported with minor modifications (Tsai et al., 2010). The cloned-in transcript in pBlueScript II SK plasmid vector was linearized with NotI. Phenol-chloroform–extracted and ethanol-precipitated template was then transcribed with T3 RNA polymerase (Promega, P2083) and biotin-RNA labeling mix (Roche, 11685597910). The in vitro transcriptions were first treated with DNase (Promega, M6101), and then purified with RNeasy Mini Kit (QIAGEN). Prior to pull-down, three micrograms of biotinylated RNA was heated to 90°C for 2 minutes, put on ice for 2 minutes, supplied with RNA structure buffer (10 mM Tris pH 7, 0.1 M KCl, 10 mM MgCl2), and then shifted to room temperature (RT) for 20 minutes to allow proper secondary structure formation. 20 million Oli-neu cells were lysed in 1 ml of lysis buffer (150 mM KCl, 25 mM Tris-HCl, pH 7.4, 5 mM EDTA, 5 mM MgCl2, 1% NP-40, 1× protease inhibitor, 0.5 mM DTT, 100 U/ml RNAseOUT) for 30 min at 4 °C. The lysate was centrifuged at 13,000 r.p.m. for 30 min. The RNA was incubated in the lysate for 2 h at 4 °C rocking, after which 40 μL of MyOne Streptavidin T1 beads was added to the mix. The beads were washed five times (5 min each) with 1 ml of the wash on a magnetic rack and boiled in SDS buffer, and the retrieved protein was detected by standard western blot technique.

RNA Extraction and RNA-Sequencing

Total RNA was extracted from samples using the RNeasy Plus mini kit (Life Technologies, Carlsbad, CA, USA). The resulting RNA samples were then used as input for library construction with TruSeq Stranded mRNA Library Prep Kit, according to the manufacturer's instructions. RNA libraries were then sequenced on the Illumina HiSeq 2000 using 100 bp paired-end reads. All RNA-seq data were aligned to mm10 using TopHat (Trapnell et al., 2009) v2.1.0 with default parameters. We used Cuffdiff (Trapnell et al., 2010) v1.3 for all differential expression (DE) analyses with either UCSC mm10 gene annotation or our custom annotation containing RefSeq entries plus OL-expressing lncRNAs as described below. In all DE tests, a gene was considered significant if the fold change was more than 1.5 and q value was less than 0.05.

Chromatin-immunoprecipitation and sequencing (ChIP-Seq)

ChIP assays were performed essentially as previously described (Yu et al., 2013b). Rabbit anti-Suz12 (Cell Signaling Technology, #3737) or rabbit anti-Chd7 (Cell Signaling Technology, # 6505) antibody was used for immunoprecipitation experiments. OLs (~20 million cells) were cross-linked in 1% formaldehyde at room temperature for 10 min and then quenched with 125 mM glycine for 5 min. Cells were rinsed, resuspended in lysis buffer (50 mM HEPES, pH 7.6, 140 mM NaCl, 1 mM EDTA, 10% Glycerol, 0.25% Triton X-100 and 0.5% NP-40 and protease inhibitor cocktail) and incubated on ice for 10 min. Lysates were centrifuged and pellets were resuspended in nuclei washing buffer (200 mM NaCl, 1 mM EDTA, 1 mM EGTA, 10 mM Tris pH 8.0, and protease inhibitor cocktail) with gentle

rocking at 4°C. Nuclei were pelleted and resuspended in 1 ml of sonication buffer (10 mM Tris-HCl [pH 8.0], 1 mM EDTA, 0.5 mM EGTA and protease inhibitor cocktail). Nuclear suspensions were sonicated with a Covaris S220 sonicator (total time 8 min). Antibody (chromatin: antibody = 4:1) was added to chromatin and incubated at 4°C overnight. Chromatin-protein complex was immunoprecipitated with protein A/G plus agarose beads and washed sequentially, twice with low salt buffer (0.1% SDS, 1% Triton X-100, 2 mM EDTA, 20 mM Tris-HCl [pH 8.0], 150 mM NaCl), twice with high salt buffer (0.1% SDS, 1% Triton X-100, 2 mM EDTA, 20 mM Tris-HCl [pH 8.0], 500 mM NaCl) and twice with LiCl buffer (0.25 M LiCl, 1% IGEPAL CA630, 1% deoxycholic acid, 1 mM EDTA, 10 mM Tris [pH 8.0]) and once with 1xTE buffer. Immunoprecipitates were then eluted in elution buffer at 65°C for 1 h. Eluted chromatin was subjected to reverse-crosslink and chromatin fragment purification with QIAGEN PCR purification columns. ChIP-Seq libraries were prepared using NEBNext ChIP-Seq Library Prep Kit according to manufacturer's instructions.

ChIP-Seq data analysis

FASTQ file was aligned to March 2012 rat genome assembly (rn5) using Bowtie with the following options: -p 8, -m 1. Resulting SAM files were converted to BAM format using SAM tools. Peak calling was performed using MACS (Model-based Analysis of ChIP-Seq) (http://liulab.dfci.harvard.edu/MACS) with a p value cut off of 1x e^{9}.

LncRNA Assembly and Annotation

We sequenced primary mouse OPCs and OLs induced to differentiate for 1 day (referred as iOL) and 3 days (referred as mOL) in duplicates (60‑80 million mate pairs each) to be used for *ab initio* transcriptome assembly with Cufflinks v2.2.1. In Brief, Cufflinks were run with the following options: -u, -N, -g (mm10 GTF file provided as guide), and -M (rRNA and 7SK RNA mask file provided). We generated transcriptome assemblies for each sample separately and then utilized Cuffmerge to combine all annotations. Any transcripts that overlapped and transcribed in the same orientation as a known coding region (RefSeq NM entries) were removed and then merged the annotations using Cuffmerge. We removed any single-exonic transcripts to reduce transcriptional noise. Any transcripts with a length < 200 nt including miRNA and snRNA host genes were removed. Next, we used the CPAT algorithm (Wang et al., 2013) to predict protein-coding potential of the remaining transcripts. Any transcript with a CPAT scores greater than 0.44 was removed. The resulting OL-expressing lncRNA annotation was then compared to the RefSeq or lncRNA annotation in order to determine the number of novel genes discovered here. Transcripts were considered divergent if their TSS was less than 2.5 kb from a RefSeq_NM TSS on the opposite strand. All other lncRNAs were considered to be intergenic. This T-ALL lncRNA annotation was merged with the RefSeqNM annotation using Cuffmerge and used for all subsequent RNA-Seq expression analyses.

Analysis of histone modification and transcription factor signatures

Published ChIP-seq (H3K4me3, H3K27Acand Sox10) datasets from transformed mouse OPCs and primary rat OPCs and OLs in NCBI were used to explore the enrichment of

histone modifications and transcription factors around mouse lncRNA transcriptional start site and corresponding genomic intervals on rat genome. Metagene plots were generated as described (Liu et al., 2011). Boxplot representations were generated using the boxplot function in R.

LncRNA-protein coding gene co-expression analysis

The co-expression network for lncRNAs and protein coding genes was as previously proposed (Necsulea et al., 2014). For each pair of genes (lncRNA or protein-coding), we computed the Pearson correlation coefficients (PCCs) of expression patterns. We detected clusters of highly inter-connected genes with the Markov Cluster (MCL) algorithm (van Dongen S, 2012), with PCC cutoff set to 0.8 and inflation coefficient set as 2.0. The resulting 19 largest clusters and interaction network were visualized with Cytoscape (Smoot et al., 2011).

Statistical analysis

All analyses were done using GraphPad Prism 6.00 (San Diego California, www.graphpad.com). Data are shown as mean ± s.e.m. or as a Box-and-whisker plot. Data distribution was assumed to be normal, but this was not formally tested. Statistical significance was determined using two-tailed Student's *t* tests or Wilcoxon rank-sum and signed-rank tests as indicated. One-way ANOVA test was performed by multiple comparisons or pairwise comparisons following Turkey's ranking tests when comparing multiple groups. Significance was set as * for $p < 0.05$, ** for $p < 0.01$, and *** $p < 0.001$, unless otherwise indicated. In MEME motif analysis, E value shows the significant

enrichment of de novo motifs while *p* value is shown the significant similarity between de novo motif and known motif. No statistical methods were used to predetermine sample sizes, but our sample sizes are similar to those generally employed in the field. Quantifications were performed from at least three independent experiments.

ACKNOWLEDGEMENTS

This dissertation would not have been possible without the support and help from many great people that I should be thankful to.

My deep gratitude goes to my mentor, Dr. Richard Lu, for providing the opportunity and invaluable resources to perform my research in his lab. I am also very grateful for his constant great support, guidance, and encouragement.

I would like to thank my thesis committee members, Drs. Lee Kraus, Jane Johnson, Eric Olson and Yi Liu, for their advice and support during my training. I was blessed to have great scientists and mentors on my committee. I also would like to thank my program coordinator Priyarama Sen for her help and support, especially after I moved to Cincinnati.

I am thankful to Dr. Carlos Parras and Corentine Marie at UPMC University for their terrific discussions and scientific input in our collaborative study on the function of Chd7 in oligodendrocyte differentiation. I would like to thank Yueh-Chiang Hu in CCHMC for generating lncOL1 KO mice. I would like to thank Dr. Yulan Lu and Lingli Xu in Children's Hospital of Fudan University for bioinformatical support.

I would like to thank all Lu lab members, present and past. I am grateful to Dr. Bongwoo Kim and Dr. Noriyoshi Usui for their initial studies, to Dr. Chuntao Zhao for his great help on CHIP-Seq experiments, to Dr. Yaqi Deng for help with surgical techniques, to

Jincheng Wang for technical support and to Jack Ma for his tremendous technical assistance.

Finally, I want to thank my fiancé Heping Xu , my parents and my brother, for their constant love and encouragement to pursue my goal of becoming a scientist.

BIBLIOGRAPHY

Aasland, R., Stewart, A.F., and Gibson, T. (1996). The SANT domain: a putative DNA-binding domain in the SWI-SNF and ADA complexes, the transcriptional co-repressor N-CoR and TFIIIB. Trends in biochemical sciences *21*, 87-88.

Ali Hassan, N.Z., Mokhtar, N.M., Kok Sin, T., Mohamed Rose, I., Sagap, I., Harun, R., and Jamal, R. (2014). Integrated analysis of copy number variation and genome-wide expression profiling in colorectal cancer tissues. PloS one *9*, e92553.

Amiel, J., Attiee-Bitach, T., Marianowski, R., Cormier-Daire, V., Abadie, V., Bonnet, D., Gonzales, M., Chemouny, S., Brunelle, F., Munnich, A.*, et al.* (2001). Temporal bone anomaly proposed as a major criteria for diagnosis of CHARGE syndrome. American journal of medical genetics *99*, 124-127.

Asakura, Y., Toyota, Y., Muroya, K., Kurosawa, K., Fujita, K., Aida, N., Kawame, H., Kosaki, K., and Adachi, M. (2008). Endocrine and radiological studies in patients with molecularly confirmed CHARGE syndrome. The Journal of clinical endocrinology and metabolism *93*, 920-924.

Bagchi, A., Papazoglu, C., Wu, Y., Capurso, D., Brodt, M., Francis, D., Bredel, M., Vogel, H., and Mills, A.A. (2007). CHD5 is a tumor suppressor at human 1p36. Cell *128*, 459-475.

Bailey, T.L., Williams, N., Misleh, C., and Li, W.W. (2006). MEME: discovering and analyzing DNA and protein sequence motifs. Nucleic acids research *34*, W369-373.

Bajpai, R., Chen, D.A., Rada-Iglesias, A., Zhang, J., Xiong, Y., Helms, J., Chang, C.P., Zhao, Y., Swigut, T., and Wysocka, J. (2010). CHD7 cooperates with PBAF to control multipotent neural crest formation. Nature *463*, 958-962.

Batista, P.J., and Chang, H.Y. (2013). Long noncoding RNAs: cellular address codes in development and disease. Cell *152*, 1298-1307.

Batsukh, T., Pieper, L., Koszucka, A.M., von Velsen, N., Hoyer-Fender, S., Elbracht, M., Bergman, J.E., Hoefsloot, L.H., and Pauli, S. (2010). CHD8 interacts with CHD7, a protein which is mutated in CHARGE syndrome. Human molecular genetics *19*, 2858-2866.

Bellucci, M., Agostini, F., Masin, M., and Tartaglia, G.G. (2011). Predicting protein associations with long noncoding RNAs. Nature methods *8*, 444-445.

Beltran, M., Puig, I., Pena, C., Garcia, J.M., Alvarez, A.B., Pena, R., Bonilla, F., and de Herreros, A.G. (2008). A natural antisense transcript regulates Zeb2/Sip1 gene expression during Snail1-induced epithelial-mesenchymal transition. Genes & development *22*, 756-769.

Bergman, J.E., Bosman, E.A., van Ravenswaaij-Arts, C.M., and Steel, K.P. (2010). Study of smell and reproductive organs in a mouse model for CHARGE syndrome. European journal of human genetics : EJHG *18*, 171-177.

Bergman, J.E., Janssen, N., Hoefsloot, L.H., Jongmans, M.C., Hofstra, R.M., and van Ravenswaaij-Arts, C.M. (2014). CHD7 mutations and CHARGE syndrome: the clinical implications of an expanding phenotype. Journal of medical genetics *48*, 334-342.

Bharti, K., Gasper, M., Ou, J., Brucato, M., Clore-Gronenborn, K., Pickel, J., and Arnheiter, H. (2012). A regulatory loop involving PAX6, MITF, and WNT signaling controls retinal pigment epithelium development. PLoS genetics *8*, e1002757.

Bischof, M., Weider, M., Kuspert, M., Nave, K.A., and Wegner, M. (2015). Brg1-dependent chromatin remodelling is not essentially required during oligodendroglial differentiation. The Journal of neuroscience : the official journal of the Society for Neuroscience *35*, 21-35.

Blake, K.D., Davenport, S.L., Hall, B.D., Hefner, M.A., Pagon, R.A., Williams, M.S., Lin, A.E., and Graham, J.M., Jr. (1998). CHARGE association: an update and review for the primary pediatrician. Clinical pediatrics *37*, 159-173.

Bond, A.M., Vangompel, M.J., Sametsky, E.A., Clark, M.F., Savage, J.C., Disterhoft, J.F., and Kohtz, J.D. (2009). Balanced gene regulation by an embryonic brain ncRNA is critical for adult hippocampal GABA circuitry. Nature neuroscience *12*, 1020-1027.

Bosman, E.A., Penn, A.C., Ambrose, J.C., Kettleborough, R., Stemple, D.L., and Steel, K.P. (2005). Multiple mutations in mouse Chd7 provide models for CHARGE syndrome. Human molecular genetics *14*, 3463-3476.

Boyer, L.A., Latek, R.R., and Peterson, C.L. (2004). The SANT domain: a unique histone-tail-binding module? Nature reviews Molecular cell biology *5*, 158-163.

Braitch, M., and Constantinescu, C.S. (2010). The role of osteopontin in experimental autoimmune encephalomyelitis (EAE) and multiple sclerosis (MS). Inflamm Allergy Drug Targets *9*, 249-256.

Briggs, J.A., Wolvetang, E.J., Mattick, J.S., Rinn, J.L., and Barry, G. (2015). Mechanisms of Long Non-coding RNAs in Mammalian Nervous System Development, Plasticity, Disease, and Evolution. Neuron *88*, 861-877.

Brookes, E., and Shi, Y. (2014). Diverse epigenetic mechanisms of human disease. Annual review of genetics *48*, 237-268.

Budde, H., Schmitt, S., Fitzner, D., Opitz, L., Salinas-Riester, G., and Simons, M. (2010). Control of oligodendroglial cell number by the miR-17-92 cluster. Development *137*, 2127-2132.

Bujalka, H., Koenning, M., Jackson, S., Perreau, V.M., Pope, B., Hay, C.M., Mitew, S., Hill, A.F., Lu, Q.R., Wegner, M.*, et al.* (2013). MYRF is a membrane-associated transcription factor that autoproteolytically cleaves to directly activate myelin genes. PLoS biology *11*, e1001625.

Bunge, M.B., Bunge, R.P., and Pappas, G.D. (1962). Electron microscopic demonstration of connections between glia and myelin sheaths in the developing mammalian central nervous system. The Journal of cell biology *12*, 448-453.

Bunge, R.P. (1968). Glial cells and the central myelin sheath. Physiological reviews *48*, 197-251.

Cabili, M.N., Trapnell, C., Goff, L., Koziol, M., Tazon-Vega, B., Regev, A., and Rinn, J.L. (2011). Integrative annotation of human large intergenic noncoding RNAs reveals global properties and specific subclasses. Genes & development *25*, 1915-1927.

Carvill, G.L., Heavin, S.B., Yendle, S.C., McMahon, J.M., O'Roak, B.J., Cook, J., Khan, A., Dorschner, M.O., Weaver, M., Calvert, S.*, et al.* (2013). Targeted resequencing in epileptic encephalopathies identifies de novo mutations in CHD2 and SYNGAP1. Nature genetics *45*, 825-830.

Casero, D., Sandoval, S., Seet, C.S., Scholes, J., Zhu, Y., Ha, V.L., Luong, A., Parekh, C., and Crooks, G.M. (2015). Long non-coding RNA profiling of human lymphoid progenitor cells reveals transcriptional divergence of B cell and T cell lineages. Nature immunology *16*, 1282-1291.

Cesana, M., Cacchiarelli, D., Legnini, I., Santini, T., Sthandier, O., Chinappi, M., Tramontano, A., and Bozzoni, I. (2011). A long noncoding RNA controls muscle differentiation by functioning as a competing endogenous RNA. Cell *147*, 358-369.

Chamberlain, K.A., Nanescu, S.E., Psachoulia, K., and Huang, J.K. (2015). Oligodendrocyte regeneration: Its significance in myelin replacement and neuroprotection in multiple sclerosis. Neuropharmacology.

Chang, A., Tourtellotte, W.W., Rudick, R., and Trapp, B.D. (2002). Premyelinating oligodendrocytes in chronic lesions of multiple sclerosis. N Engl J Med *346*, 165-173.

Chen, K., Deng, S., Lu, H., Zheng, Y., Yang, G., Kim, D., Cao, Q., and Wu, J.Q. (2013). RNA-seq characterization of spinal cord injury transcriptome in acute/subacute phases: a resource for understanding the pathology at the systems level. PloS one *8*, e72567.

Chen, Y., Balasubramaniyan, V., Peng, J., Hurlock, E.C., Tallquist, M., Li, J., and Lu, Q.R. (2007). Isolation and culture of rat and mouse oligodendrocyte precursor cells. Nature protocols *2*, 1044-1051.

Clapier, C.R., and Cairns, B.R. (2009). The biology of chromatin remodeling complexes. Annual review of biochemistry *78*, 273-304.

Colbert, L.E., Petrova, A.V., Fisher, S.B., Pantazides, B.G., Madden, M.Z., Hardy, C.W., Warren, M.D., Pan, Y., Nagaraju, G.P., Liu, E.A.*, et al.* (2014). CHD7 expression predicts survival outcomes in patients with resected pancreatic cancer. Cancer research *74*, 2677-2687.

Comi, C., Cappellano, G., Chiocchetti, A., Orilieri, E., Buttini, S., Ghezzi, L., Galimberti, D., Guerini, F., Barizzone, N., Perla, F.*, et al.* (2012). The impact of osteopontin gene variations on multiple sclerosis development and progression. Clinical & developmental immunology *2012*, 212893.

Conway, E., Healy, E., and Bracken, A.P. (2015). PRC2 mediated H3K27 methylations in cellular identity and cancer. Current opinion in cell biology *37*, 42-48.

Dai, J., Bercury, K.K., Ahrendsen, J.T., and Macklin, W.B. (2015). Olig1 function is required for oligodendrocyte differentiation in the mouse brain. The Journal of neuroscience : the official journal of the Society for Neuroscience *35*, 4386-4402.

Das Sarma, J., Kenyon, L.C., Hingley, S.T., and Shindler, K.S. (2009). Mechanisms of primary axonal damage in a viral model of multiple sclerosis. The Journal of neuroscience : the official journal of the Society for Neuroscience *29*, 10272-10280.

Delmas, V., Stokes, D.G., and Perry, R.P. (1993). A mammalian DNA-binding protein that contains a chromodomain and an SNF2/SWI2-like helicase domain. Proceedings of the National Academy of Sciences of the United States of America *90*, 2414-2418.

Derrien, T., Johnson, R., Bussotti, G., Tanzer, A., Djebali, S., Tilgner, H., Guernec, G., Martin, D., Merkel, A., Knowles, D.G.*, et al.* (2012). The GENCODE v7 catalog of human long noncoding RNAs: analysis of their gene structure, evolution, and expression. Genome research *22*, 1775-1789.

Diederichs, S. (2014). The four dimensions of noncoding RNA conservation. Trends in genetics : TIG *30*, 121-123.

Dong, X., Chen, K., Cuevas-Diaz Duran, R., You, Y., Sloan, S.A., Zhang, Y., Zong, S., Cao, Q., Barres, B.A., and Wu, J.Q. (2015). Comprehensive Identification of Long Non-coding RNAs in Purified Cell Types from the Brain Reveals Functional LncRNA in OPC Fate Determination. PLoS genetics *11*, e1005669.

Doudna, J.A., and Charpentier, E. (2014). Genome editing. The new frontier of genome engineering with CRISPR-Cas9. Science *346*, 1258096.

Dugas, J.C., Cuellar, T.L., Scholze, A., Ason, B., Ibrahim, A., Emery, B., Zamanian, J.L., Foo, L.C., McManus, M.T., and Barres, B.A. (2010). Dicer1 and miR-219 Are required for normal oligodendrocyte differentiation and myelination. Neuron *65*, 597-611.

Dugas, J.C., Tai, Y.C., Speed, T.P., Ngai, J., and Barres, B.A. (2006). Functional genomic analysis of oligodendrocyte differentiation. The Journal of neuroscience : the official journal of the Society for Neuroscience *26*, 10967-10983.

Eberharter, A., Vetter, I., Ferreira, R., and Becker, P.B. (2004). ACF1 improves the effectiveness of nucleosome mobilization by ISWI through PHD-histone contacts. The EMBO journal *23*, 4029-4039.

Emery, B., Agalliu, D., Cahoy, J.D., Watkins, T.A., Dugas, J.C., Mulinyawe, S.B., Ibrahim, A., Ligon, K.L., Rowitch, D.H., and Barres, B.A. (2009). Myelin gene regulatory factor is a critical transcriptional regulator required for CNS myelination. Cell *138*, 172-185.

Emery, B., and Lu, Q.R. (2015). Transcriptional and Epigenetic Regulation of Oligodendrocyte Development and Myelination in the Central Nervous System. Cold Spring Harbor perspectives in biology *7*.

Engelen, E., Akinci, U., Bryne, J.C., Hou, J., Gontan, C., Moen, M., Szumska, D., Kockx, C., van Ijcken, W., Dekkers, D.H.*, et al.* (2011). Sox2 cooperates with Chd7 to regulate genes that are mutated in human syndromes. Nature genetics *43*, 607-611.

Falkenberg, K.J., and Johnstone, R.W. (2014). Histone deacetylases and their inhibitors in cancer, neurological diseases and immune disorders. Nature reviews Drug discovery *13*, 673-691.

Feng, W., Khan, M.A., Bellvis, P., Zhu, Z., Bernhardt, O., Herold-Mende, C., and Liu, H.K. (2013). The chromatin remodeler CHD7 regulates adult neurogenesis via activation of SoxC transcription factors. Cell stem cell *13*, 62-72.

Finzsch, M., Stolt, C.C., Lommes, P., and Wegner, M. (2008). Sox9 and Sox10 influence survival and migration of oligodendrocyte precursors in the spinal cord by regulating PDGF receptor alpha expression. Development *135*, 637-646.

Flynn, R.A., and Chang, H.Y. (2014). Long noncoding RNAs in cell-fate programming and reprogramming. Cell stem cell *14*, 752-761.

Franklin, R.J. (2002). Why does remyelination fail in multiple sclerosis? Nat Rev Neurosci *3*, 705-714.

Franklin, R.J., and Ffrench-Constant, C. (2008). Remyelination in the CNS: from biology to therapy. Nat Rev Neurosci *9*, 839-855.

Frederick, T.J., and Wood, T.L. (2004). IGF-I and FGF-2 coordinately enhance cyclin D1 and cyclin E-cdk2 association and activity to promote G1 progression in oligodendrocyte progenitor cells. Molecular and cellular neurosciences *25*, 480-492.

Friedmann, D.R., Amoils, M., Germiller, J.A., Lustig, L.R., Glastonbury, C.M., Pramanik, B.K., and Lalwani, A.K. (2012). Venous malformations of the temporal bone are a common feature in CHARGE syndrome. The Laryngoscope *122*, 895-900.

Gaspar-Maia, A., Alajem, A., Polesso, F., Sridharan, R., Mason, M.J., Heidersbach, A., Ramalho-Santos, J., McManus, M.T., Plath, K., Meshorer, E.*, et al.* (2009). Chd1 regulates open chromatin and pluripotency of embryonic stem cells. Nature *460*, 863-868.

Graw, J. (2010). Eye development. Current topics in developmental biology *90*, 343-386.

Gregory, L.C., Gevers, E.F., Baker, J., Kasia, T., Chong, K., Josifova, D.J., Caimari, M., Bilan, F., McCabe, M.J., and Dattani, M.T. (2013). Structural pituitary abnormalities associated with CHARGE syndrome. The Journal of clinical endocrinology and metabolism *98*, E737-743.

Grote, P., Wittler, L., Hendrix, D., Koch, F., Wahrisch, S., Beisaw, A., Macura, K., Blass, G., Kellis, M., Werber, M.*, et al.* (2013). The tissue-specific lncRNA Fendrr is an essential regulator of heart and body wall development in the mouse. Developmental cell *24*, 206-214.

Gui, Y., Guo, G., Huang, Y., Hu, X., Tang, A., Gao, S., Wu, R., Chen, C., Li, X., Zhou, L.*, et al.* (2011). Frequent mutations of chromatin remodeling genes in transitional cell carcinoma of the bladder. Nature genetics *43*, 875-878.

Gupta, R.A., Shah, N., Wang, K.C., Kim, J., Horlings, H.M., Wong, D.J., Tsai, M.C., Hung, T., Argani, P., Rinn, J.L.*, et al.* (2010). Long non-coding RNA HOTAIR reprograms chromatin state to promote cancer metastasis. Nature *464*, 1071-1076.

Guttman, M., Amit, I., Garber, M., French, C., Lin, M.F., Feldser, D., Huarte, M., Zuk, O., Carey, B.W., Cassady, J.P.*, et al.* (2009). Chromatin signature reveals over a thousand highly conserved large non-coding RNAs in mammals. Nature *458*, 223-227.

Guttman, M., Donaghey, J., Carey, B.W., Garber, M., Grenier, J.K., Munson, G., Young, G., Lucas, A.B., Ach, R., Bruhn, L.*, et al.* (2011). lincRNAs act in the circuitry controlling pluripotency and differentiation. Nature *477*, 295-300.

Guzman-Ayala, M., Sachs, M., Koh, F.M., Onodera, C., Bulut-Karslioglu, A., Lin, C.J., Wong, P., Nitta, R., Song, J.S., and Ramalho-Santos, M. (2015). Chd1 is essential for the high transcriptional output and rapid growth of the mouse epiblast. Development *142*, 118-127.

Hacisuleyman, E., Goff, L.A., Trapnell, C., Williams, A., Henao-Mejia, J., Sun, L., McClanahan, P., Hendrickson, D.G., Sauvageau, M., Kelley, D.R.*, et al.* (2014). Topological organization of multichromosomal regions by the long intergenic noncoding RNA Firre. Nature structural & molecular biology *21*, 198-206.

He, D., Marie, C., Zhao, C., Kim, B., Wang, J., Deng, Y., Clavairoly, A., Frah, M., Wang, H., He, X.*, et al.* (2016). Chd7 cooperates with Sox10 and regulates the onset of CNS myelination and remyelination. Nature neuroscience.

He, Y., Dupree, J., Wang, J., Sandoval, J., Li, J., Liu, H., Shi, Y., Nave, K.A., and Casaccia-Bonnefil, P. (2007). The transcription factor Yin Yang 1 is essential for oligodendrocyte progenitor differentiation. Neuron *55*, 217-230.

Hedtjarn, M., Mallard, C., Arvidsson, P., and Hagberg, H. (2005). White matter injury in the immature brain: role of interleukin-18. Neuroscience letters *373*, 16-20.

Ho, L., and Crabtree, G.R. (2010). Chromatin remodelling during development. Nature *463*, 474-484.

Hu, X., Feng, Y., Zhang, D., Zhao, S.D., Hu, Z., Greshock, J., Zhang, Y., Yang, L., Zhong, X., Wang, L.P.*, et al.* (2014). A Functional Genomic Approach Identifies FAL1 as an Oncogenic Long Noncoding RNA that Associates with BMI1 and Represses p21 Expression in Cancer. Cancer cell *26*, 344-357.

Huang, J.K., Jarjour, A.A., Nait Oumesmar, B., Kerninon, C., Williams, A., Krezel, W., Kagechika, H., Bauer, J., Zhao, C., Baron-Van Evercooren, A.*, et al.* (2011). Retinoid X receptor gamma signaling accelerates CNS remyelination. Nature neuroscience *14*, 45-53.

Huang, S., Gulzar, Z.G., Salari, K., Lapointe, J., Brooks, J.D., and Pollack, J.R. (2012). Recurrent deletion of CHD1 in prostate cancer with relevance to cell invasiveness. Oncogene *31*, 4164-4170.

Huang, W., Thomas, B., Flynn, R.A., Gavzy, S.J., Wu, L., Kim, S.V., Hall, J.A., Miraldi, E.R., Ng, C.P., Rigo, F.W.*, et al.* (2015). DDX5 and its associated lncRNA Rmrp modulate TH17 cell effector functions. Nature *528*, 517-522.

Hung, H., Kohnken, R., and Svaren, J. (2012). The nucleosome remodeling and deacetylase chromatin remodeling (NuRD) complex is required for peripheral nerve myelination. The Journal of neuroscience : the official journal of the Society for Neuroscience *32*, 1517-1527.

Hung, T., and Chang, H.Y. (2010). Long noncoding RNA in genome regulation: prospects and mechanisms. RNA biology *7*, 582-585.

Hurd, E.A., Capers, P.L., Blauwkamp, M.N., Adams, M.E., Raphael, Y., Poucher, H.K., and Martin, D.M. (2007). Loss of Chd7 function in gene-trapped reporter mice is embryonic lethal and associated with severe defects in multiple developing tissues. Mammalian genome : official journal of the International Mammalian Genome Society *18*, 94-104.

Hurd, E.A., Poucher, H.K., Cheng, K., Raphael, Y., and Martin, D.M. (2010). The ATP-dependent chromatin remodeling enzyme CHD7 regulates pro-neural gene expression and neurogenesis in the inner ear. Development *137*, 3139-3150.

Jakovcevski, M., and Akbarian, S. (2012). Epigenetic mechanisms in neurological disease. Nature medicine *18*, 1194-1204.

Jongmans, M.C., Admiraal, R.J., van der Donk, K.P., Vissers, L.E., Baas, A.F., Kapusta, L., van Hagen, J.M., Donnai, D., de Ravel, T.J., Veltman, J.A.*, et al.* (2006). CHARGE syndrome: the phenotypic spectrum of mutations in the CHD7 gene. Journal of medical genetics *43*, 306-314.

Jongmans, M.C., van Ravenswaaij-Arts, C.M., Pitteloud, N., Ogata, T., Sato, N., Claahsen-van der Grinten, H.L., van der Donk, K., Seminara, S., Bergman, J.E., Brunner, H.G.*, et al.* (2009). CHD7 mutations in patients initially diagnosed with Kallmann syndrome--the clinical overlap with CHARGE syndrome. Clinical genetics *75*, 65-71.

Jung, M., Kramer, E., Grzenkowski, M., Tang, K., Blakemore, W., Aguzzi, A., Khazaie, K., Chlichlia, K., von Blankenfeld, G., Kettenmann, H.*, et al.* (1995). Lines of murine oligodendroglial precursor cells immortalized by an activated neu tyrosine kinase show distinct degrees of interaction with axons in vitro and in vivo. Eur J Neurosci *7*, 1245-1265.

Kaminsky, E.B., Kaul, V., Paschall, J., Church, D.M., Bunke, B., Kunig, D., Moreno-De-Luca, D., Moreno-De-Luca, A., Mulle, J.G., Warren, S.T.*, et al.* (2011). An evidence-based approach to establish the functional and clinical significance of copy number variants in intellectual and developmental disabilities. Genetics in medicine : official journal of the American College of Medical Genetics *13*, 777-784.

Kaneko, S., Son, J., Bonasio, R., Shen, S.S., and Reinberg, D. (2014). Nascent RNA interaction keeps PRC2 activity poised and in check. Genes & development *28*, 1983-1988.

Kang, S.H., Fukaya, M., Yang, J.K., Rothstein, J.D., and Bergles, D.E. (2010). NG2+ CNS glial progenitors remain committed to the oligodendrocyte lineage in postnatal life and following neurodegeneration. Neuron *68*, 668-681.

Katayama, Y., Nishiyama, M., Shoji, H., Ohkawa, Y., Kawamura, A., Sato, T., Suyama, M., Takumi, T., Miyakawa, T., and Nakayama, K.I. (2016). CHD8 haploinsufficiency results in autistic-like phenotypes in mice. Nature.

Kim, M.S., Chung, N.G., Kang, M.R., Yoo, N.J., and Lee, S.H. (2011). Genetic and expressional alterations of CHD genes in gastric and colorectal cancers. Histopathology *58*, 660-668.

Kino, T., Hurt, D.E., Ichijo, T., Nader, N., and Chrousos, G.P. (2010). Noncoding RNA gas5 is a growth arrest- and starvation-associated repressor of the glucocorticoid receptor. Science signaling *3*, ra8.

Klattenhoff, C.A., Scheuermann, J.C., Surface, L.E., Bradley, R.K., Fields, P.A., Steinhauser, M.L., Ding, H., Butty, V.L., Torrey, L., Haas, S.*, et al.* (2013). Braveheart, a long noncoding RNA required for cardiovascular lineage commitment. Cell *152*, 570-583.

Koenning, M., Jackson, S., Hay, C.M., Faux, C., Kilpatrick, T.J., Willingham, M., and Emery, B. (2012). Myelin gene regulatory factor is required for maintenance of myelin and mature oligodendrocyte identity in the adult CNS. The Journal of neuroscience : the official journal of the Society for Neuroscience *32*, 12528-12542.

Konze, K.D., Ma, A., Li, F., Barsyte-Lovejoy, D., Parton, T., Macnevin, C.J., Liu, F., Gao, C., Huang, X.P., Kuznetsova, E.*, et al.* (2013). An orally bioavailable chemical probe of the Lysine Methyltransferases EZH2 and EZH1. ACS chemical biology *8*, 1324-1334.

Kretz, M., Siprashvili, Z., Chu, C., Webster, D.E., Zehnder, A., Qu, K., Lee, C.S., Flockhart, R.J., Groff, A.F., Chow, J.*, et al.* (2013). Control of somatic tissue differentiation by the long non-coding RNA TINCR. Nature *493*, 231-235.

Kretz, M., Webster, D.E., Flockhart, R.J., Lee, C.S., Zehnder, A., Lopez-Pajares, V., Qu, K., Zheng, G.X., Chow, J., Kim, G.E.*, et al.* (2012). Suppression of progenitor differentiation requires the long noncoding RNA ANCR. Genes & development *26*, 338-343.

Krogan, N.J., Kim, M., Ahn, S.H., Zhong, G., Kobor, M.S., Cagney, G., Emili, A., Shilatifard, A., Buratowski, S., and Greenblatt, J.F. (2002). RNA polymerase II elongation factors of Saccharomyces cerevisiae: a targeted proteomics approach. Molecular and cellular biology *22*, 6979-6992.

Kwon, Y.J., Baek, H.S., Ye, D.J., Shin, S., Kim, D., and Chun, Y.J. (2016). CYP1B1 Enhances Cell Proliferation and Metastasis through Induction of EMT and Activation of Wnt/beta-Catenin Signaling via Sp1 Upregulation. PLoS One *11*, e0151598.

Lathrop, M.J., Chakrabarti, L., Eng, J., Rhodes, C.H., Lutz, T., Nieto, A., Liggitt, H.D., Warner, S., Fields, J., Stoger, R.*, et al.* (2010). Deletion of the Chd6 exon 12 affects motor coordination. Mammalian genome : official journal of the International Mammalian Genome Society *21*, 130-142.

Layman, W.S., McEwen, D.P., Beyer, L.A., Lalani, S.R., Fernbach, S.D., Oh, E., Swaroop, A., Hegg, C.C., Raphael, Y., Martens, J.R.*, et al.* (2009). Defects in neural stem cell proliferation and olfaction in Chd7 deficient mice indicate a mechanism for hyposmia in human CHARGE syndrome. Human molecular genetics *18*, 1909-1923.

Le Gallo, M., O'Hara, A.J., Rudd, M.L., Urick, M.E., Hansen, N.F., O'Neil, N.J., Price, J.C., Zhang, S., England, B.M., Godwin, A.K.*, et al.* (2012). Exome sequencing of serous endometrial tumors identifies recurrent somatic mutations in chromatin-remodeling and ubiquitin ligase complex genes. Nature genetics *44*, 1310-1315.

Letzen, B.S., Liu, C., Thakor, N.V., Gearhart, J.D., All, A.H., and Kerr, C.L. (2010). MicroRNA expression profiling of oligodendrocyte differentiation from human embryonic stem cells. PloS one *5*, e10480.

Li, H., Lu, Y., Smith, H.K., and Richardson, W.D. (2007a). Olig1 and Sox10 interact synergistically to drive myelin basic protein transcription in oligodendrocytes. The Journal of neuroscience : the official journal of the Society for Neuroscience *27*, 14375-14382.

Li, W., and Mills, A.A. (2014). Architects of the genome: CHD dysfunction in cancer, developmental disorders and neurological syndromes. Epigenomics *6*, 381-395.

Li, W., Notani, D., Ma, Q., Tanasa, B., Nunez, E., Chen, A.Y., Merkurjev, D., Zhang, J., Ohgi, K., Song, X.*, et al.* (2013). Functional roles of enhancer RNAs for oestrogen-dependent transcriptional activation. Nature *498*, 516-520.

Li, W., Zhang, B., Tang, J., Cao, Q., Wu, Y., Wu, C., Guo, J., Ling, E.A., and Liang, F. (2007b). Sirtuin 2, a mammalian homolog of yeast silent information regulator-2 longevity regulator, is an oligodendroglial protein that decelerates cell differentiation through deacetylating alpha-tubulin. The Journal of neuroscience : the official journal of the Society for Neuroscience *27*, 2606-2616.

Lin, N., Chang, K.Y., Li, Z., Gates, K., Rana, Z.A., Dang, J., Zhang, D., Han, T., Yang, C.S., Cunningham, T.J.*, et al.* (2014). An evolutionarily conserved long noncoding RNA TUNA controls pluripotency and neural lineage commitment. Molecular cell *53*, 1005-1019.

Lin, S.T., and Fu, Y.H. (2009). miR-23 regulation of lamin B1 is crucial for oligodendrocyte development and myelination. Disease models & mechanisms *2*, 178-188.

Lin, S.T., Huang, Y., Zhang, L., Heng, M.Y., Ptacek, L.J., and Fu, Y.H. (2013). MicroRNA-23a promotes myelination in the central nervous system. Proceedings of the National Academy of Sciences of the United States of America *110*, 17468-17473.

Liu, A., Li, J., Marin-Husstege, M., Kageyama, R., Fan, Y., Gelinas, C., and Casaccia-Bonnefil, P. (2006). A molecular insight of Hes5-dependent inhibition of myelin gene expression: old partners and new players. The EMBO journal *25*, 4833-4842.

Liu, H., Hu, Q., D'Ercole A, J., and Ye, P. (2009). Histone deacetylase 11 regulates oligodendrocyte-specific gene expression and cell development in OL-1 oligodendroglia cells. Glia *57*, 1-12.

Liu, J., Magri, L., Zhang, F., Marsh, N.O., Albrecht, S., Huynh, J.L., Kaur, J., Kuhlmann, T., Zhang, W., Slesinger, P.A.*, et al.* (2015). Chromatin landscape defined by repressive histone methylation during oligodendrocyte differentiation. The Journal of neuroscience : the official journal of the Society for Neuroscience *35*, 352-365.

Liu, J., Moyon, S., Hernandez, M., and Casaccia, P. (2016). Epigenetic control of oligodendrocyte development: adding new players to old keepers. Current opinion in neurobiology *39*, 133-138.

Liu, L., Yu, T., Wang, L., Mo, X., and Yu, Y. (2014). A novel CHD7 mutation in a Chinese patient with CHARGE syndrome. Meta Gene *2*, 469-478.

Liu, T., Ortiz, J.A., Taing, L., Meyer, C.A., Lee, B., Zhang, Y., Shin, H., Wong, S.S., Ma, J., Lei, Y.*, et al.* (2011). Cistrome: an integrative platform for transcriptional regulation studies. Genome biology *12*, R83.

Lopez-Anido, C., Sun, G., Koenning, M., Srinivasan, R., Hung, H.A., Emery, B., Keles, S., and Svaren, J. (2015). Differential Sox10 genomic occupancy in myelinating glia. Glia.

Lu, F., Chen, Y., Zhao, C., Wang, H., He, D., Xu, L., Wang, J., He, X., Deng, Y., Lu, E.E.*, et al.* (2016a). Olig2-Dependent Reciprocal Shift in PDGF and EGF Receptor Signaling Regulates Tumor Phenotype and Mitotic Growth in Malignant Glioma. Cancer Cell *29*, 669-683.

Lu, F., Chen, Y., Zhao, C., Wang, H., He, D., Xu, L., Wang, J., He, X., Deng, Y., Lu, E.E.*, et al.* (2016b). Olig2-Dependent Reciprocal Shift in PDGF and EGF Receptor Signaling Regulates Tumor Phenotype and Mitotic Growth in Malignant Glioma Cancer cell *29*.

Lu, Q.R., Sun, T., Zhu, Z., Ma, N., Garcia, M., Stiles, C.D., and Rowitch, D.H. (2002). Common developmental requirement for Olig function indicates a motor neuron/oligodendrocyte connection. Cell *109*, 75-86.

Lu, Q.R., Yuk, D., Alberta, J.A., Zhu, Z., Pawlitzky, I., Chan, J., McMahon, A.P., Stiles, C.D., and Rowitch, D.H. (2000). Sonic hedgehog--regulated oligodendrocyte lineage genes encoding bHLH proteins in the mammalian central nervous system. Neuron *25*, 317-329.

Luna-Zurita, L., and Bruneau, B.G. (2013). Chromatin modulators as facilitating factors in cellular reprogramming. Curr Opin Genet Dev *23*, 556-561.

Maass, P.G., Luft, F.C., and Bahring, S. (2014). Long non-coding RNA in health and disease. J Mol Med (Berl) *92*, 337-346.

Marfella, C.G., and Imbalzano, A.N. (2007). The Chd family of chromatin remodelers. Mutation research *618*, 30-40.

Marfella, C.G., Ohkawa, Y., Coles, A.H., Garlick, D.S., Jones, S.N., and Imbalzano, A.N. (2006). Mutation of the SNF2 family member Chd2 affects mouse development and survival. Journal of cellular physiology *209*, 162-171.

Marin-Husstege, M., Muggironi, M., Liu, A., and Casaccia-Bonnefil, P. (2002). Histone deacetylase activity is necessary for oligodendrocyte lineage progression. The Journal of neuroscience : the official journal of the Society for Neuroscience *22*, 10333-10345.

Martin, D.M. (2010). Chromatin remodeling in development and disease: focus on CHD7. PLoS genetics *6*, e1001010.

Menon, T., Yates, J.A., and Bochar, D.A. (2010). Regulation of androgen-responsive transcription by the chromatin remodeling factor CHD8. Mol Endocrinol *24*, 1165-1174.

Mercer, T.R., Qureshi, I.A., Gokhan, S., Dinger, M.E., Li, G., Mattick, J.S., and Mehler, M.F. (2010). Long noncoding RNAs in neuronal-glial fate specification and oligodendrocyte lineage maturation. BMC neuroscience *11*, 14.

Meyer zum Gottesberge, A.M., Gross, O., Becker-Lendzian, U., Massing, T., and Vogel, W.F. (2008). Inner ear defects and hearing loss in mice lacking the collagen receptor DDR1. Laboratory investigation; a journal of technical methods and pathology *88*, 27-37.

Micucci, J.A., Layman, W.S., Hurd, E.A., Sperry, E.D., Frank, S.F., Durham, M.A., Swiderski, D.L., Skidmore, J.M., Scacheri, P.C., Raphael, Y.*, et al.* (2014). CHD7 and retinoic acid signaling cooperate to regulate neural stem cell and inner ear development in mouse models of CHARGE syndrome. Human molecular genetics *23*, 434-448.

Mills, J.D., Kavanagh, T., Kim, W.S., Chen, B.J., Waters, P.D., Halliday, G.M., and Janitz, M. (2015). High expression of long intervening non-coding RNA OLMALINC in the human cortical white matter is associated with regulation of oligodendrocyte maturation. Molecular brain *8*, 2.

Mitsui, Y., Chang, I., Fukuhara, S., Hiraki, M., Arichi, N., Yasumoto, H., Hirata, H., Yamamura, S., Shahryari, V., Deng, G.*, et al.* (2015). CYP1B1 promotes tumorigenesis via altered expression of CDC20 and DAPK1 genes in renal cell carcinoma. BMC cancer *15*, 942.

Murawska, M., and Brehm, A. (2011). CHD chromatin remodelers and the transcription cycle. Transcription *2*, 244-253.

Nakagawa, S. (2016). Lessons from reverse-genetic studies of lncRNAs. Biochimica et biophysica acta *1859*, 177-183.

Nakashima, K., Zhou, X., Kunkel, G., Zhang, Z., Deng, J.M., Behringer, R.R., and de Crombrugghe, B. (2002). The novel zinc finger-containing transcription factor osterix is required for osteoblast differentiation and bone formation. Cell *108*, 17-29.

Neale, B.M., Kou, Y., Liu, L., Ma'ayan, A., Samocha, K.E., Sabo, A., Lin, C.F., Stevens, C., Wang, L.S., Makarov, V.*, et al.* (2012). Patterns and rates of exonic de novo mutations in autism spectrum disorders. Nature *485*, 242-245.

Necsulea, A., Soumillon, M., Warnefors, M., Liechti, A., Daish, T., Zeller, U., Baker, J.C., Grutzner, F., and Kaessmann, H. (2014). The evolution of lncRNA repertoires and expression patterns in tetrapods. Nature *505*, 635-640.

Ng, S.Y., Johnson, R., and Stanton, L.W. (2012). Human long non-coding RNAs promote pluripotency and neuronal differentiation by association with chromatin modifiers and transcription factors. The EMBO journal *31*, 522-533.

Nielsen, J.A., Hudson, L.D., and Armstrong, R.C. (2002). Nuclear organization in differentiating oligodendrocytes. Journal of cell science *115*, 4071-4079.

Nishiyama, M., Nakayama, K., Tsunematsu, R., Tsukiyama, T., Kikuchi, A., and Nakayama, K.I. (2004). Early embryonic death in mice lacking the beta-catenin-binding protein Duplin. Molecular and cellular biology *24*, 8386-8394.

O'Shaughnessy-Kirwan, A., Signolet, J., Costello, I., Gharbi, S., and Hendrich, B. (2015). Constraint of gene expression by the chromatin remodelling protein CHD4 facilitates lineage specification. Development *142*, 2586-2597.

Ounzain, S., and Pedrazzini, T. (2015). The promise of enhancer-associated long noncoding RNAs in cardiac regeneration. Trends in cardiovascular medicine *25*, 592-602.

P., D.R.H. (1922). Son homologables la glía de escasas radiaciones y las células de Schwann. Bol Soc Esp Biol 2.

P., D.R.H. (1928). Tercera aportación al conocimiento morfológico e interpretación funcional de la oligodendroglía. Mem Real Soc Esp Hist Nat, 5-122.

Pauley, S., Lai, E., and Fritzsch, B. (2006). Foxg1 is required for morphogenesis and histogenesis of the mammalian inner ear. Developmental dynamics : an official publication of the American Association of Anatomists *235*, 2470-2482.

Pleasance, E.D., Stephens, P.J., O'Meara, S., McBride, D.J., Meynert, A., Jones, D., Lin, M.L., Beare, D., Lau, K.W., Greenman, C.*, et al.* (2010). A small-cell lung cancer genome with complex signatures of tobacco exposure. Nature *463*, 184-190.

Ragvin, A., Valvatne, H., Erdal, S., Arskog, V., Tufteland, K.R., Breen, K., AM, O.Y., Eberharter, A., Gibson, T.J., Becker, P.B.*, et al.* (2004). Nucleosome binding by the bromodomain and PHD finger of the transcriptional cofactor p300. Journal of molecular biology *337*, 773-788.

Ramos, A.D., Diaz, A., Nellore, A., Delgado, R.N., Park, K.Y., Gonzales-Roybal, G., Oldham, M.C., Song, J.S., and Lim, D.A. (2013). Integration of genome-wide approaches identifies lncRNAs of adult neural stem cells and their progeny in vivo. Cell stem cell *12*, 616-628.

Ran, F.A., Hsu, P.D., Wright, J., Agarwala, V., Scott, D.A., and Zhang, F. (2013). Genome engineering using the CRISPR-Cas9 system. Nature protocols *8*, 2281-2308.

Ratajczak, M.Z. (2012). Igf2-H19, an imprinted tandem gene, is an important regulator of embryonic development, a guardian of proliferation of adult pluripotent stem cells, a regulator of longevity, and a 'passkey' to cancerogenesis. Folia histochemica et cytobiologica / Polish Academy of Sciences, Polish Histochemical and Cytochemical Society *50*, 171-179.

Rinn, J.L., and Chang, H.Y. (2012). Genome regulation by long noncoding RNAs. Annual review of biochemistry *81*, 145-166.

Robert P. Erickson , A.J.W.-B. (2004). Epstein's Inborn Errors of Development: The Molecular Basis of Clinical Disorders of Morphogenesis (Oxford Monographs on Medical Genetics).

Roughton, K., Bostrom, M., Kalm, M., and Blomgren, K. (2013). Irradiation to the young mouse brain impaired white matter growth more in females than in males. Cell death & disease *4*, e897.

Sahlman, J., Inkinen, R., Hirvonen, T., Lammi, M.J., Lammi, P.E., Nieminen, J., Lapvetelainen, T., Prockop, D.J., Arita, M., Li, S.W.*, et al.* (2001). Premature vertebral endplate ossification and mild disc degeneration in mice after inactivation of one allele belonging to the Col2a1 gene for Type II collagen. Spine *26*, 2558-2565.

Saito, A., Hino, S., Murakami, T., Kanemoto, S., Kondo, S., Saitoh, M., Nishimura, R., Yoneda, T., Furuichi, T., Ikegawa, S.*, et al.* (2009). Regulation of endoplasmic reticulum stress response by a BBF2H7-mediated Sec23a pathway is essential for chondrogenesis. Nature cell biology *11*, 1197-1204.

Samanta, J., and Kessler, J.A. (2004). Interactions between ID and OLIG proteins mediate the inhibitory effects of BMP4 on oligodendroglial differentiation. Development *131*, 4131-4142.

Sandell, J.H., and Peters, A. (2002). Effects of age on the glial cells in the rhesus monkey optic nerve. The Journal of comparative neurology *445*, 13-28.

Sanlaville, D., Etchevers, H.C., Gonzales, M., Martinovic, J., Clement-Ziza, M., Delezoide, A.L., Aubry, M.C., Pelet, A., Chemouny, S., Cruaud, C.*, et al.* (2006). Phenotypic spectrum of CHARGE syndrome in fetuses with CHD7 truncating mutations correlates with expression during human development. Journal of medical genetics *43*, 211-217.

Sanlaville, D., and Verloes, A. (2007). CHARGE syndrome: an update. European journal of human genetics : EJHG *15*, 389-399.

Schimmang, T. (2013). Transcription factors that control inner ear development and their potential for transdifferentiation and reprogramming. Hearing research *297*, 84-90.

Schmitt, A.M., and Chang, H.Y. (2016). Long Noncoding RNAs in Cancer Pathways. Cancer cell *29*, 452-463.

Schnetz, M.P., Handoko, L., Akhtar-Zaidi, B., Bartels, C.F., Pereira, C.F., Fisher, A.G., Adams, D.J., Flicek, P., Crawford, G.E., Laframboise, T.*, et al.* (2010). CHD7 targets active gene enhancer elements to modulate ES cell-specific gene expression. PLoS genetics *6*, e1001023.

Schuster, N., Bender, H., Philippi, A., Subramaniam, S., Strelau, J., Wang, Z., and Krieglstein, K. (2002). TGF-beta induces cell death in the oligodendroglial cell line OLI-neu. Glia *40*, 95-108.

Shalem, O., Sanjana, N.E., and Zhang, F. (2015). High-throughput functional genomics using CRISPR-Cas9. Nature Reviews Genetics *16*, 299-311.

Shen, S., Li, J., and Casaccia-Bonnefil, P. (2005). Histone modifications affect timing of oligodendrocyte progenitor differentiation in the developing rat brain. The Journal of cell biology *169*, 577-589.

Shen, X., Liu, Y., Hsu, Y.J., Fujiwara, Y., Kim, J., Mao, X., Yuan, G.C., and Orkin, S.H. (2008). EZH1 mediates methylation on histone H3 lysine 27 and complements EZH2 in maintaining stem cell identity and executing pluripotency. Molecular cell *32*, 491-502.

Sher, F., Boddeke, E., Olah, M., and Copray, S. (2012). Dynamic Changes in Ezh2 Gene Occupancy Underlie Its Involvement in Neural Stem Cell Self-Renewal and Differentiation towards Oligodendrocytes. PloS one *7*.

Sher, F., Rossler, R., Brouwer, N., Balasubramaniyan, V., Boddeke, E., and Copray, S. (2008). Differentiation of neural stem cells into oligodendrocytes: involvement of the polycomb group protein Ezh2. Stem Cells *26*, 2875-2883.

Shi, J., Wang, E., Zuber, J., Rappaport, A., Taylor, M., Johns, C., Lowe, S.W., and Vakoc, C.R. (2013). The Polycomb complex PRC2 supports aberrant self-renewal in a mouse model of MLL-AF9;Nras(G12D) acute myeloid leukemia. Oncogene *32*, 930-938.

Simic, R., Lindstrom, D.L., Tran, H.G., Roinick, K.L., Costa, P.J., Johnson, A.D., Hartzog, G.A., and Arndt, K.M. (2003). Chromatin remodeling protein Chd1 interacts with transcription elongation factors and localizes to transcribed genes. The EMBO journal *22*, 1846-1856.

Sims, R.J., 3rd, Millhouse, S., Chen, C.F., Lewis, B.A., Erdjument-Bromage, H., Tempst, P., Manley, J.L., and Reinberg, D. (2007). Recognition of trimethylated histone H3 lysine 4 facilitates the recruitment of transcription postinitiation factors and pre-mRNA splicing. Molecular cell *28*, 665-676.

Smith, C.L., and Peterson, C.L. (2005). ATP-dependent chromatin remodeling. Current topics in developmental biology *65*, 115-148.

Smoot, M.E., Ono, K., Ruscheinski, J., Wang, P.L., and Ideker, T. (2011). Cytoscape 2.8: new features for data integration and network visualization. Bioinformatics *27*, 431-432.

Spitale, R.C., Tsai, M.C., and Chang, H.Y. (2011). RNA templating the epigenome: long noncoding RNAs as molecular scaffolds. Epigenetics : official journal of the DNA Methylation Society *6*, 539-543.

Stokes, D.G., and Perry, R.P. (1995). DNA-binding and chromatin localization properties of CHD1. Molecular and cellular biology *15*, 2745-2753.

Stolt, C.C., Rehberg, S., Ader, M., Lommes, P., Riethmacher, D., Schachner, M., Bartsch, U., and Wegner, M. (2002). Terminal differentiation of myelin-forming oligodendrocytes depends on the transcription factor Sox10. Genes & development *16*, 165-170.

Stolt, C.C., Schlierf, A., Lommes, P., Hillgartner, S., Werner, T., Kosian, T., Sock, E., Kessaris, N., Richardson, W.D., Lefebvre, V.*, et al.* (2006). SoxD proteins influence multiple stages of oligodendrocyte development and modulate SoxE protein function. Developmental cell *11*, 697-709.

Sumi-Ichinose, C., Ichinose, H., Metzger, D., and Chambon, P. (1997). SNF2beta-BRG1 is essential for the viability of F9 murine embryonal carcinoma cells. Molecular and cellular biology *17*, 5976-5986.

Swiss, V.A., Nguyen, T., Dugas, J., Ibrahim, A., Barres, B., Androulakis, I.P., and Casaccia, P. (2011). Identification of a gene regulatory network necessary for the initiation of oligodendrocyte differentiation. PloS one *6*, e18088.

Tahara, T., Yamamoto, E., Madireddi, P., Suzuki, H., Maruyama, R., Chung, W., Garriga, J., Jelinek, J., Yamano, H.O., Sugai, T.*, et al.* (2014). Colorectal carcinomas with CpG island methylator phenotype 1 frequently contain mutations in chromatin regulators. Gastroenterology *146*, 530-538 e535.

Trapnell, C., Pachter, L., and Salzberg, S.L. (2009). TopHat: discovering splice junctions with RNA-Seq. Bioinformatics *25*, 1105-1111.

Trapnell, C., Williams, B.A., Pertea, G., Mortazavi, A., Kwan, G., van Baren, M.J., Salzberg, S.L., Wold, B.J., and Pachter, L. (2010). Transcript assembly and quantification by RNA-Seq reveals unannotated transcripts and isoform switching during cell differentiation. Nature biotechnology *28*, 511-515.

Trimarchi, T., Bilal, E., Ntziachristos, P., Fabbri, G., Dalla-Favera, R., Tsirigos, A., and Aifantis, I. (2014). Genome-wide mapping and characterization of Notch-regulated long noncoding RNAs in acute leukemia. Cell *158*, 593-606.

Tripathi, V., Ellis, J.D., Shen, Z., Song, D.Y., Pan, Q., Watt, A.T., Freier, S.M., Bennett, C.F., Sharma, A., Bubulya, P.A.*, et al.* (2010). The nuclear-retained noncoding RNA

MALAT1 regulates alternative splicing by modulating SR splicing factor phosphorylation. Molecular cell *39*, 925-938.

Tsai, M.C., Manor, O., Wan, Y., Mosammaparast, N., Wang, J.K., Lan, F., Shi, Y., Segal, E., and Chang, H.Y. (2010). Long noncoding RNA as modular scaffold of histone modification complexes. Science *329*, 689-693.

Tsukiyama, T. (2002). The in vivo functions of ATP-dependent chromatin-remodelling factors. Nature reviews Molecular cell biology *3*, 422-429.

Ulitsky, I., and Bartel, D.P. (2013). lincRNAs: genomics, evolution, and mechanisms. Cell *154*, 26-46.

Valerius, M.T., Patterson, L.T., Witte, D.P., and Potter, S.S. (2002). Microarray analysis of novel cell lines representing two stages of metanephric mesenchyme differentiation. Mech Dev *112*, 219-232.

Vallstedt, A., Klos, J.M., and Ericson, J. (2005). Multiple dorsoventral origins of oligodendrocyte generation in the spinal cord and hindbrain. Neuron *45*, 55-67.

van Dongen S, A.-G.C. (2012). Using MCL to extract clusters from networks. Methods Mol Biol *804*, 281-295.

van Dongen, S., and Abreu-Goodger, C. (2012). Using MCL to extract clusters from networks. Methods Mol Biol *804*, 281-295.

Vissers, L.E., van Ravenswaaij, C.M., Admiraal, R., Hurst, J.A., de Vries, B.B., Janssen, I.M., van der Vliet, W.A., Huys, E.H., de Jong, P.J., Hamel, B.C.*, et al.* (2004). Mutations in a new member of the chromodomain gene family cause CHARGE syndrome. Nature genetics *36*, 955-957.

Voss, T.C., and Hager, G.L. (2014). Dynamic regulation of transcriptional states by chromatin and transcription factors. Nature reviews Genetics *15*, 69-81.

Walfridsson, J., Khorosjutina, O., Matikainen, P., Gustafsson, C.M., and Ekwall, K. (2007). A genome-wide role for CHD remodelling factors and Nap1 in nucleosome disassembly. The EMBO journal *26*, 2868-2879.

Wang, L., Park, H.J., Dasari, S., Wang, S., Kocher, J.P., and Li, W. (2013). CPAT: Coding-Potential Assessment Tool using an alignment-free logistic regression model. Nucleic acids research *41*, e74.

Wang, S., Sdrulla, A., Johnson, J.E., Yokota, Y., and Barres, B.A. (2001). A role for the helix-loop-helix protein Id2 in the control of oligodendrocyte development. Neuron *29*, 603-614.

Wang, X., Arai, S., Song, X., Reichart, D., Du, K., Pascual, G., Tempst, P., Rosenfeld, M.G., Glass, C.K., and Kurokawa, R. (2008). Induced ncRNAs allosterically modify RNA-binding proteins in cis to inhibit transcription. Nature *454*, 126-130.

Waxman, S.G. (2006). Axonal conduction and injury in multiple sclerosis: the role of sodium channels. Nat Rev Neurosci *7*, 932-941.

Weng, Q., Chen, Y., Wang, H., Xu, X., Yang, B., He, Q., Shou, W., Higashi, Y., van den Berghe, V., Seuntjens, E.*, et al.* (2012). Dual-mode modulation of Smad signaling by Smad-interacting protein Sip1 is required for myelination in the central nervous system. Neuron *73*, 713-728.

Williams, C.J., Naito, T., Arco, P.G., Seavitt, J.R., Cashman, S.M., De Souza, B., Qi, X., Keables, P., Von Andrian, U.H., and Georgopoulos, K. (2004). The chromatin remodeler Mi-2beta is required for CD4 expression and T cell development. Immunity *20*, 719-733.

Woodage, T., Basrai, M.A., Baxevanis, A.D., Hieter, P., and Collins, F.S. (1997). Characterization of the CHD family of proteins. Proceedings of the National Academy of Sciences of the United States of America *94*, 11472-11477.

Xin, M., Yue, T., Ma, Z., Wu, F.F., Gow, A., and Lu, Q.R. (2005). Myelinogenesis and axonal recognition by oligodendrocytes in brain are uncoupled in Olig1-null mice. The Journal of neuroscience : the official journal of the Society for Neuroscience *25*, 1354-1365.

Xu, D., Yang, F., Yuan, J.H., Zhang, L., Bi, H.S., Zhou, C.C., Liu, F., Wang, F., and Sun, S.H. (2013). Long noncoding RNAs associated with liver regeneration 1 accelerates hepatocyte proliferation during liver regeneration by activating Wnt/beta-catenin signaling. Hepatology *58*, 739-751.

Yang, L., Froberg, J.E., and Lee, J.T. (2014). Long noncoding RNAs: fresh perspectives into the RNA world. Trends in biochemical sciences *39*, 35-43.

Yang, L., Lin, C., Liu, W., Zhang, J., Ohgi, K.A., Grinstein, J.D., Dorrestein, P.C., and Rosenfeld, M.G. (2011). ncRNA- and Pc2 methylation-dependent gene relocation between nuclear structures mediates gene activation programs. Cell *147*, 773-788.

Ye, F., Chen, Y., Hoang, T., Montgomery, R.L., Zhao, X.H., Bu, H., Hu, T., Taketo, M.M., van Es, J.H., Clevers, H.*, et al.* (2009). HDAC1 and HDAC2 regulate oligodendrocyte differentiation by disrupting the beta-catenin-TCF interaction. Nature neuroscience *12*, 829-838.

Yu, T., Meiners, L.C., Danielsen, K., Wong, M.T., Bowler, T., Reinberg, D., Scambler, P.J., van Ravenswaaij-Arts, C.M., and Basson, M.A. (2013a). Deregulated FGF and homeotic gene expression underlies cerebellar vermis hypoplasia in CHARGE syndrome. eLife *2*, e01305.

Yu, Y., Chen, Y., Kim, B., Wang, H., Zhao, C., He, X., Liu, L., Liu, W., Wu, L.M., Mao, M.*, et al.* (2013b). Olig2 targets chromatin remodelers to enhancers to initiate oligodendrocyte differentiation. Cell *152*, 248-261.

Yue, F., Cheng, Y., Breschi, A., Vierstra, J., Wu, W., Ryba, T., Sandstrom, R., Ma, Z., Davis, C., Pope, B.D.*, et al.* (2014). A comparative encyclopedia of DNA elements in the mouse genome. Nature *515*, 355-364.

Zaret, K.S., and Carroll, J.S. (2011). Pioneer transcription factors: establishing competence for gene expression. Genes & development *25*, 2227-2241.

Zentner, G.E., Layman, W.S., Martin, D.M., and Scacheri, P.C. (2010). Molecular and phenotypic aspects of CHD7 mutation in CHARGE syndrome. American journal of medical genetics Part A *152A*, 674-686.

Zhang, L., He, X., Liu, L., Jiang, M., Zhao, C., Wang, H., He, D., Zheng, T., Zhou, X., Hassan, A.*, et al.* (2016). Hdac3 Interaction with p300 Histone Acetyltransferase Regulates the Oligodendrocyte and Astrocyte Lineage Fate Switch. Developmental cell *37*, 582.

Zhang, Y., Chen, K., Sloan, S.A., Bennett, M.L., Scholze, A.R., O'Keeffe, S., Phatnani, H.P., Guarnieri, P., Caneda, C., Ruderisch, N.*, et al.* (2014). An RNA-sequencing transcriptome and splicing database of glia, neurons, and vascular cells of the cerebral cortex. The Journal of neuroscience : the official journal of the Society for Neuroscience *34*, 11929-11947.

Zhang, Y., Jalili, F., Ouamara, N., Zameer, A., Cosentino, G., Mayne, M., Hayardeny, L., Antel, J.P., Bar-Or, A., and John, G.R. (2010). Glatiramer acetate-reactive T lymphocytes regulate oligodendrocyte progenitor cell number in vitro: role of IGF-2. Journal of neuroimmunology *227*, 71-79.

Zhao, C., Deng, Y., Liu, L., Yu, K., Zhang, L., Wang, H., He, X., Wang, J., Lu, C., Wu, L.N.*, et al.* (2016). Dual regulatory switch through interactions of Tcf7l2/Tcf4 with stage-specific partners propels oligodendroglial maturation. Nature communications *7*, 10883.

Zhao, S., Choi, M., Overton, J.D., Bellone, S., Roque, D.M., Cocco, E., Guzzo, F., English, D.P., Varughese, J., Gasparrini, S.*, et al.* (2013). Landscape of somatic single-nucleotide and copy-number mutations in uterine serous carcinoma. Proceedings of the National Academy of Sciences of the United States of America *110*, 2916-2921.

Zhao, X., Dai, J., Ma, Y., Mi, Y., Cui, D., Ju, G., Macklin, W.B., and Jin, W. (2014). Dynamics of ten-eleven translocation hydroxylase family proteins and 5-hydroxymethylcytosine in oligodendrocyte differentiation. Glia *62*, 914-926.

Zhao, X., He, X., Han, X., Yu, Y., Ye, F., Chen, Y., Hoang, T., Xu, X., Mi, Q.S., Xin, M.*, et al.* (2010). MicroRNA-mediated control of oligodendrocyte differentiation. Neuron *65*, 612-626.

Zhou, Q., and Anderson, D.J. (2002). The bHLH transcription factors OLIG2 and OLIG1 couple neuronal and glial subtype specification. Cell *109*, 61-73.

Zhou, Q., Wang, S., and Anderson, D.J. (2000). Identification of a novel family of oligodendrocyte lineage-specific basic helix-loop-helix transcription factors. Neuron *25*, 331-343.

Zhuang, T., Hess, R.A., Kolla, V., Higashi, M., Raabe, T.D., and Brodeur, G.M. (2014). CHD5 is required for spermiogenesis and chromatin condensation. Mechanisms of development *131*, 35-46.

Zuchero, J.B., and Barres, B.A. (2013). Intrinsic and extrinsic control of oligodendrocyte development. Current opinion in neurobiology *23*, 914-920.